Core–hole–clock spectroscopy : Characterization of the method and dynamics of charge transfer at adsorbate metal interfaces

Dissertation
zur Erlangung des Doktorgrades
des Department Physik
der Universität Hamburg

vorgelegt von
Vijayalakshmi Sethuraman
aus Indien in Kuvanur

Hamburg
2007

Dissertation an der Universität Hamburg

Gutachter der Dissertation :	Prof. Dr. Wilfried Wurth Prof. Dr. Michael Rübhausen
Gutachter der Disputation :	Prof. Dr. Wilfried Wurth Prof. Dr. Edgar Weckert
Datum der Disputation:	20.12.2006
Vorsitzender des Prüfungsausschusses:	Dr. Klaus Petermann
MIN-Fakultät des Department Physik :	Prof. Dr. Arno Frühwald
Vorsitzender des Promotionaussschusses :	Prof. Dr. Günter Huber

Kurzfassung

Core–hole–clock Spektroskopie: Untersuchung der Methodik und Ladungstransferdynamik an Adsorbat-Metall-Grenzflächen

In dieser Doktorarbeit wird die Dynamik des Ladungstransfers sowohl an atomaren, als auch an molekularen Adsorbaten mit der Core–hole–clock (CHC) Spektroskopie untersucht. Zuerst wird überprüft, ob die Ladungstransferzeiten unabhängig von der Referenz sind, der Lebensdauer des Rumpflochs, welches die Grundannahme der core–hole–clock-Methode bildet. Dies wird an fest auf einer Ru-Oberfläche chemisorbierten S-Atomen mittels zweier unabhängiger Rumpflöcher (S(1s), S(2s)) gezeigt. Weiterhin haben kleine Änderungen in der elektronischen Struktur der Oberfläche einen Einfluss auf die Lebensdauer des angeregten Zustands des Adsorbats. Diese wurden mit Hilfe der CHC Spektroskopie bei physisorbiertem Argon auf Cu(111) und Cu(100)-Oberflächen gefunden. Kombinierte, theoretische Berechnungen sind konsistent mit den experimentellen Ergebnissen. Schlussendlich werden Ladungstransferzeiten von Moleküladsorbaten in das darunterliegende Substrat für das Moleküladsorbatsystem (C_6F_6) (ein aromatisches Molekül mit äquivalenten Atomen) bei verschiedenen Bedeckungen bestimmt. Zusätzliche Vibrationsbewegungen, die für Moleküladsorbate typisch sind, stören dabei die Ermittlung der Ladungstransferzeiten. Daher wird der Vergleich zur Gasphase herangezogen, um den Ladungstransfer im Adsorbat zu bestimmen. Die Ladungstransferzeiten, die mit der Core hole clock Spektroskopie für dieses molekulare System gemessen werden, werden mit Ergebnissen der zeitaufgelösten Zwei-Photon-Photoemission vergleichen. Diese Technik bildet einen alternativen Ansatz, um Ladungstransferzeiten zu bestimmen. Übereinstimmungen und Unterschiede der beiden Spektroskopiemethoden werden diskutiert.

Abstract

Core–hole–clock spectroscopy : Investigation of the method and charge transfer dynamics at adsorbate metal interfaces

In this thesis, charge transfer dynamics has been investigated with the core–hole–clock method (CHC) for both atomic and molecular adsorbates. As a first step, the basic assumption of the core–hole–clock method that the charge transfer time is independent of the reference core hole lifetime has been tested. This is shown for the strongly chemisorbed S atom on the Ru surface for two independent core hole clocks (S(1s), S(2s)). Furthermore, fine changes in surface electronic structure affect the excited adsorbate state lifetime and has been detected by CHC spectroscopy for physisorbed Ar on Cu(111) and Cu(100) surfaces. Combined theoretical computations are consistent with the experimental findings. Finally, charge transfer times from the molecular adsorbate to the underlying substrate have been determined for the molecular adsorbate system (C_6F_6)(aromatic molecule with equivalent atoms) with core–hole–

clock spectroscopy for various adsorbate coverages. There additional vibrational motion typical of the molecular adsorbates complicates the determination of charge transfer times and comparison to gas phase has been used to determine the charge transfer in the adsorbate. The charge transfer times obtained with core–hole–clock spectroscopy for this molecular system have been compared to those from time resolved two-photon photoemission which is an alternative approach to determine charge transfer times and the similarities/and differences between the two spectroscopic methods are discussed.

List of Papers

This thesis is based on the following papers. They will be referred to in the text by their roman numbers.

[**Paper I**] Verification of the core–hole–clock method using two different time references : Attosecond charge transfer in c(4x2)S/Ru(0001)
A. Föhlisch and S. Vijayalakshmi and F. Hennies and W. Wurth and V. R. R. Medicherla and W. Drube, Chem. Phys. Lett.434 (2007) 214.

[**Paper II**] Surface projected electronic band structure and adsorbate charge transfer dynamics : Ar adsorbed on Cu(111) and Cu(100)
S. Vijayalakshmi and A. Föhlisch and F. Hennies and A. Pietzsch and M. Nagasono and W. Wurth and A. G. Borisov and J. P. Gauyacq, Chem. Phys. Lett.427 (2006) 91.

[**Paper III**] Bond polarization and image-potential screening in adsorbed C_6F_6 on Cu(111)
S. Vijayalakshmi and A. Föhlisch and P. S. Kirchmann and F. Hennies and A. Pietzsch and M. Nagasono and W. Wurth, Surf. Sci. 600 (2006) 4972.

[**Paper IV**] Investigation of charge transfer dynamics in C_6F_6/Cu(111) with core–hole–clock spectroscopy
S. Vijayalakshmi and A. Föhlisch and F. Hennies and A. Pietzsch and M. Nagasono and W. Wurth, in manuscript.

[**Paper V**] Comparative study of charge transfer dynamics between core–hole–clock method and time resolved two-photon photoemission on C_6F_6/Cu(111)
S. Vijayalakshmi and A. Föhlisch and F. Hennies and A. Pietzsch and M. Nagasono and W. Wurth, P. S. Kirchmann and U. Bovensiepen and M. Wolf, in manuscript.

Die aufregendste in Wissenschaft, die zu hören Phrase, die neue Entdeckungen ankündigt, ist nicht Eureka! (ich fand sie!) aber eher, "hmm...., das...." lustig ist – Isaac Asimov

The most exciting phrase to hear in science, the one that heralds new discoveries, is not Eureka! (I found it!) but rather, "hmm.... that's funny...." – Isaac Asimov

Contents

Scope of the present investigations

The driving force for the study carried out here is to get a complete understanding of the core–hole–clock (CHC) method and to evaluate the potential of the method as an experimental tool in various fields of research in deriving electron transfer dynamics. Important information on local electronic structure within the adsorbate-substrate and core-hole dynamics can be obtained from investigations of the deexcitation spectra.

First, to justify the assumption made in the method itself. The major assumption made in core–hole–clock spectroscopy is that the dynamics of the excited electron is not influenced by the speed of the core–hole–clock which serves as a reference in determining the charge transfer times. The validity of this assumption is checked by evaluating the rate of charge transfer from the atomic adsorbate S on Ru(0001) surface with two independent core hole clocks which are of different speed. The charge transfer times remain unaffected by the nature of the clocks within the experimental resolution thereby, proving the approximation to be good.

Next, to determine the sensitivity of the method to subtle changes of the substrate electronic structure. This can be realized with a simple atomic adsorbate like Ar on two different surfaces of Cu, Cu(100) and Cu(111) where the adsorbed atom couples weakly to the substrate. The dissimilar electronic structure of Cu(100) and Cu(111) should be reflected in the charge transfer time from the excited Ar to the substrate surfaces.

Evidently, comparison of the CHC method to the traditional time resolved laser technique would facilitate to differentiate or find similarities between the methods while studying the systems of technological importance. The charge transfer dynamics in the system C_6F_6/Cu(111) for the adsorbate coverages ranging from submonolayer to multilayers is studied with core–hole–clock method and pump-probe technique.

(a) Before investigating the molecular adsorbate system for charge transfer dynamics, it is essential to know exactly the adsorption geometry of the molecule. Hence polarization dependency of Near Edge X-ray Absorption Fine Structure (NEXAFS) spectroscopy has been utilized to determine the orientation of C_6F_6 on Cu(111) for various adsorbate coverages.

(b) The system C_6F_6/Cu(111) is subjected to study by core hole clock spectroscopy and time resolved two-photon photoemission (tr-2PPE) and the charge transfer times obtained from these two methods are compared.

Chapter 1

Introduction

Charge transfer dynamics

Electron transfer is a key concept in surface science. This can be realized on looking back into the history of surface science. For instance, work function changes occurring upon e.g. alkali-atom adsorption have been driving forces behind essential conceptual developments. Electron transfer plays central role in many situations of both scientific and technological importance [1].

Electronic excitations in condensed matter are another important study. Quantum mechanically an excited electronic state of a system is an electronic state that has a higher energy than the ground state. Lifetime of the excited state is usually short; either by spontaneous or via stimulated emission the excess quanta of energy leave the system and the excited system returns to the ground state. Alternatively the excited state may lose its absorbed energy via electronic decay processes.

Motivation

By and large, photo induced electron transfer is the primary step in systems capable of converting light into information. Basic understanding of the electron transfer dynamics is thus essential for instance in disentangling the reaction mechanisms at catalytic surfaces and photochemistry, in synthesizing efficient solar cells and improving optoelectronic devices, light emitting diodes, FRET (Förster Resonant Energy Transfer) devices etc. The success of these fields lies mainly in tailoring excited state lifetimes and in controlling those intermediate electronic states with high flexibility. Here the concept of electron transfer can be associated with an energy dissipation process where the excited electrons in these systems lose their energy to their surroundings via resonant electron transfer or by inelastic electron-electron collision. It is necessary to understand the contribution of different electronic decay channels in order to obtain maximum benefit.

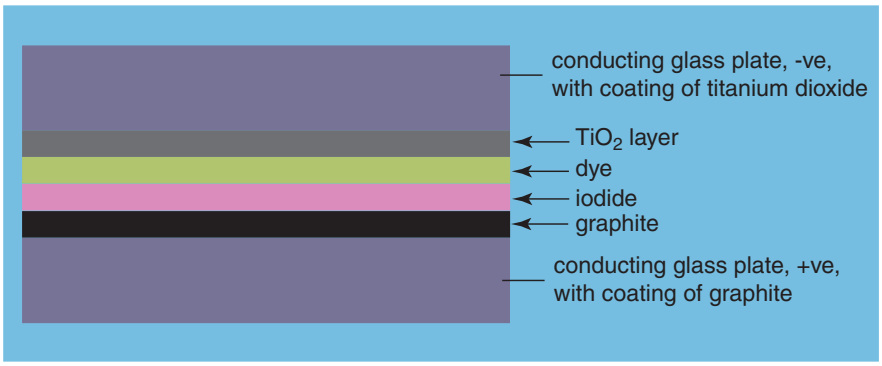

Figure 1.1: Operation of the Grätzel cell

In Fig. 1.1 is shown the working principle of the well known Grätzel cell where the leading role of charge transfer dynamics in determining the efficiency of the device is made evident.

Prof. Grätzel ⟨http://isic2.epfl.ch/page58671-en.html⟩ at the EPFL (Ecole Polytechnique Fédérale de Lausanne) discovered and developed this new type of solar cell based on dye sensitized mesoscopic oxide particles [2]. Grätzel cells are produced at much lower cost compared to the industry standard based on silicon layers. A Grätzel cell works by mimicking photosynthesis. Incident light excites electrons in the dye which tunnel through the conduction band of the TiO_2 particles and are collected through the glass plate to the external circuit. Recombination of the electrons with the dye is prevented by intercepting the latter with the electrons supplied by an electrolyte I_3^-/I_2 redox couple. The oxidized mediator is in turn regenerated at the counter electrode. Here the excited electron lifetime and the dynamics of charge transfer are the major factors determining the efficiency of the device. Thus understanding electron dynamics is essential.

Vital importance of electron transfer was realized not only in the field of physics but also widely in chemistry and biology of both normal and photon induced reactions. Here the electron transfer is associated with dissociation dynamics of molecules and non-adiabatic electronic processes accompanying chemical reactions. Surface catalysed chemical reactions, nanocatalysis are based on electron transfer, to name a few. Often spoken in chemical and biological reactions is the Resonant Charge Transfer (RCT) i.e., transfer of an electron from the acceptor (A) to the donor (D) in the localized picture. The energy levels of A and D and the distance between A and D are crucial factors in determining efficient RCT processes. Likewise in the spectroscopic sense transfer of an resonantly excited electron to the surroundings with delocalized states is called RCT [3]. Therefore, spectroscopic investigation of RCT process leads to the better control of reaction pathways and the end products.

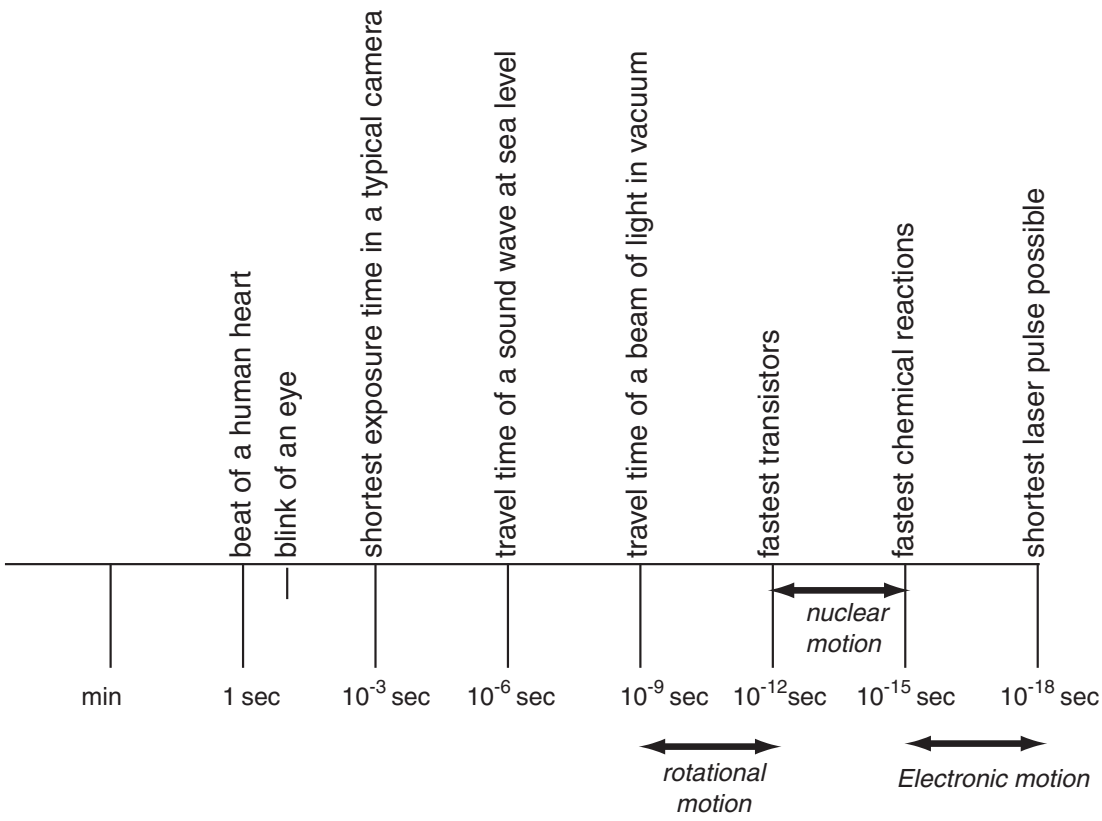

Figure 1.2: Comparison of timescales of primary processes in a molecule with universal processes

Electrochemistry and photography are few other fields where electron transfer in the form of oxidation/reduction is of fundamental importance. A well-known example where electron transfer is initiated by photons is photosynthesis.

A closely related aspect to electron transfer is the excited state lifetime. For instance, in organic photochemical reactions, lifetime of the electronically excited molecules dictate the pathway of the reaction mechanism.

Charge transfer is an important phenomena at surfaces and interfaces. The dynamics of electronic excitations in general including charge transfer between the surface and the adsorbate proceed on a femtosecond timescale. In Fig. 1.2 the timescale of electron dynamics is compared with the primary molecular processes and with universal processes.

Chapter 2

Methods of investigation

2.1 Background

Electron transfer plays a prominent role widely from day-to-day life to high-tech industry. Therefore, it is of foremost importance to device methods which can provide deep knowledge on such processes. There are techniques that can deal with initial and final states of electron transfer. While static aspects of electron transfer can be looked through by means of work function measurements, dynamic aspects of charge transfer need very sensitive and sophisticated techniques. Principal reason for the lack of methods is that electron transfer dynamics occur in the ultrafast timescale, femtoseconds to sub-femto seconds [4].

A direct and appealing approach to studying charge transfer processes at surfaces and interfaces is the pump-probe measurement in which an electron is optically excited and the excited state is probed as a function of time. The use of lasers with pulse lengths as short as a few tenths of fs for this is now established. These methods are quite attractive as they operate in the time domain, which allows one to more or less directly derive relaxation times as low as around 10fs.

With the advent of ultrafast lasers, reaction intermediates and transition states in chemistry which live only few hundreds of femtoseconds could be observed by performing pump-probe measurements. Snapshots of intermediate reaction stages could be photographed by applying femtosecond optical pulses [5]. Ahmed Zewail of California Institute of Technology was awarded Nobel Prize in Chemistry for his significant work in the development of femtochemistry.

Time Resolved Two Photon Photoemission (tr-2PPE)

Briefly, the tr-2PPE works as follows. A pump laser pulse creates hot electrons near the Fermi level of the substrate by exciting electrons below the E_F into normally unoccupied states. These hot electrons can subsequently tunnel into the intermediate state (image

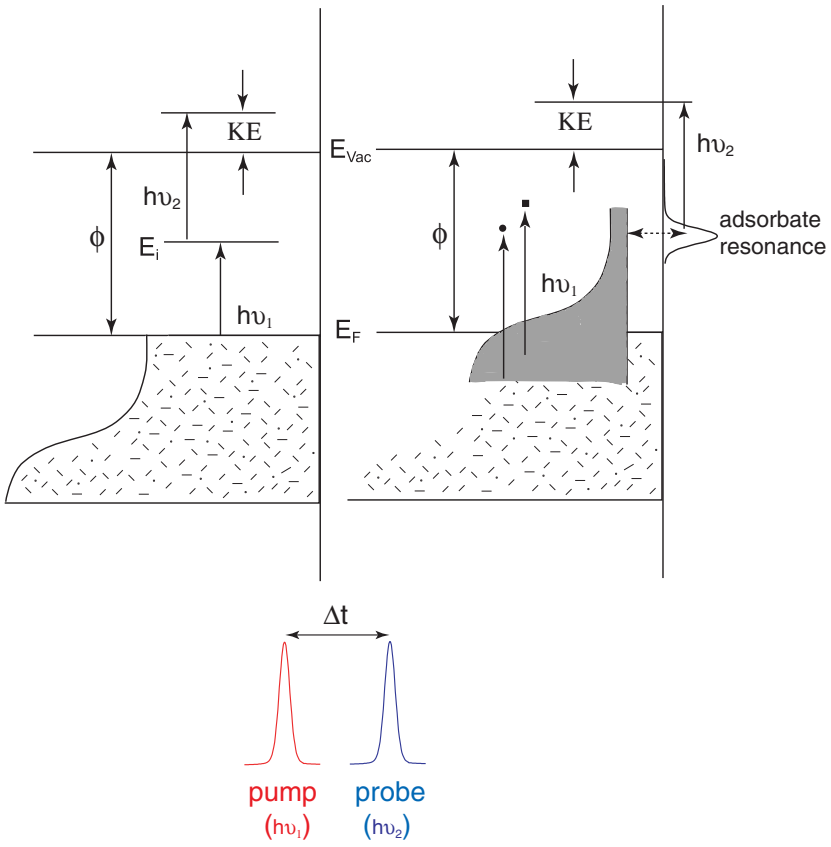

Figure 2.1: Time resolved two photon photoemission scheme

state or adsorbate resonance, for instance). The second probe pulse photoemits the electron from the intermediate state and is detected. Upon varying the time delay between the pump and the probe laser pulse, lifetime of the electron in the intermediate resonance can be measured against other inelastic decay channels. For elaborate details on 2PPE and tr-2PPE see references [6, 7].

In spectroscopic mode, the first and second photons come from the same laser pulse; in time-resolved measurement, the two photons are from two time-delayed pulses.

The lifetimes of electronic excitons in tr-2PPE are determined by performing cross-correlation (CC) measurements. In these experiments, photoelectron signal at the intermediate state (image state (or) adsorbate resonance) is recorded as a function of pump-probe delay time. As the intermediate state can decay with a finite lifetime, the cross-correlation trace consists of three components: (1) a coherent component (also called coherent artifact) which results from the fact that the optical fields from both laser pulses add coherently and enhance transition probabilities in both excitation steps; (2) an incoherent component which reflects the dynamics of the transiently populated intermediate state; and (3) the constant background. In principle the intensity ratio

at zero time-delay is 1:1:1 for the three components. In practice, the background signal is usually higher because the spatial overlap of the two laser pulses is less than 100%. Two-photon photo-ionization from an occupied state which involves only virtual intermediate state gives auto-correlation (AC) curve. Here the optical fields from the two laser pulses add coherently. Fitting the auto-correlation curve to the well-known Gaussian or hyperbolic sech functions gives the pulse width. The cross-correlation curve should be broader than the auto-correlation curve which is due to finite lifetime of the intermediate state. If we assume a single-exponential decay with lifetime of τ_{life} the experimental cross-correlation data can be described by the sum of the AC function S_{AC} and the incoherent component, S_{inc}, which is a convolution of the AC function and a symmetric exponential decay function.

$$S_{inc}(\tau) \propto \int S_{AC}(t-\tau) e_{life}^{-|t|\tau} dt \tag{2.1}$$

The technique has been exploited to study the dynamics of hot electrons and holes on the metal surfaces [7] and the lifetime of image potential [8, 9] and surface states. Later on lifetimes of unoccupied resonances of adsorbates became more interesting. Two photon photoemission experiments provided evidence for the existence of adsorbate anionic resonances from atomic [10, 11] and molecular [12–17] adsorbates and their lifetimes can be measured with a resolution of few femtoseconds with the advent of ultrafast lasers [13]. Tr-2PPE is widely applicable to study underlying mechanisms of photochemical reactions occurring on surfaces and charge injection in optoelectronic devices.

We here used UV (pump) and visible (probe) lasers for pump-probe measurements and hence valence electrons are probed.

Core–hole–clock spectroscopy

Charge transfer dynamics in the fs regime can also be investigated with core–hole–clock spectroscopy which is based on core-level excitation and decay. This method is analogous to pump-probe technique, with an intrinsic time scale based on the lifetime of the core-hole, leading to the description as core-hole–clock method. Due to the shortness of the core-hole lifetime, electron dynamics can be studied in much shorter timescales compared to tens of fs. However, core–hole–clock method differs from pump-probe technique in two aspects.

(1) Lifetimes of the excited state is calculated from the intensities in the deexcitation spectrum, so it is often termed as excitation-decay.

(2) Core electrons are involved which enables the general atomic specificity unique to core spectroscopies.

Two step model

Core–hole–clock spectroscopy for either an atom or a molecule coupled to a substrate can be described in a two step model as the core excitation and the core-hole decay. Resonant excitation of a core electron to a nominally unoccupied level resulting in a core-hole corresponds to X-ray absorption maximum. Decay of the core-hole takes place both radiatively, (X-ray Emission Spectrosocpy - XES) and non-radiatively (Auger Electron Spectrosocpy - AES). The systems investigated in this thesis are studied within the framework of non-radiative decay (Auger resonant Raman spectroscopy). Fig. 2.2 shows the principle behind core–hole–clock method.

Briefly, a core electron of the adsorbate is excited to one of the unoccupied orbitals of the later by absorption of a soft x-ray photon. Consequently, a valence electron fills the core-hole whereas another valence electron escapes into vacuum as an Auger electron. During the lifetime of the core-hole the excited electron can either stay at the core-hole site and watch the decay as a spectator (spectator Auger decay) or can take part in the decay process (participator Auger decay). Alternatively, the excited electron may tunnel to the substrate conduction band resulting in charge transfer decay (CT Auger decay). The core- hole serves as an internal clock to monitor the decay processes [18].

The branching ratio of Raman channel (spectator and participator Auger) to the CT Auger gives charge transfer time in reference to the core-hole life time. Inset of Fig. 2.2 shows the schematic representation of autoionization decay spectral output corresponding to charge transfer times compared to core-hole life time.

When charge transfer time (τ_{CT}) and core-hole life time (τ_C) are considered as an exponential decay processes then the relation between them can be written as

$$\frac{\tau_{CT}}{\tau_C} = \frac{f}{1-f} \qquad where, f = \frac{I_{Raman}}{I_{Raman} + I_{Auger}} \tag{2.2}$$

I_{Raman} and I_{Auger} are the respective intensities of the Raman and CT Auger decay channels. In Fig. 2.3 the ratio of CT time to core-hole lifetime is plotted as a function of Raman fraction f. The core–hole–clock method is most accurate for charge transfer times not too different from the core-hole lifetime ie. in the range of $0.1\tau \leq \tau_{CT} \geq \tau$.

We used soft x-rays in the regime of C1s, Ar2p and S1s to study charge transfer dynamics. Core–hole–clock measurements are carried out on adsorbate systems coupled to the substrate ranging from weak to strong coupling limits. The excitation and decay are both centered around the adsorbate system. In pump-probe measurements the initial excitation occurs at the substrate and the decay dynamics are focussed for the adsorbate resonance.

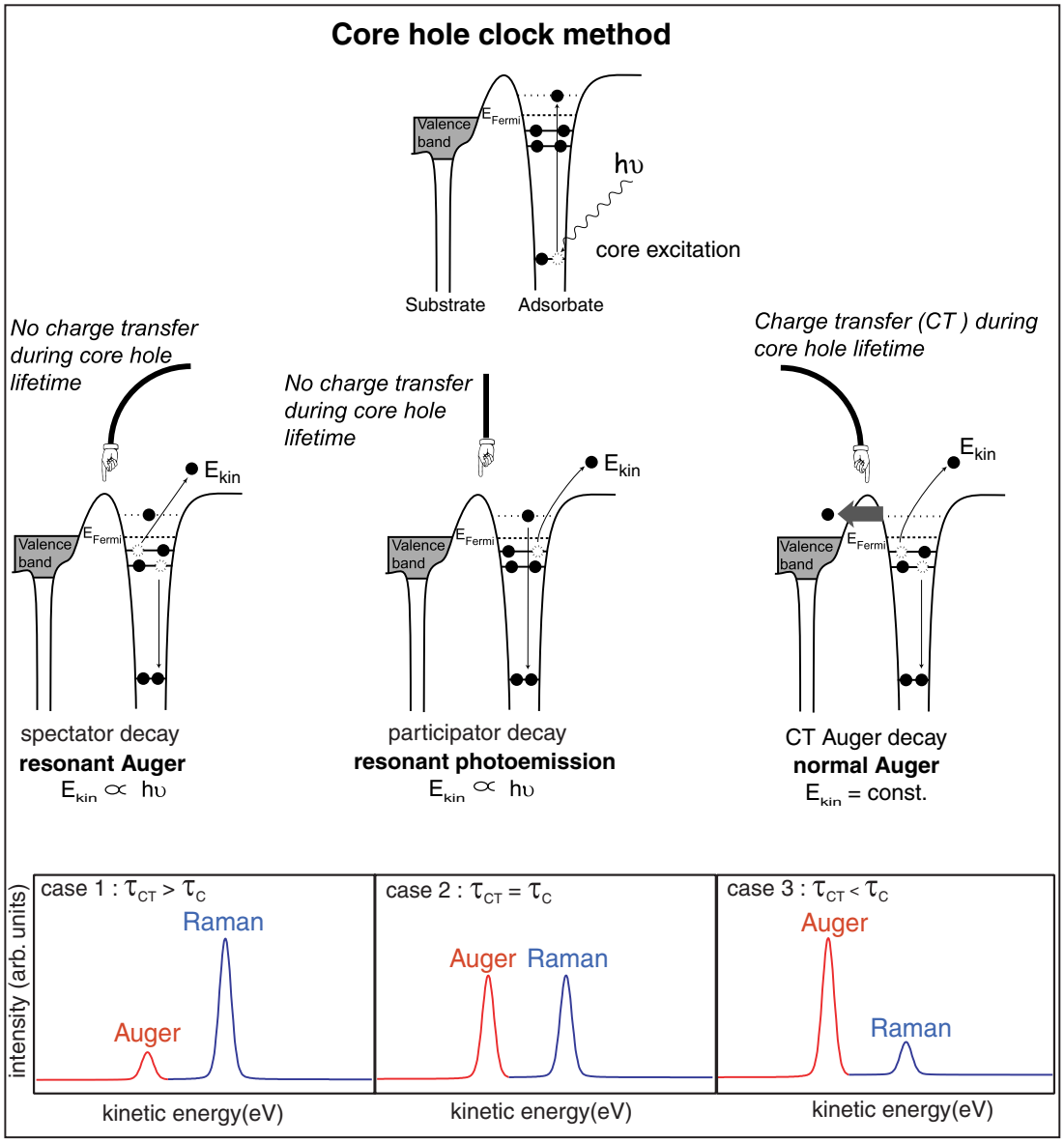

Figure 2.2: Principle of core–hole–clock method. Inset: Schematic illustration of ratio of Raman Auger to charge transfer Auger intensity when charge transfer times greater than, smaller than or equivalent to core-hole lifetime.

Auger resonant Raman conditions - one-step picture:

When the bandwidth of the exciting radiation is much narrower than the core-hole lifetime broadening of the neutral core-excited state, it is not possible to disentangle excitation - de-excitation processes in a two-step framework, but the whole phenomenon should be considered as a scattering process and treated in a one-step picture.

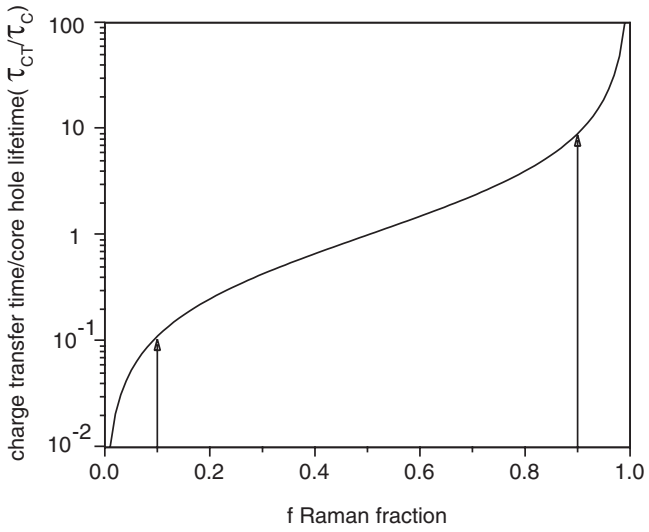

Figure 2.3: Charge transfer time in reference to core-hole lifetime as a function of Raman fraction (f). Experimentally accessible limits of f are shown by arrows.

Under such conditions linear dispersion of the resonant Auger lines with the excitation energy (as in Fig. 2.4) and narrowing of their linewidths compared to the natural linewidth of the intermediate neutral state is observed. Other interesting effects include lifetime/vibrational interference, detuning effects, non-linear dispersion and fragmentation dynamics.

Experimental observations of the Auger resonant Raman effect have become feasible with state-of-the art light sources (such as undulator beamlines and high resolution and high flux monochromators in the soft-x-ray regime at synchrotron radiation facilities) and high-resolution electron energy analyzers. First observation of Auger resonant Raman effect was by Brown et al.[19–21].

Energy considerations and Interference phenomena

The core excitation-deexcitation of a molecule or an atom is a coherent process and therefore various types of interference phenomena may be observed in the resonant Auger decay spectra. Two hole-one particle states and singly ionized states can be reached via interference between direct and resonant Auger photoionization. Energetically, the participator features resemble valence photoemission features. Energetically, the spectator Auger features resemble the satellite structures associated with valence photoemission (2h-1p). However, as the matrix elements are different for the core-hole mediated resonant Auger decay from the normal photoemission or normal Auger processes the relative intensities of the resonant decay features are consequently not similar to that of normal photoemission or normal Auger. Interference effects show

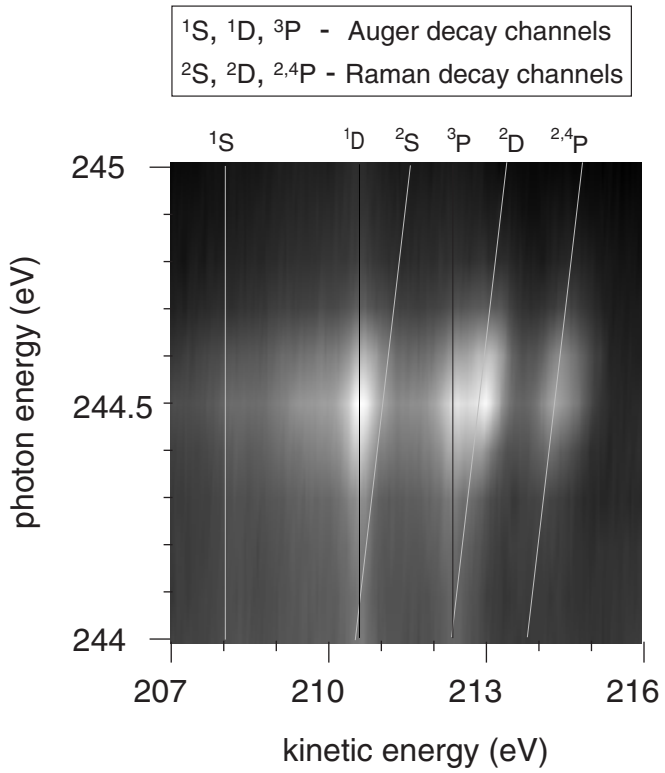

Figure 2.4: Photon energy dependence of CT Auger and Raman channels for the autoionization decay of $Ar2p_{3/2}^{-1}\ 4s^1$ in Ar/Cu(111).

Fano-type profile on detuning the exciting radiation. In addition for molecules also lifetime vibrational interference comes into play. The intensities of the decay spectra reveal the extent of overlap between the core-vacancy and the various valence orbitals.

Autoionization vs Auger

The distinction between Auger decay and autoionization decay is very important in Auger resonant Raman spectroscopy. The absorption of a x-ray photon in XAS or XPS leaves the system in an excited state. Subsequent decay of the excited state via non-radiative dominates for low atomic elements over radiative decay. Decay by electron emission is roughly divided into normal Auger decay and autoionization depending on the energy of the excitation with respect to the absorption maximum. If the excitation is done far above the absorption threshold, it is a very good approximation that the interaction between the outgoing photoelectron and the remaining system is negligible. The relaxation of the excited state in this regime is denoted as Auger decay. The Auger electron comes out with constant kinetic energy independent of the energy of the exciting radiation and the system is at 2 hole final state. As the excitation energy

approaches the core-level threshold from above, treatment of the excitation and decay as independent processes is not valid. Relaxation of the excited state in this regime is called autoionization. The excited photoelectron will interact significantly with the remaining electrons in the system and the kinetic energy of the Auger electron will depend on the exciting radiation. Autoionization branches into spectator (2h-1p) and participator (1h) type Auger decay depending on whether the initially excited electron participates in the decay or remains passively localized at the core-hole site during the decay.

Advantages of studying deexcitation spectrosocpy:

Spectator final states offer a unique way to study electron correlation since the spectator electron in the bound orbital, Rydberg orbital or higher above influence the rest of the electrons. Participator decay provides information on the localization of the electronic wavefunctions on the core-excited state. So dynamic charge rearrangements and core-hole screening processes by the valence electrons can be understood. The CT Auger decay intensity depends upon the hybridization width and the density of empty donor states.

2.2 Experimental set-up

Beamline

The experiments were performed at beamline UE56/1(SGM) of BESSY II in Germany (http://www.bessy.de/users_info/02.beamlines/linespdf/ID_11_3.pdf), BW2 of HASYLAB in Germany (http://www-hasylab.desy.de/facility/experimental_stations/BW2/BW2_new.html) and I311 of MAX-Lab (http://www.maxlab.lu.se/beamlines/bli311/) in Sweden. The third generation synchrotron radiation source provides with very high flux, of the order of $\sim 10^{13}$ photons/sec. The advantage is that the photon energy bandwidth can be made much narrower than the core-hole lifetime width while maintaining reasonably high photon flux. Thus the source fulfills the Auger Resonant Raman conditions (page 12) and is well suited for the core–hole–clock spectroscopic investigations.

For instance, the polarization characteristics of the outcoming radiation and the working energy range of Spherical Grating Monochromator (SGM) of Fig. 2.5 BESSY II UE56/1(SGM) beamline are considered below [1].

The photons coming out of the undulator are focussed both horizontally and vertically in a successive manner. The photon beam then passes through the entrance slit into the gratings assembly where it is energy analyzed. Required energy resolution of

[1] Private communication

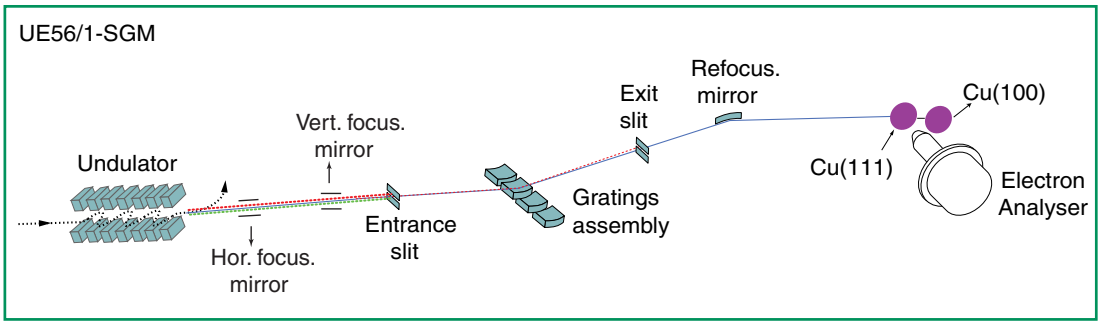

Figure 2.5: Layout of the UE56/1 (SGM) beamline

the incident radiation is achieved by proper choice of the grating. The monochromotized photon beam then passes through the exit slit, is refocussed again by the mirrors and finally enters the experimental chamber where it is directed on the sample, Fig. 2.5. The spot size of the incident beam is of the order of 100μm.

Gratings	lines/mm	working energy range (eV)
Grating 1	200	60-270 eV
Grating 2	350	100-480 eV
Grating 3	800	220-1080 eV
Grating 4	1200	325-1600 eV
Grating 5	1600	440-1600 eV

The electric polarization of the photon beam can be varied between linear/perpendicular to the plane of the ring or between left/right circular polarization by moving the undulator assembly, UE56.

End station

The experimental setup called HIXSS (Hamburg Inelastic X-ray Scattering Station), consists of a transportable UHV surface science spectroscopy system at a base pressure below 2×10^{-10} mbar with a preparation and an analysis chamber. Fig. 2.6 shows HIXSS and its components. The preparation chamber is equipped with standard surface science preparation tools, i.e. sputter gun, quadrupole mass spectrometer and Low Energy Electron Diffraction. The analysis chamber houses an electron analyser, a partial yield detector, a X-ray Emission Spectrometer (XES), a X-ray gun as well as an electron gun for use in the laboratory.

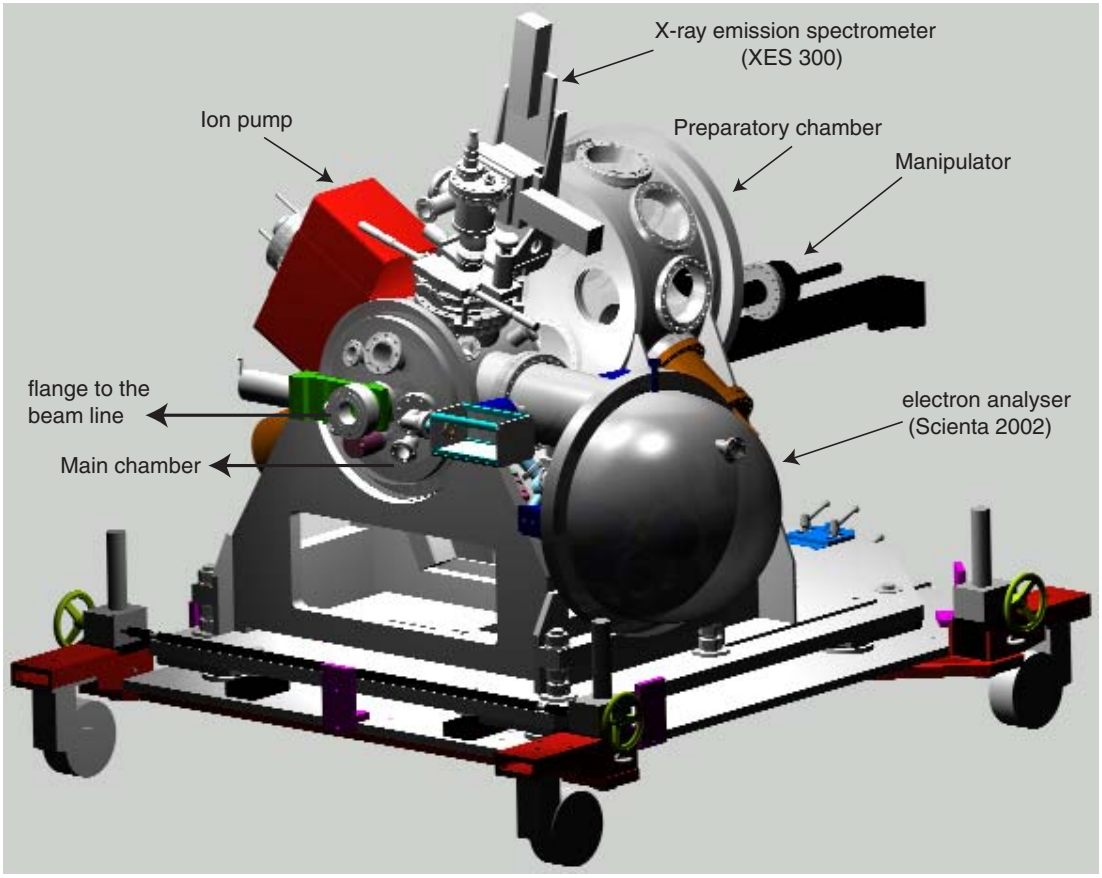

Figure 2.6: Layout of the endstation, HIXSS

Manipulator

The manipulator has got provisions for both cooling and heating the sample. The sample can be cooled down to 10K by means of a cryostat and the temperature can be controlled. The sample can also be heated by radiative means and electron bombardment with tungsten filaments. The chromel-Alumel thermocouples measure the sample temperature and are read out at the thermocouple heads on the outer side of the manipulator.

Sample holder

The sample holder shown in Fig. 2.7 is made of oxygen free copper. The single crystals Cu(100) and Cu(111) are mounted side by side separated by ∼0.5 cm and are attached to the holder by means of a thick Tantalum wire each fused at the bottom of the crystal. The Tantalum wire on the side of the Cu holder is held by Ta screws. Under each of the single crystal, roughly at a mm of distance close is a thin Tungsten (W) filament (0.1mm

Figure 2.7: Photography of the sample holder: Assembly of Cu(100) and Cu(111) single crystals.

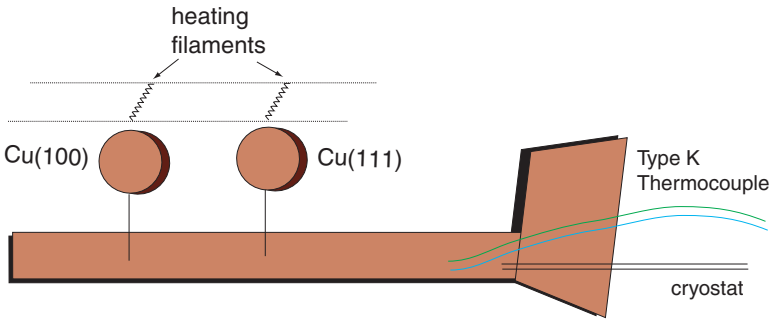

Figure 2.8: Schematic drawing of the assembly of Cu(100) and Cu(111) single crystals mounted on the sample holder.

diameter) that heats the crystal radiatively. Each crystal can be heated independently (one after the other or both at the same time). The sample holder is designed in a such a way that when it is mounted on the manipulator, the crystals receive the photon beam at an angle of 7° degree off the surface plane.

sample preparation

The Cu(100) and Cu(111) crystals were cleaned by sputtering with Ar^+ beam of 1.5KeV energy while the pure Ar gas was leaked at a pressure of $\sim 2 \times 10^{-6}$ mbar. Each crystal was sputtered for roughly 12 minutes. Then the crystals were annealed for 5 minutes and the surface was checked with XPS for impurities like carbon, oxygen. The sputter-anneal cycle was repeated until negligible amount of surface impurities were detected after which the crystals were briefly annealed for a minute to get smooth surfaces.

The adsorbate molecules were either in the gaseous or in the liquid form. The liquid sample was further purified by freeze-pump-thaw cycles and both the liquid and gaseous samples were ensured for purity with the Quadrupole Mass Spectrometer (QMS) prior

to dosing. The adsorbing gas and the liquid were leaked through fine leak valves to be adsorbed on the freshly prepared single crystals.

Measurement

Electron analyser

The end station HIXSS is equipped with a Scienta type hemispherical analyser which performs the actual energy dispersion of the electrons. The schematic drawing of the electron analyser is shown in Fig. 2.9. The main radius is 200mm. The two hemispheres are concentric and are 80mm apart. The electrons from the sample pass through the entrance slit before entering the hemisphere where their trajectories are bent in the radial electrostatic field between two hemispheres with a voltage difference. The bending radius will depend on the electron kinetic energies and an energy dispersion is achieved. The electrons are then detected by the detector system with their exact position in two dimensions. This makes it possible to determine their energy and one additional parameter, either the position or angular direction (in the dimension along the slit). The 180° hemisphere analyser has some advantages compared to other analyser types, the most prominent of which is the existence of an image plane unit with magnification perpendicular to the trajectories. The shape of the entrance slit can be adjusted between straight and curved and its width is variable as well. Due to the imaging properties of the analyser a narrow (straight) line of monochromatic electrons will be imaged as a narrow (slightly bent) line at the detector. The energy dispersion is determined by the pass energy and the analyser radius, and the resolution is then given by the ratio of the imaged line width to the dispersion. The spheres, like all other surfaces seen by the electrons are graphite coated to provide surfaces with a very even potential distribution.

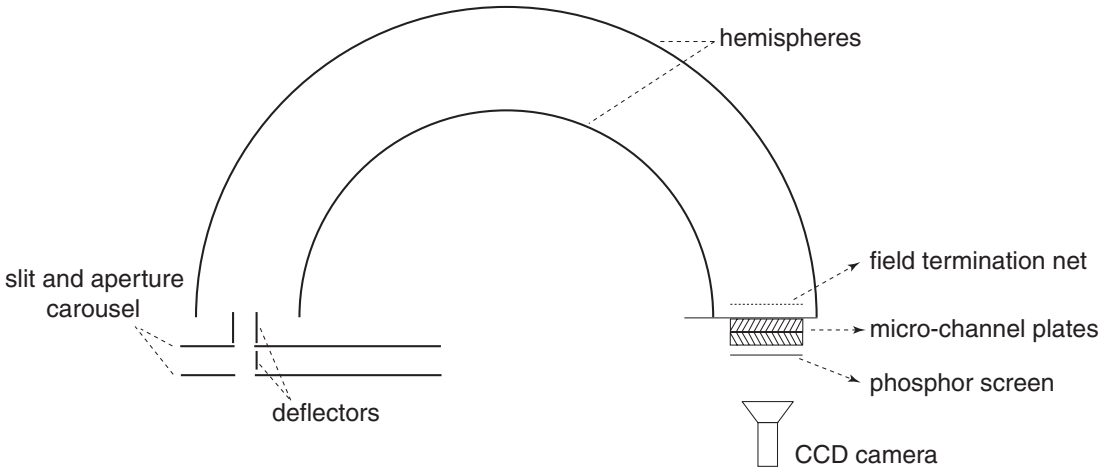

Figure 2.9: Schematic diagram of a Scienta type hemispherical elecron analyser

The Scienta type analyser can measure electrons either in the constant pass energy mode or in the constant electron energy mode. The detector assembly consists of two Micro Channel Plates (MCP) and a phosphor screen. The MCP pair multiplies each incoming electron $\sim 10^6$ times and this electron pulse is accelerated to the phosphor screen, where they produce a light flash. This is subsequently detected by the CCD camera. The position of the light flash corresponds to the position of the incoming electron. With the standard 40mm diameter detector, the energy range that can be simultaneously recorded is about $E_p/10$, where E_p is the pass energy. Specification on the analyzer such as technical details and general information on the analyzer can be found from the manuals supplied with the instrument from the supplier, Gammadata.

Partial yield detector

The NEXAFS spectrum of adsorbates and/or substrates can be recorded in different modes; namely, by monitoring total electron yield (TEY), partial electron yield (PEY), Auger electron yield (AEY) or fluorescence yield (FY) whereas each mode has its own advantage. In the Auger electron yield mode Auger peak from the atom of interest is monitored as a function of the excitation energy while the fluorescence peak is monitored for the fluorescence yield (FY). Since the fluorescence cross section for the light elements is very much lower than the Auger cross section, NEXAFS spectra for the light/heavy atoms are preferred in the AEY/FY mode respectively. However, high photon flux is necessary for both Auger and fluorescence yield detection. In the partial yield mode inelastic Auger electrons along with main Auger peak are detected so as to give higher signal to noise ratio. PEY detection is best carried out in the retarding grid detector, also called a Partial yield detector, where a negative grid potential -E_p is used to prevent electrons with kinetic energy less than E_p from entering the detector. Finally, the TEY measurement consists of collecting electrons of all the energies from the sample and is the simplest of all the modes. The detailed discussion on the components and functioning of the partial yield detector along with various electron yield detection techniques can be found in [22].

Core–hole–clock spectroscopy on atomic adsorbates

Chapter 3

Verification of the core–hole–clock method

In core–hole–clock spectroscopy of non-radiative decay, the relationship between the charge transfer time and core-hole lifetime is derived by considering the removal of the excited electron as a tunnelling process with exponential probability as a function of time and the core-hole decay rate also as exponential. Implicit in the description of the two processes as exponential decay is the assumption that the two events are independent [18].

In general, the exponential decay law says that the decay rate is proportional to the number of identical systems available in the initial, unstable state, i.e., the decay rate dN/dt is given by

$$\frac{dN(t)}{dt} = -\frac{\Gamma}{\hbar}N(t) \tag{3.1}$$

$\frac{\hbar}{\Gamma} = \tau$ is the characteristic time for the decay.

The quantity Γ in Eq. 3.1 is generally given the interpretation of the imaginary part of a complex energy often denoted the self-energy. It is apparent that Γ itself is proportional to the decay rate. For a particular core-excited state this quantity is also proportional to the total intensity in the measured spectrum. A solution of Eq. 3.1 is given by

$$N(t) = N_0 \times \exp^{-\frac{t}{\tau}} = N_0 \exp^{-\frac{\Gamma}{\hbar}\times t} \tag{3.2}$$

Where N_0 is the number of systems prepared in the decaying state at some (arbitrarily) chosen time zero and N(t) is the number of systems left in the excited state at time t. We can use Eq. 3.1 to derive time-dependent probabilities by dividing by N_0 and integrating to some time T to determine the likelihood of no decay event for times smaller than or equal to that time. This yields,

$$P(T) = 1 - \int_0^T \frac{\Gamma}{\hbar} exp^{-\frac{\Gamma}{\hbar}t} dt \tag{3.3}$$

Where P(T) is the probability that no decay has taken place up to time T. By identifying $\frac{\hbar}{\Gamma}$ with the characteristic times for charge transfer ($\tau_{CT} \equiv \frac{\hbar}{\Gamma_{CT}}$) and core-hole lifetime ($\tau_C \equiv \frac{\hbar}{\Gamma_C}$) respectively, we may write the relations corresponding to Eq. 3.3 for the processes in which we are interested here. This is done below, where we derive a useful relationship between the characteristic times and the intensities found in the decay spectrum.

As stated above in connection to Eq. 3.3, we may write the probability for no charge-transfer event to occur before time T as

$$P_{No}CT = 1 - \int_0^T \frac{\Gamma_C T}{\hbar} exp^{-\frac{\Gamma_{CT}}{\hbar}t} dt \tag{3.4}$$

The same form holds for the probability relation $P_C(T)$ that the excited state of an isolated small system has decayed before a given time T after excitation of the core electron,

$$P_C(T) = \int_0^T \frac{\Gamma_C}{\hbar} exp^{-\frac{\Gamma_C}{\hbar}t} dt \tag{3.5}$$

Note the difference in sign between Eqs. 3.4 and 3.5. Whereas we are considering the situation of "nothing happened" (no charge transfer) in Eq. 3.4 while we are considering the probability of "something happened" (core-hole decay) in this case, Eq. 3.5.

If we would like to consider both channels simultaneously, with independent rates, we have to consider the conditional probability for the combined events. The branching ratio of the events is indicated in Fig. 3.1. Let us first consider the sequence: A core-excited system decays before or at some time T, with no charge transfer during this time. This is given by,

$$P_C^{NoCT}(T) = \int_0^T \frac{\Gamma_C}{\hbar} exp^{-\frac{\Gamma_C}{\hbar}t_1} \times (1 - \int_0^{t_1} \frac{\Gamma_{CT}}{\hbar} exp^{-\frac{\Gamma_{CT}}{\hbar}t_2}) dt_2) dt_1 = \frac{\Gamma_C}{\Gamma_C + \Gamma_{CT}} (1 - e^{-\frac{\Gamma_C + \Gamma_{CT}}{\hbar}T}) \tag{3.6}$$

Measuring a spectrum corresponds to T$\rightarrow \infty$ in Eq. 3.6. When the excited systems have definitely decayed, and we obtain

$$P^{No}CT_C = \frac{\Gamma_C}{\Gamma_C + \Gamma_{CT}} \tag{3.7}$$

Equation 3.8 tells us that a fraction $\frac{\Gamma_C}{\Gamma_C + \Gamma_{CT}}$ of the spectral intensity stems from decays where no charge transfer has occurred before core-hole decay. The remaining fractional intensity in the spectrum is given analogously by

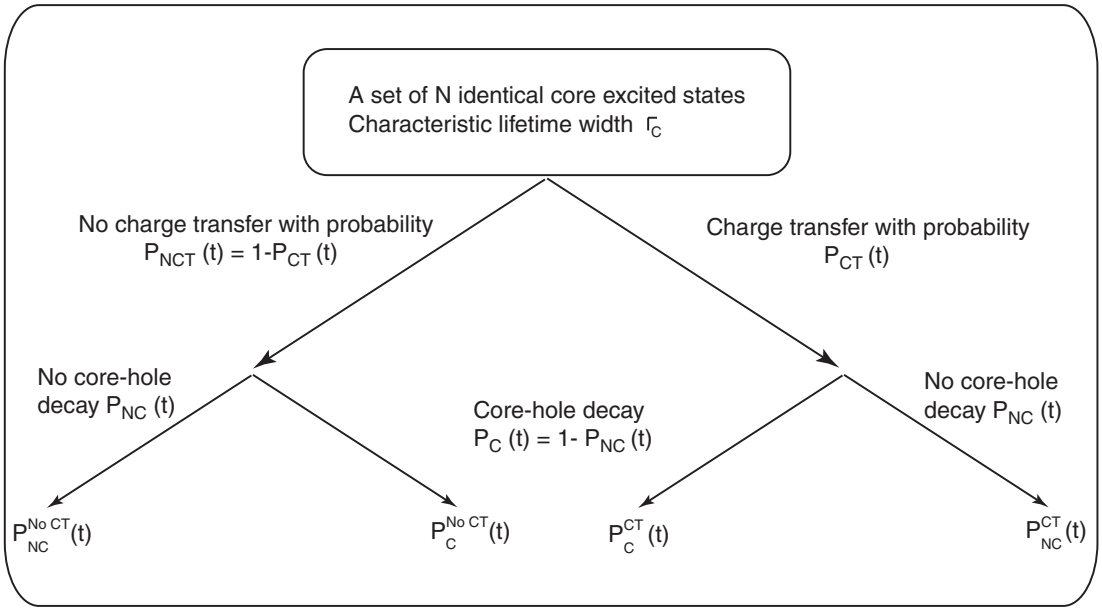

Figure 3.1: Illustration of the core-hole decay and charge transfer process as two independent mechanisms governed by exponential decay laws. Within the time interval [t,t+dt] the system may or may not undergo charge transfer. Both cases may or may not decay during this time interval.

$$P_C^{CT} = \frac{\Gamma_{CT}}{\Gamma_C + \Gamma_{CT}} \tag{3.8}$$

These equations show that, while Γ_C is proportional to the Auger transition rate which defines the absolute intensity of the entire spectrum (resonant and nonresonant) if this is available, its magnitude relative to Γ_{CT} emerges in the intensity ratios. This can also be confirmed by taking certain limits, such as $\Gamma_{CT} \to \infty$ and $\Gamma_{CT} \to 0$. Since we did not need to specify which core-excited state was originally produced, the expressions above apply, within the stated approximations, to all cases of dynamic charge transfer to be considered. These cases, and their spectral signatures, are given schematically in Fig. 3.1

We can now apply the relationships above to obtain expressions relating the measured spectral intensities I to the corresponding quantities Γ. For the case of resonant excitation in which the core-excited adsorbate transfers charge to the surrounding (adsorbate neighbors/substrate) system, the total intensity in the spectrum corresponds to the core lifetime broadening (transition rate) Γ_C, whereas the Auger fraction corresponds to the tunnelling bandwidth Γ_{CT}. Hence the relationship we seek is

$$\frac{\Gamma_{CT}}{\Gamma_C + \Gamma_{CT}} = \frac{I_{Aug}}{I_{res} + I_{Aug}} \tag{3.9}$$

For which I_{Aug} represents the intensity of the Auger component in the spectrum, and I_{res} that of the resonant Auger, or spectator component.

One may ask about the validity of the assumption made in the derivation of charge transfer times namely, the core-hole decay and charge transfer times as independent events. In the following article we would like to address this question. There we compared the charge transfer times from the adsorbate (atomic S) on to the Ru(0001) substrate with two independent core-hole clocks, ie., S(1s) and S(2s). The charge transfer time after excitation of the S(1s) electron to S(3p) level is independently monitored from that of the S(2s) electron to S(3p) level. Within the experimental uncertainty the charge transfer times obtained independently with the two core-hole clocks are similar. This is the experimental evidence for the validity of the assumption.

Whereas S(1s) hole decays by normal Auger process, S(2s) hole undergoes Coster-Kronig decay. Coster-Kronig decay is a special type of Auger process in which the final doubly charged ion has one hole in a shell of the same principal quantum number as that of the original ion. There is also super Coster-Kronig decay process in which the final doubly charged ion has both the holes in a shell of the same principal quantum number as that of the original ion. Both Coster-Kronig and super Coster-Kronig processes are extremely fast.

3.1 Verification of the core–hole–clock method using two different time references : Attosecond charge transfer in c(4x2)S/Ru(0001)

Abstract

Core–hole–clock spectroscopy is increasingly used to determine femtosecond and attosecond charge transfer processes initiated at an atomically defined starting point. We give proof that the time constant of a charge transfer process determined by the core–hole–clock method is probed, but not governed by the spectroscopic process. To this end, charge transfer in c(4x2)S/Ru(0001) has been probed by two investigations using core level resonances with identical symmetry but excitation photon energies one order of magnitude apart (S2s→ 3p at 227.5 eV, S1s → 3p at 2471.1±0.3 eV). Despite the large difference in excitation energy, the measured charge transfer times agree [1].

Introduction

Core–hole–clock spectroscopy has been used to study electron and nuclear dynamics with an atomically defined starting point on attosecond [24] and femtosecond [18, 25–36] timescales, tracking the dynamics of a core excited state through spectral signatures in autoionization or resonant inelastic X–ray scattering (see Reviews given in Refs. [18, 32, 37]). Implicit to the core–hole–clock method is the assumption that the temporal evolution of the excited wave packet is highly independent of the scattering process creating and probing it. This assumption has not been experimentally verified so far due to the difficulty of finding a suitable system, where core hole resonances of identical symmetry can be prepared at different resonance energies, which nevertheless have both core hole life times on a similar timescale than the dynamic process under investigation. With this work we have identified a suitable system and conducted this fundamental proof of the core–hole–clock method.

The atomic adsorbate of Sulphur on the Ru(0001) surface allows to create two different core hole resonances of identical symmetry and to monitor their non-radiative or autoionization decay. In particular, the Sulphur 3p electronic states can be populated by resonant X-ray absorption via the S1s → 3p (K-edge) and the S2s → 3p (L_1-edge) core hole resonances. With the electric field vector of the linearly polarized exciting radiation along the surface normal, selectively the $3p_z$ state polarized along the surface normal is populated. Both at the K-edge and the L_1-edge, these excited states have identical symmetry but the excitation energies differ by an order of magnitude (S2s →

[1] This section is intended for publication as Paper I : A. Föhlisch, S. Vijayalakshmi, F. Hennies, W. Wurth, V. R. R. Medicherla, W. Drube [23]

$3p_z$ at 227.5 eV, S1$s \rightarrow 3p_z$ at 2471.1±0.3 eV), where the Sulphur 2s core hole life time is τ_{2s}=0.5 fs [38] and the Sulphur 1s core hole life time we find at τ_{1s}=0.99 ± 0.07 fs.

In both experiments the survival probability of these atomically localized, core excited states and their relaxation into itinerant electronic states (delocalization) which can be seen as electron hopping or charge transfer (CT) have been investigated. Spectroscopically, the dynamic processes on the timescale of a transient core excited state in resonant inelastic X-ray scattering or autoionization can be separated through a branching into different inelastic scattering channels, which can be distinguished according to their energy and dispersion [39–41]. In a two step description of the inelastic scattering process, first, a previously unoccupied adsorbate state is populated by the promotion of a core–level electron by X–ray absorption. Then the core excited state can on the timescale set by the finite core hole life time τ either remain unchanged, i.e. survive as atomically localized, or relax (charge transfer), before core hole decay takes place. As charge transfer is equivalent with coupling to the quasi-continuum of the substrate, charge transfer spectral features are found in autoionization at the constant kinetic energy of normal Auger decay independent of the incident photon energy. Autoionization involving the atomically localized resonance exhibits Raman–like, linear dispersion with the photon energy, as the scattering process directly relates energy and momentum between incoming and outgoing particles. Thus, in a kinetic model of two independent exponential decays the timescales of charge transfer τ_{CT} and the natural core hole life time τ are directly related to the intensity ratio of the atomically localized Raman and the charge transfer (CT) spectral features of autoionization $\frac{I_{Raman}}{I_{CT}} = \frac{\tau_{CT}}{\tau}$ [18, 26, 27].

Experiment

Due to the very different photon energies required, the experiments at the Sulphur L_1-edge were performed at beamline I311 at Max-Lab in Lund, Sweden [24], whereas the experiments at the Sulphur K-edge took place at BW2 at HASYLAB/DESY in Hamburg, Germany. At 5×10^{-11} torr base pressure, a clean Ru(0001) surface was prepared by cycles of Ar^+-ion sputtering, oxygen-exposure and annealing. The c(4x2)S/Ru(0001) surface, with Sulphur atoms chemisorbed in hcp and fcc hollow sites [42, 43], was prepared by dissociative adsorption of 400 L H_2S at 550 K and annealing to 850 K. The surface quality was checked by core level photoelectron spectroscopy (XPS) and low energy electron diffraction (LEED). At less than 1° grazing incidence at BW2 and 7° at I311, the electric field vector of the incident radiation was near-normal to the surface, exciting preferentially into the S$3p_z$ orbital oriented normal to the surface. In both experimental stations, the electron spectrometer (Scienta SES 200) was mounted in the polarization plane at 45° to the incident radiation. At I311 the bandwidth of the incident radiation and the ΔE of the electron analyzer were set to 100 meV. At

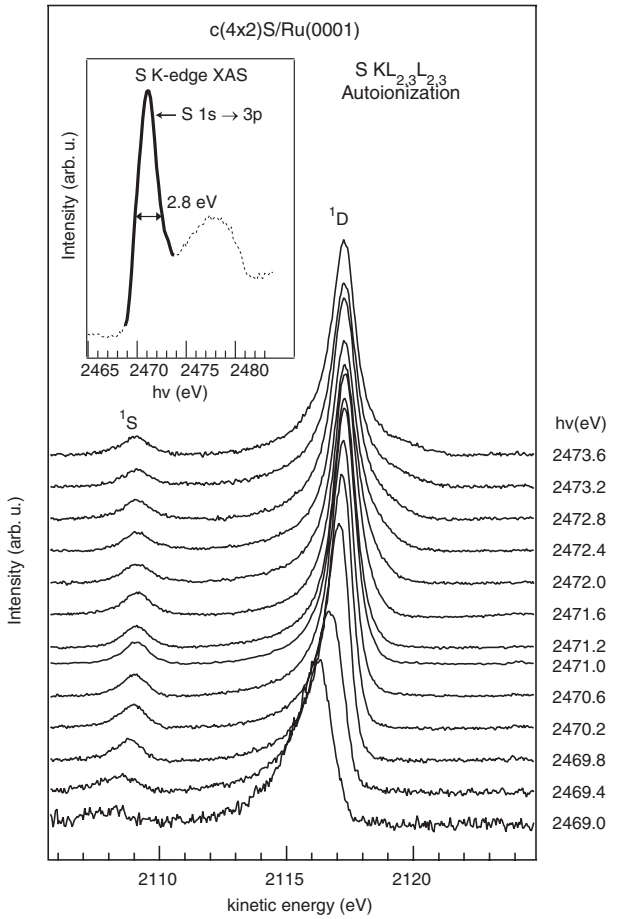

Figure 3.2: Sulphur $KL_{2,3}L_{2,3}$ autoionization spectra as a function of photon energy across the S $1s \rightarrow 3p$ core hole resonance. Inset: Sulphur K-edge X-ray absorption spectrum. The bold black part of the spectrum corresponds to the photon energy range used in autoionization. The autoionization spectra are normalized by the measured S K-edge X-ray absorption strength.

BW2, the experimental broadening was determined to be 0.43 eV with photoemission at 2820 eV using the Ru $3d_{5/2}$ line as a benchmark.

Results and discussion

In Fig. 3.2 the Sulphur $KL_{2,3}L_{2,3}$ autoionization spectra, normalized by the experimental X-ray absorption strength, are shown as a function of photon energy varied across the S1s $\rightarrow$ $3p_z$ X-ray absorption resonance maximum. The X-ray absorption spectrum is shown as an inset in Fig.3.2. Comparing the S1s $\rightarrow$ $3p_z$ X-ray absorption resonance maximum at 2471.1 ± 0.3 eV to the S1s binding energy at 2469.6 ± 0.1 eV, the S1s $\rightarrow$ $3p_z$ absorption resonance maximum lies 1.5 ± 0.4 eV above the Fermi level.

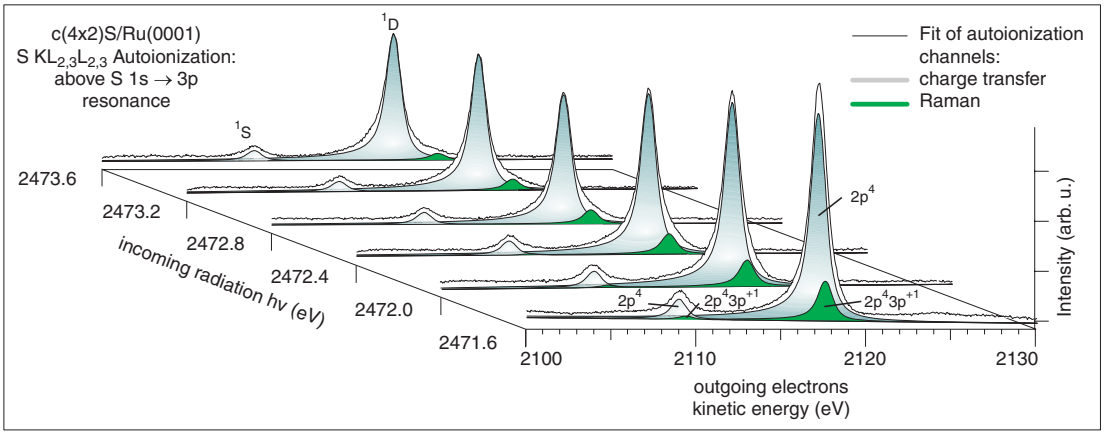

Figure 3.3: Decomposition of the Sulphur $KL_{2,3}L_{2,3}$ autoionization spectra into the atomically localized S $2p^4$ $3p^{+1}$ final state multiplets (linear dispersion with photon energy), and the charge transfer S $2p^4$ final states represented by the ^1S, ^1D normal Auger multiplets at constant kinetic energy.

For photon energies above the resonance maximum, the Sulphur $KL_{2,3}L_{2,3}$ normal Auger multiplet components of the S $2p^4$ final state at constant kinetic energy dominate the spectra at 2109 eV (^1S) and 2117.5 eV (^1D)[2]. These are the charge transfer spectral features. The corresponding localized Raman features (S $2p^4$ $3p^{+1}$) with linear dispersion are clearly visible below threshold, whereas they are just a shoulder to the CT spectral features above threshold.

To quantify these experimental findings we performed a curve fitting analysis as depicted in Fig. 3.3. Under the constraint of identical peak shapes of all four Raman and Auger features we obtained for the autoionization spectra above resonance an overall best fit for Doniach-Sunjic line-profiles [45] with Γ=0.7 eV Lorentzian FWHM (Full Width at Half Maximum), an asymmetry parameter of 0.074 and convolution with a Gaussian of 0.55 eV FWHM. With this parameterization the relative intensities of the Raman and the CT spectral features have been extracted. Taking also the Lorentzian life time broadening of the S1s photoemission line into account, which we determined to Γ=0.63 ± 0.01 eV FWHM, using the experimental Gaussian broadening of 0.43 eV, determined at the Ru $3d_{5/2}$ photoemission lines at 2820 eV, we find a S K-edge core hole life time of τ_{1s}=0.99 ± 0.07 fs. We can now directly translate the relative intensities of the Raman and the CT spectral features to the charge transfer time $\tau_{CT} = \frac{I_{Raman}}{I_{CT}} \cdot \tau$.

In Fig. 3.4 the measured charge transfer time in c(4x2)S/Ru(0001) for Sulphur core excitation via the S1s → $3p_z$ resonance (upper half) is compared to excitation via the S2s → $3p_z$ resonance (lower half) from our previous investigation Ref. [24]. Let us

[2]The $KL_{2,3}L_{2,3}$ normal Auger multiplet component ^3P is only faintly visible around 2124 eV as in other Sulphur containing systems [44].

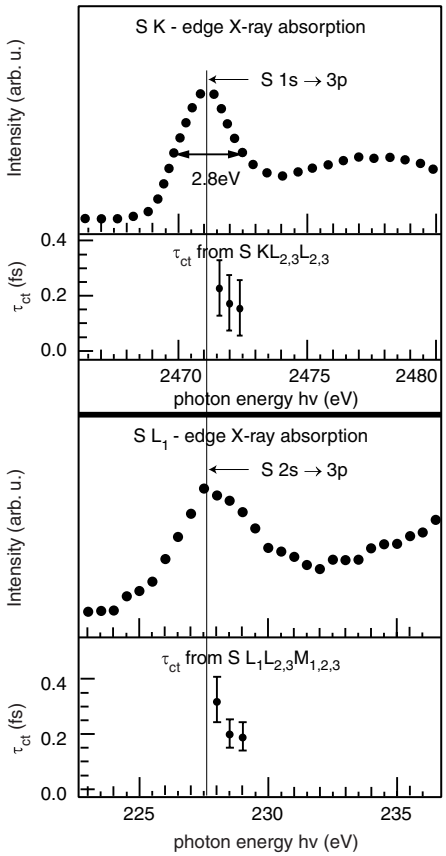

Figure 3.4: Comparison of the charge transfer times τ_{CT} extracted from independent core–hole–clock spectroscopic investigations using the Sulphur $KL_{2,3}L_{2,3}$ (upper panel) and $L_1L_{2,3}M_{1,2,3}$ (lower panel)[24] autoionization. The photon energy scales are aligned to the respective X-ray absorption resonance maxima into the Sulphur 3p state.

first discuss the result of core–hole–clock spectroscopy at the Sulphur K-edge in the upper half of Fig. 3.4. As seen in the X-ray absorption spectrum, photon energies between 2471.6 eV 2472.4 eV prepare core excited Sulphur species just above the S1s $\rightarrow$ $3p_z$ X-ray absorption resonance maximum at 2471.1 ± 0.3 eV, 1.5 ± 0.4 eV above the Fermi level. The corresponding charge transfer times, extracted from the autoionization spectra shown in Fig. 3.3 lie at 0.22 ± 0.1 fs (2471.6 eV), 0.16 ± 0.1 fs (2472.0 eV) and 0.14 ± 0.1 fs (2472.4 eV), respectively. The error bars are the result of the uncertainty of the spectral fit and the core hole life time τ_{1s}=0.99 $\pm$ 0.07 fs.

In the lower part of Fig. 3.4, the results from core–hole–clock spectroscopy using the Sulphur $L_1L_{2,3}M_{1,2,3}$ Coster Kronig decay of S2s $\rightarrow$ $3p_z$ core excited c(4x2)S/Ru(0001) are shown [24]. The photon energy scale is aligned relative to the respective S1s $\rightarrow$ $3p_z$ and S2s $\rightarrow$ $3p_z$ X-ray absorption resonance maxima. The S2s $\rightarrow$ $3p_z$ resonance maximum at 227.5 eV is found to lie 1.68 ± 0.1 eV above the Fermi level, as the S2s

binding energy is 225.82 eV. As seen in the lowest panel in Fig. 3.4, the charge transfer time obtained from core–hole–clock spectroscopy using the Sulphur $L_1L_{2,3}M_{1,2,3}$ Coster Kronig decay (Sulphur L_1 core hole life time τ_{2s}=0.5 fs [38]) lies between 0.32 ± 0.09 fs, 0.20 ± 0.06 fs and 0.19 ± 0.06 fs for the three photon energies just above the X-ray absorption resonance maximum. Thus, the charge transfer times extracted from the two independent investigations at the S1s $\rightarrow$ $3p_z$ and S2s $\rightarrow$ $3p_z$ resonances agree in magnitude and the relative change relative to the absorption resonance maximum within the experimental uncertainty (See Fig. 3.4). This is remarkable in the light that the energies of the two involved core-hole resonances differ by one order of magnitude (S2s $\rightarrow$ $3p_z$ at 227.5 eV, S1s $\rightarrow$ $3p_z$ at 2471.1 eV). Without going here into the nature of the charge transfer process in detail, we can interpret our finding as an experimental confirmation that core–hole–clock spectroscopy is indeed a measurement of electronic delocalization or charge transfer in a core excited atomic adsorbate. The choice of a given core hole resonance does select the time scale of reference through the core hole life time. However, the charge transfer time constant is found to be independent of the excited core level and its life time.

Summary

In summary, we have determined in c(4x2)S/Ru(0001) with two independent core–hole–clock spectroscopic investigations the charge transfer between the S1s $\rightarrow$ $3p_z$ and S2s $\rightarrow$ $3p_z$ core excited Sulphur and the substrate. Both core hole resonances have identical symmetry, but are in energy one order of magnitude apart. For both core hole resonances we extract charge transfer times. In spite of their large energetic difference, the measured attosecond charge transfer times extracted from the Sulphur $KL_{2,3}L_{2,3}$ and $L_1L_{2,3}M_{1,2,3}$ autoionization do not differ within experimental uncertainty. This agreement of the charge transfer times obtained with different internal clocks indicates that the charge transfer times derived from core–hole–clock spectroscopy are dominated by the physics of the charge transfer process in the core excited intermediate state and are probed, but not governed by the ultra fast core hole decay life time.

Acknowledgments

We gratefully acknowledge technical support by the staff of MAX-lab, Lund, Sweden, in particular J. N. Andersen and by the staff of HASYLAB/DESY, Hamburg, Germany. This work was supported by the Deutsche Forschungsgemeinschaft under Schwerpunktprogramm 1093 'Dynamik von Elektronentransferprozessen an Grenzflächen' and at MAX-lab by the EU Access to Research Infrastructure Program.

Chapter 4

Control of excited state lifetimes

Physisorbed atoms/molecules retain many of their properties in the gas phase. However, unique dynamic effects due to weak interactions in the physisorbed overlayers have been demonstrated recently [46]. The coupling of the adsorbate with the substrate band structure is reflected in the dynamics of charge transfer in the case of Ar adsorbed on graphite [46]. The coupling nature of the adsorbate due to differences in the surface electronic structure are delicate to be distinguished with the experimental techniques. Theoretical studies point out the role of surface electronic structure [47].

The above is true for chemisorbed systems. Time resolved two-photon photoemission technique can already reveal the differences in the case of adsorbed Cs on Cu(111) and Cu(100) [11, 48]. Both Cu(111) and Cu(100) exhibit a wide band gap in their projected band structure yet differ delicately in their electronic structure. The energetic position of adsorbed Cs on these two surfaces are different and hence the lifetime of excited Cs on the two surfaces also differ. On the other hand, lifetime of CO^- ($2\pi^*$) resonance on Cu(111) is not different from that on Cu(100) as the adsorbate resonance is quite broad [49]. The studies are relevant to surface chemical and surface photochemical reactions where the lifetime of reaction intermediates determine the reaction mechanism. In general, surface chemical reactions are sensitive to

- geometric surface structure
- electronic structure
- electronic relaxation times
- substrate-adsorbate electronic coupling
- adsorbate excited state lifetimes also
- phonon structure, relaxation times and its coupling to the substrate

Here we would like to check the sensitivity of the core–hole–clock spectroscopy to subtle differences in surface electronic structure. One can prepare a long-lived (10-100fs) intermediate state on a surface and study the influence of the substrate. As a model system we have chosen to study the lifetime of core-excited Ar adsorbate $Ar2p_{3/2}^{-1}\ 4s^1$ in a thick monolayer on (100) and (111) surfaces of Cu. First of all Ar couples weakly to the substrate. Secondly, the autoionization decay spectrum of Ar is less complex as it is an atomic system. Hence the system is well suited for core–hole– clock spectroscopy investigations.

The transfer of the excited electron from the core-excited $Ar^*(2p_{3/2}^{-1}\ 4s^1)$ atom to the Cu(111) and Cu(100) has also been studied theoretically by Wave Packet Propagation (WPP) approach.

Wave Packet Propagation (WPP) method:

The dynamics of the charge transfer between a core-excited $Ar^*(2p_{3/2}^{-1}\ 4s^1)$ atom and a metal surface is studied using a one-electron 3-D WPP method developed for surface problems by Emoshin and Kazansky [50]. It can be used in direct contexts.

(1) In the static situation i.e. at fixed projectile-surface distance one can obtain the atomic level characteristics such as energy and width of the projectile.

(2) One can also directly study the dynamics of the Resonant Charge Transfer (RCT) by following the wave-packet evolution during the projectile motion in front of the surface.

WPP approach provides the exact solution of the dynamical problem and it is free of approximations. In particular, it naturally includes the non-adiabatic effects.

The basis of the approach in core-excited Ar/Cu(111) and Ar/Cu(100) is to look at the time evolution of the wave function of the electron active in the resonant charge transfer process. It consists in studying the time evolution of the 4s outer electron in the $Ar^*(2p_{3/2}^{-1}\ 4s^1)$ state, the Ar^+ excited core being a spectator. In such an approach, the decay of the Ar^* state is entirely due to the atom-surface charge transfer and thus the level width yields the charge transfer rate.

The interaction of the outer electron in the $Ar^*(2p_{3/2}^{-1}\ 4s^1)$ state with the various parts of the system is described via the following Hamiltonian, H;

$$H = T + V_{e-surf} + V_{e-Ar^+core} + V_{e-Ar^+image} + V_{e-Arlayer} - iV_{ee} \tag{4.1}$$

Where T is the electron kinetic energy, V_{e-surf} is the interaction of the electron with the clean metal surface, V_{e-Ar^+core} is the interaction between the electron and the Ar^+ core, V_{e-Ar^+image} is the interaction of the electron with the image of the Ar^+ ion core, $V_{e-Arlayer}$ is the interaction between the electron and the adsorbed Ar layer and V_{ee} is an effective representation of the inelastic electron-electron interaction. For

the description of potentials we refer to the recent review [51]. Within the chosen model, the system is invariant by rotation around O_z the axis normal to the surface and going through the Ar^* center. WPP method has been utilized to investigate charge transfer dynamics in several adsorbate systems of core-excited neutral and negative ions in nature [47, 49, 52].

4.1 Surface projected electronic band structure and adsorbate charge transfer dynamics : Ar adsorbed on Cu(111) and Cu(100)

Abstract

The influence of the surface projected electronic structure on resonant charge transfer is investigated on the Cu(111) and Cu(100) surfaces using core–hole–clock spectroscopy and wave packet propagation computations. The charge transfer time of core-excited Ar ($2p^5_{3/2}4s^1$) adsorbed in a dense Ar monolayer is 5.6 ± 0.1 fs and 3.5 ± 0.1 fs for the Cu(111) and Cu(100) surfaces. A two times longer residence time on Cu(111) than on Cu(100) is also obtained from theory and is attributed to the differences in the projected electronic band structure of the two metal surfaces, especially to the different energies of the surface projected band gap [1].

Introduction

On a fundamental level, the lifetimes of excited states at surfaces have drawn considerable interest from experiment and theory [54] as they form the basis for the description and prediction of reaction mechanisms in surface chemistry, largely governed by the lifetimes of metastable reaction intermediates [55, 56]. Thus, particular attention was given to the observation that on certain metal surfaces very long-lived adsorbate-localized excited states have been found. Here, the charge transfer time is strongly influenced by the orbital overlap and the energetic position of the adsorbate resonance with respect to the surface electronic structure. For adsorbed Cs on the Cu(111) surface, lifetimes of the Cs 6s resonance in the range from 10 fs [11, 48] up to 50 fs [57, 58] have been observed in time resolved two photon photoemission (tr–2PPE), which has been attributed to the combined effect of the Cu L-band gap and the polarization of the Cs 6s electron due to its interaction with the surface [59, 60]. Theoretically, the main features of the alkali/Cu excited states on different surfaces have been quantitatively described [47, 59, 61].

Compared to tr–2PPE (limited by pulse length), core–hole–clock spectroscopy on surface systems gives an unprecedented accuracy in the range of few femtoseconds [18, 25, 29, 30, 33, 34, 46] [62–69] and attoseconds [24] as the charge transfer (CT) time is determined in comparison to the ultrashort natural core-hole lifetime. The electronic configuration of core-excited Ar ($2p^5_{3/2}$ $4s^1$) resembles the one of a K atom and the binding energy of the 4s electron is similar in both cases, though the total excitation

[1] This section has been published as Paper II : S. Vijayalakshmi, A. Föhlisch, F. Hennies, A. Pietzsch, M. Nagasono, W. Wurth, A. G. Borisov, J. P. Gauyacq [53] Chem. Phys. Lett. 427 (2006) 91.

energy is very different. Therefore, the dynamic behavior of the excited 4s electron for K and core-excited Ar is expected to be fundamentally similar. Theoretically, on a Cu(111) surface, the 4s electron residence time of core-excited Ar ($2p^5_{3/2}$ $4s^1$) was shown to be significantly larger than on a free–electron metal [51].

Besides the much faster charge transfer timescales accessible with core–hole–clock spectroscopy in comparison to tr–2PPE there is a qualitative difference in the excitation: in a tr–2PPE experiment the adsorbate 4s orbital is populated by a pump pulse transferring an electron from the substrate to the K adsorbate, whereas in core–hole–clock spectroscopy the 4s orbital is populated by an internal excitation on the adsorbed Ar atom via the absorption of a x-ray photon, without any associated charge transfer in the excitation process. The autoionization of this core-excited adsorbed Ar ($2p^5_{3/2}$ $4s^1$) branches into two channels: an atomically localized state (Raman-channel) or a delocalized state due to resonant transfer of the 4s electron into the substrate (CT-channel). Their branching ratio directly relates the Ar $2p_{3/2}$ core-hole lifetime τ=6 fs to the charge transfer time τ_{CT} [2].

In the present work, we investigate the stabilization of the 4s resonance state of adsorbed, core-excited Ar ($2p^5_{3/2}4s^1$) on the Cu(111) surface in comparison to the Cu(100) surface, which occurs on a fast femtosecond timescale with core–hole–clock spectroscopy and theoretical computations. The charge transfer takes two times longer on the Cu(111) than on the Cu(100) substrate. In both cases, the charge transfer is significantly slower than what is expected for a free-electron substrate. These results therefore extend our understanding of the decisive influence of the surface electronic structure to resonance stabilization and electron transfer to shorter timescales of only few femtoseconds, where crucial steps of transient formation of many surface reaction mechanisms take place.

Experiment

The experiments were performed at beamline UE56/1(SGM) at BESSY II in Berlin, Germany, with our transportable UHV surface science spectroscopy system at a base pressure below 2×10^{-10} mbar housing a Scienta 2002 hemispherical photoelectron analyzer and a partial electron yield detector. We have mounted two Cu(111) and Cu(100) single crystals (purity $\geq$ 99.9%), cleaned by Ar^+ sputter-anneal cycles (875 K) and checked by X-ray photoelectron spectroscopy. A dense Ar monolayer was prepared by multilayer desorption after dosing 2L of Ar at 25 K. In particular, the removal of the second layer Ar was monitored by photoemission as the Ar $2p_{3/2}$ binding energy shows a chemical shift between the first and second layer. The close packed Argon monolayer forms a hexagonal lattice [70, 71]. The bandwidth of the exciting synchrotron radiation

[2] $\frac{I_{Raman}}{I_{CT}} = \frac{\tau_{CT}}{\tau}$

was set to 42 meV. At 7° grazing incidence, the electric field vector $\overrightarrow{E}$ of the incident radiation was in the surface plane. The direction of photoelectron detection was in the plane normal to the incident photon beam at 45° with respect to the surface normal. The Scienta SES 2002 was operated at 50 eV pass energy at a bandwidth of 56 meV. The samples were scanned during measurement to minimize the radiation induced desorption.

Results and discussion

In Fig. 4.1, the autoionization spectra of adsorbed Ar on the (100) and (111) faces of Cu are shown for exciting photon energies across the Ar $2p^5_{3/2}4s^1$ resonances at 244.74 eV and 244.64 eV, respectively. Using the Ar $2p_{3/2}$ photoemission binding energies (Ar/Cu(100): E_B=242.44 eV and Ar/Cu(111): E_B=242.10 eV), the Ar $2p^5_{3/2}4s^1$ resonance lies on the Cu(100) and Cu(111) surfaces at 2.3 eV and 2.54 eV above the Fermi level, respectively. The autoionization spectra are characterized by the atomic multiplet structure of the final states. As indicated in the upper panels of Fig. 4.1, the prominent final states are the Ar $3p^4 4s^1$ (^{2,4}P, ^{2}D and ^{2}S) final states with the excited electron localized at the Ar atom and the Ar $3p^4$ (^{3}P, ^{1}D and ^{1}S) final states corresponding to charge transfer.

The variation of the excitation energy above and below the resonance (in steps of 0.1 eV) allows for direct distinction of the localized (Raman) vs. the charge transfer contributions: the latter occur at constant kinetic energy (^{1}S, ^{1}D, ^{3}P), whereas the former (^{2}S, ^{2}D, ^{2,4}P) show a linear dispersion with the excitation energy on both surfaces. However, the relative intensities of these channels are clearly different and the ^{2}S, ^{2}D, ^{2,4}P components of the atomically localized Ar $3p^4 4s^1$ final state have a significantly higher relative intensity on the Cu(111) surface than on the Cu(100) surface.

To quantify this observation, we have decomposed the autoionization spectra measured at the resonance maximum for Argon adsorbed on Cu(111) and Cu(100) into the Raman and CT contributions using least squares peak fitting. Each multiplet component is described by a Voigt line profile with a fixed Lorentzian linewidth of FWHM Γ=120 meV, representing the Ar $2p_{3/2}$ core-hole lifetime broadening, and a Gaussian broadening of 660 meV, which was obtained from the fit. The peak shape of the various components was kept constant for both surfaces. Likewise the energy separation between the multiplet components are the same on both surfaces. The resulting decomposition of the autoionization spectra is shown in the lower panels of Fig. 4.1. The tail of intensity between 204 eV and 210 eV, that is due to satellite features to the atomic multiplet components, is phenomenologically modelled by additional peaks. Using the relative intensities of the Raman and CT atomic multiplet components determined for the two surfaces, the charge transfer time constant τ_{CT} becomes accessible

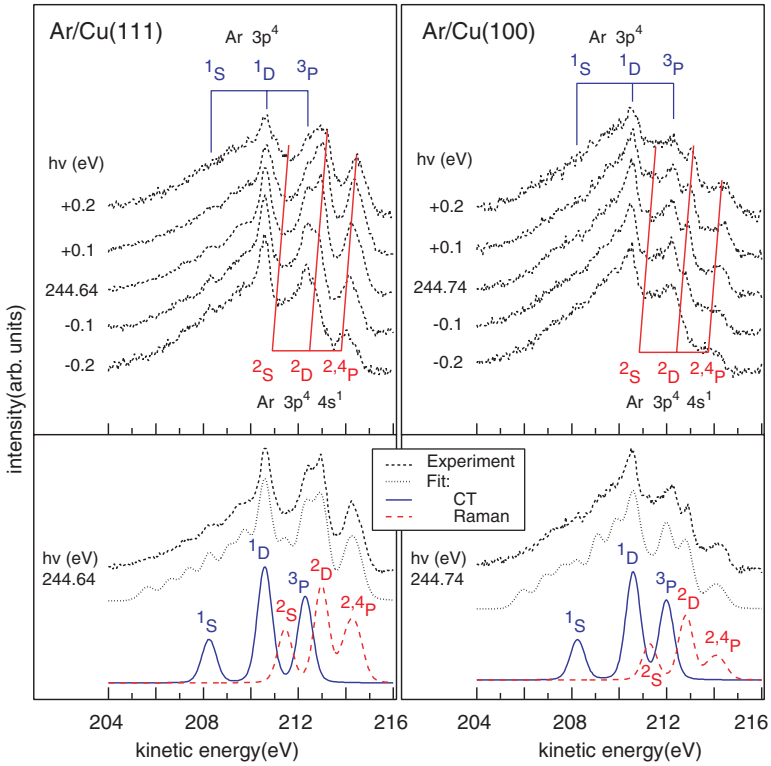

Figure 4.1: Autoionization spectra of $2p^5_{3/2}$ $4s^1$ core-excited Ar adsorbed on Cu(111) and Cu(100). Top panels: Excitation energy dependence around the respective Ar ($2p^5_{3/2}$ $4s^1$) X-ray absorption resonance. Bottom panels: Decomposition of the on-resonance excited autoionization spectra into the atomic localized (Raman) and the charge transfer (CT) contributions.

on the timescale of the Ar $2p_{3/2}$ lifetime of τ=6 fs. We obtain charge transfer times of 5.6 ± 0.1 fs and 3.5 ± 0.1 fs for the Cu(111) and Cu(100) surfaces, respectively.

Our theoretical approach extends our earlier study of the excited Ar($2p^5_{3/2}4s^1$)/ Cu(111) system [51] using a Wave Packet Propagation (WPP) approach. It consists in studying the time dependence of a 3–dimensional electronic wave packet representing the excited 4s electron. The electron evolves in a model potential built from the superposition of four parts: (i) a model potential for the electron–Cu surface interaction accounting for the specificity of the Cu(100) and (111) electronic structure and taken from [72], (ii) a pseudo–potential of Kleynman–Bylander form representing the interaction of the excited electron with the Ar^+ ($2p^5_{3/2}$) core, (iii) the interaction of the electron with the image of the Ar^+ ion core and (iv) a potential representing the interaction of the electron with the other Ar atoms in the adsorbate layer. The latter fully incorporates the mutual polarization of the various Ar atoms, accounting for the dielectric nature of the Ar layer[70]. The effect of inelastic interactions with substrate electrons is modelled by a local complex potential located inside the Cu metal (details

in [51]). The 3–dimensional electronic wave packet is expressed in cylindrical coordinates, (ρ,ϕ,z) with the z axis normal to the surface and going through the excited atom center. The time propagation of the wave packet is performed using the split operator approximation combined with finite differences and Cayley transform (ρ coordinate) and Fourier grid representation (ϕ and z coordinates) (details on propagation [59]). The initial wave packet is taken equal to the 4s orbital in the free atom and the analysis of the time dependence of the survival amplitude yields the characteristics of the excited states of the system (energy and charge transfer rate)[59].

Fig. 4.2 schematically represents the surface projected electronic structure of Cu(111) and Cu(100) modelled by the potentials from [72]. A projected band gap is present in both cases however at a different energy. The 4s resonance energy is represented by a horizontal line in both panels. Due to the projected band gap, the 4s resonant charge transfer (RCT) into the metal can only occur toward a bulk state (or toward the surface state in the Cu(111) case) with a large $k_{\|}$ momentum parallel to the surface. Since RCT corresponds to tunnelling of the electron through the barrier separating the adsorbate and the metal, it is favored along the surface normal and its efficiency rapidly decreases as the final electron momentum $k_{\|}$ increases. As a consequence, the RCT is drastically reduced on surfaces like Cu(111) or Cu(100), as compared to a free-electron metal surface. On Cu(111) and (100), the 4s RCT rate is equal to 48 meV and 89 meV, respectively, compared to 600 meV on a free-electron metal. One can notice that the RCT quasi-blocking by the projected band gap is weaker than found in the Cs/Cu(111) system; this is attributed to the larger adsorption distance of Ar (see discussions in [51, 60]). Being a one electron process, RCT is usually thought to be dominant. However, if RCT is much reduced, one should also consider the effect of inelastic interactions with the bulk electrons. In the present case, these only weakly contribute to the population decay rate (around 10% on both surfaces) and the 4s orbital population decay is thus dictated by RCT. In the $Ar(2p^5_{3/2}4s^1)$/Cu systems, the presence of Ar neighbors surrounding the excited $Ar(2p^5_{3/2}4s^1)$ also influences the dynamics of the charge transfer between atom and substrate. This effect has been discussed in Ref.[51] for Cu(111); although it does weaken the projected band gap stabilization effect, it is expected to play a similar role on both surfaces and not to influence the crystal face dependence.

The theoretical predictions for the total charge transfer time amount to 12 fs and 6.6 fs for the (111) and (100) surfaces, respectively. On a free-electron metal, it amounts to 1.1 fs. Thus, a comparable relative magnitude for the two surfaces as in the experimental data is retrieved, however with an overestimation of the CT time. The crystal face dependent charge transfer in the $Ar(2p^5_{3/2}4s^1)$/Cu system is driven by RCT: due to the different position of the 4s orbital in the surface projected band gap, RCT on Cu(100) can occur towards metal states with smaller $k_{\|}$ than on Cu(111), leading to a faster CT on Cu(100).

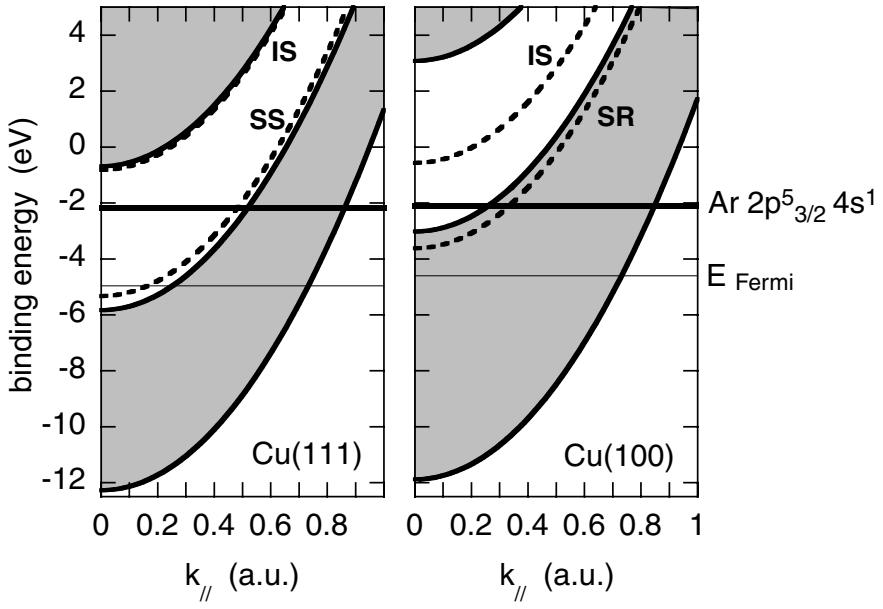

Figure 4.2: Schematic picture of the surface projected electronic structure in the $Ar(2p^5_{3/2}4s^1)$/Cu(111) and (100) systems as a function of $k_{\|}$, the electron momentum parallel to the surface. The energies are defined with respect to vacuum. The shaded area presents the 3D-propagation Cu states. The surface (SS) and image (IS) states and the surface resonance(SR) are shown as dashed lines. The thick full line gives the energy position of the 4s orbital and the thin full line that of Fermi energy.

This feature is further illustrated in Fig. 4.3 which presents a cut of the wave packet describing the resonant 4s orbital on the two Cu surfaces in a plane perpendicular to the surface and containing one of the nearest Ar neighbors. The 4s orbital is localized around the adsorbate center at the origin of coordinates. It is strongly polarized away from the surface. The structures appearing in the z=0 plane are due to the first two Ar neighbors in the adsorbate layer.

The wave packet oscillations inside the metal are associated with the periodicity of the Cu crystal along the surface normal. No electron transfer is seen to occur along the surface normal. Resonant electron transfer occurs beyond a finite angle from the surface normal for both surfaces. It appears as an electron flux propagating from the excited atom to the upper right corner of the figure in both cases. In addition, transfer to the surface state is observed in the (111) case as an electron flux propagating parallel to the surface and close to it. Consistently with the discussion of Fig.4.2, we note that RCT occurs closer to the surface normal for Cu(100), accounting for the faster RCT in this case. The difference in the RCT times also appears as a very different wave packet amplitude inside the metal, the flux being much larger in the (100) case.

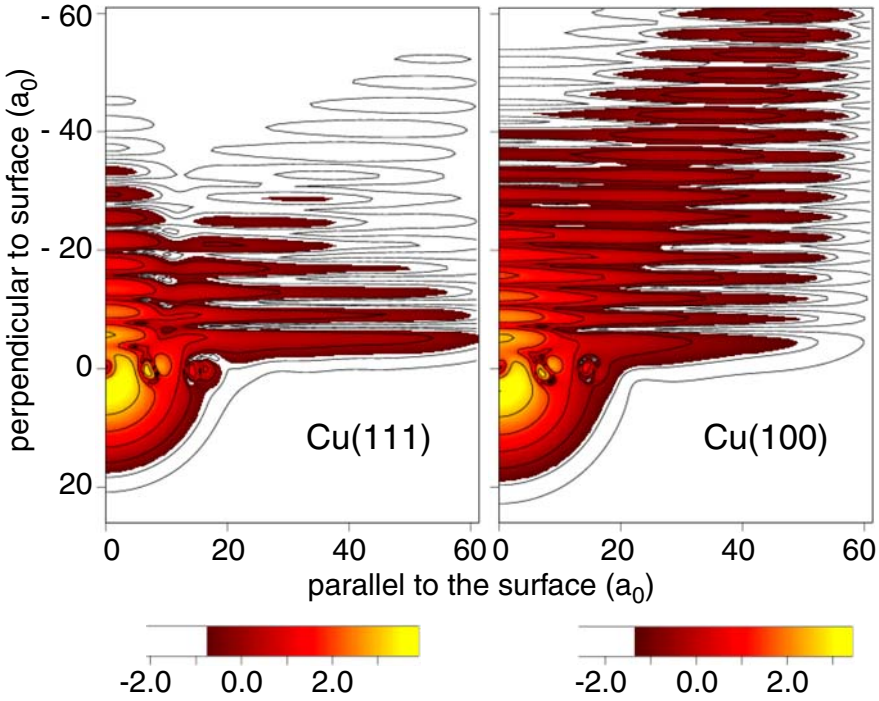

Figure 4.3: Contour plot of a cut of the resonant 4s wave packet in the $Ar(2p^5_{3/2}4s^1)$/ Cu systems. It presents the logarithm of the electron density in cylindrical coordinates parallel (ρ) and perpendicular (z) to the surface. The z-coordinate is positive in vacuum. The adsorbate is centered at the origin. The ρ-axis is in a plane that contains one of the nearest Ar neighbors. The coordinates are in atomic units $a_0 = 0.529$ Å. The electron density decreases when going from yellow to dark red. White corresponds to very small densities. The contour lines are separated by a factor e.

In contrast to the previously investigated resonance stabilization of the Cs 6s state on the Cu(111) surface [47, 48], the main difference between the Ar and Cs systems lies in the relative importance of the RCT and multi-electron charge transfer. Contrarily to the Cs/Cu(111) case, where multi-electron charge transfer is dominant, we find RCT to be dominant for Ar. This is a consequence of the larger adsorption distance for Ar and the presence of the Ar neighbours.

Although the present theoretical charge transfer times are longer than the experimental ones, the difference between the two surfaces is the same in experiment and theory. The remaining discrepancy could come from inaccuracies in the theoretical and/or experimental parts. Experimentally, some imperfections of the Cu(111) and Cu(100) surfaces could lead to a shortening of the experimentally determined charge transfer times. Theoretically, the relative importance of the RCT and multi-electron charge transfer and the adsorption distance could play a role, as well as to what detail the experimental signals are represented comparing experiment to theory [73].

Summary

In summary, we have determined with core–hole–clock spectroscopy and theoretical computations the charge transfer time between adsorbate and substrate of core-excited Ar ($2p^5_{3/2}$ $4s^1$) on the (111) and (100) faces of Cu. Due to the existence of a projected band gap in both cases, the charge transfer time of the Ar 4s electron ($2p^5_{3/2}4s^1$) to Cu is significantly longer than the one expected on a free–electron metal surface. In addition, the charge transfer time on the two surfaces is found to differ by a factor two, a direct consequence of their difference in electronic structure. The similarity of the excited electron in the Ar*/Cu and K/Cu systems leads to similar adsorbate/substrate charge transfer properties in the two systems, although the total excitation energy is very different. In particular, the decisive influence of the surface electronic structure on the charge transfer time on a timescale of only few femtoseconds is further revealed, as well as the stabilization effect of the surface projected band gap of the noble metal (100) and (111) surfaces. This is of fundamental importance for any reaction mechanism at surfaces involving the transient formation of an excited electronic state.

Acknowledgments

We are grateful to S. Cramm and the BESSY II staff. Financial support by the DFG under SPP 1093 and support to M. N. from MEXT Japan, Grant in aid for Young Scientists (B) 2003 is acknowledged.

Core–hole–clock spectroscopy to molecular adsorbates

Chapter 5

Near Edge X-ray Absorption Spectroscopy : Electronic structure of unoccupied states

Near Edge X-ray Absorption Fine Structure spectroscopy (NEXAFS) or X-ray Absorption Spectroscopy (XAS) is a tool for mapping out the unoccupied density of states. The probability of absorbing a photon is measured as a function of exciting photon energy by monitoring secondary processes as Auger and fluorescence. Here for all the measurements Auger electron yield was detected. Inner Shell Electron Energy Loss Spectroscopy (ISEELS), Inverse Photoemission (IPE) and two-photon photoemission (2PPE) also probe unoccupied density of states. However, the polarization dependence of NEXAFS makes it a special tool in spectroscopy to study the adsorption geometry of molecules on surfaces. Figure.5.1 shows the basic principle of XAS.

The sketch of NEXAFS spectrum of unoccupied resonances for an unsaturated molecule is shown in Figure below, Fig. 5.3.

When the electric field of the incident radiation is parallel to the symmetry axis of the unoccupied final state, then excitation into this orbital is dipole allowed. By using polarized radiation we can therefore use XAS as a structural tool to determine the orientation of, e.g., an adsorbate. Polarization dependency of NEXAFS is shown schematically in Fig. 5.3.

The orientation of adsorbed benzene on Cu(111) surface has been studied by NEXAFS spectroscopy for its orientation in the monolayer [74], bilayer [75] and multilayer [76] coverages. The adsorption geometry as found from polarization dependence of NEXAFS is shown in Fig. 5.4. The monolayer molecules adsorb with their aromatic ring parallel to the surface whereas the second layer molecules adsorb in perpendicular geometry to those in the monolayer. Evidently, the NEXAFS spectrum of monolayer coverage showed dominant $1\pi^*$ resonance when the $\overrightarrow{E}$ of the exciting radiation was

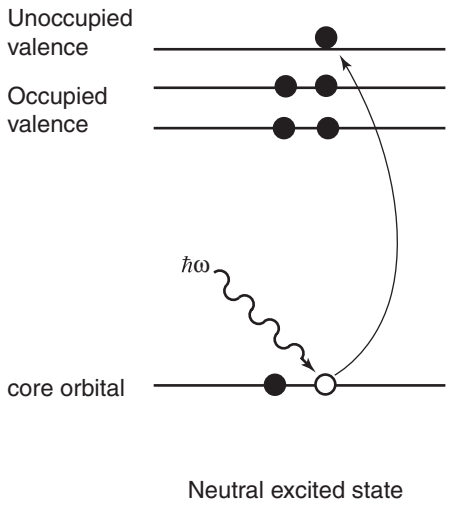

Figure 5.1: A simplistic outline of the principle of X-ray absorption

perpendicular to the surface and the $1\pi^*$ resonance got suppressed when the $\overrightarrow{E}$ of the exciting radiation was parallel to the surface accompanied by enhancement of σ type resonances. In contrast, on bilayer opposite effects were observed regarding the $1\pi^*$ resonance on varying the electrical polarization of the incident radiation between parallel/perpendicular. This indicates that the second layer molecules adsorb with perpendicular orientation to those in the first layer. Multilayer spectrum did not show considerable difference on switching the electrical polarization of the incident light between parallel/perpendicular. Therefore, it was concluded that the molecules are randomly oriented in multilayers.

Similarly, benzene adsorbs on Si(100) with a butterfly geometry with the C-C bond parallel to the Silicon dimer [77]. From polarization anisotropy for ethylene adsorbed on Si(100), on varying the electrical polarization of the incident radiation along x, parallel to the Si dimer axis, along y, perpendicular to the Si dimer axis and along z perpendicular to the Si(100) surface a full picture of the spatial orientation of unoccupied states has been derived [78]. NEXAFS investigations indicate that Ethylene molecules not only adsorb on top, along the dimer but also give direct evidence of a slight rotation of the C-C bond axis around the surface normal against the dimer axis. In cases of strong chemisorption, changes in the valence electronic structure of the adsorbate combined with the adsorption geometry provides useful information on chemical bonds. We use polarization dependent NEXAFS at the C K-edge to determine the adsorption geometry of the adsorbed C_6F_6 at various coverages ranging from submonolayer to multilayers. It is very essential to get complete spectrum of unoccupied density of states in order to specifically prepare a required core-excited state for resonant Auger decay spectroscopic studies.

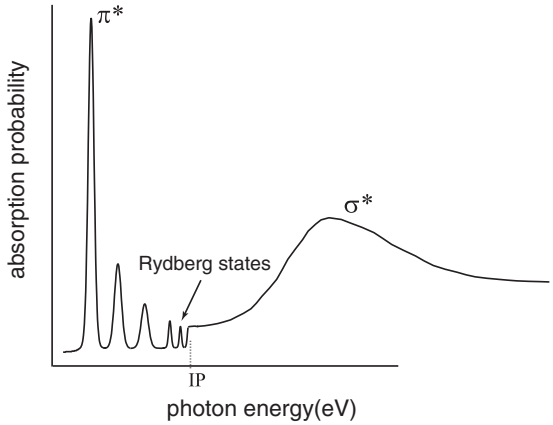

Figure 5.2: Schematic drawing of a typical NEXAFS spectrum for an unsaturated molecule

The adsorbate coverages were characterized by Temperature Programmed Thermal Desorption Spectroscopy (TP-TDS) and X-ray Photoelectron Spectroscopy (XPS).

Thermal Desorption Spectroscopy (TDS)

TDS was employed to measure the thickness of the C_6F_6 adsorbate layers. In general, the sample surface after dosing the adsorbate is heated slowly at constant rate and simultaneously the signal from the desorbing fragments is measured with Quadrupole Mass Spectrometer (QMS). The ionized fragments from the adsorbate which showed maximum intensity was used to record the TDS spectrum. Each of the sharp features in the spectrum correspond to a single phase. The saturation coverage is determined by increasing the dosage slowly from very low amount until a single feature in TDS is obtained.

X-ray Photoelectron Spectroscopy (XPS)

XPS is a method used for identification of elements under various chemical environments. In XPS of adsorbates, one of the core electron of the atom present in the adsorbate is ionized by absorption of an x-ray photon. The kinetic energy of the ionizing electron is then measured. The binding energy of the core electron is calculated from the relationship between the kinetic energy of the ionizing electron, incident photon energy, and the work function of the metal.

$$B.E(eV) = h\nu - K.E(eV) - \phi \tag{5.1}$$

The differentiation between elements and their different electronic structure is made by the chemical shift which is directly evident from the binding energy.

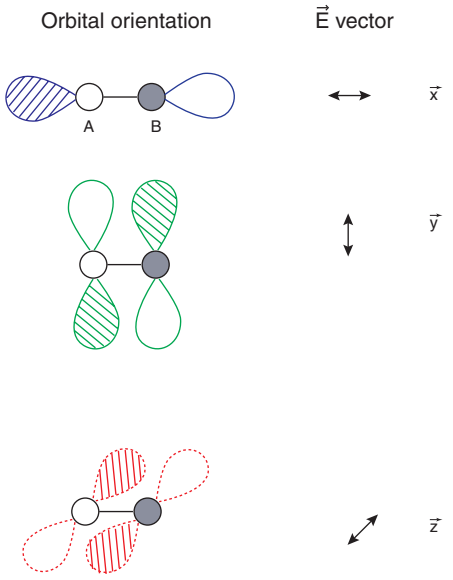

Figure 5.3: Polarization dependence of NEXAFS

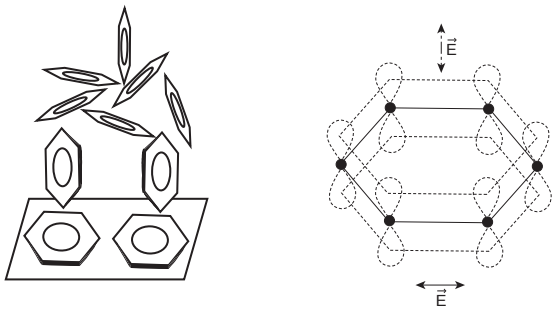

Figure 5.4: Adsorption geometry of benzene on Cu(111) for the coverages ranging from monolayer to multilayers.

The atoms/molecules in the first layer close to the metal substrate show lower binding energy than those at the higher coverages due to differential screening from the underlying substrate.

One may expect for C_6F_6 on Cu(111) similar adsorption characteristics as that of C_6H_6 for different coverages. However, the substitution of all the hydrogens by fluorine atoms in benzene probably changes the adsorption mode and bonding interaction with the substrate as fluorine has strong electron affinity. In the following chapter, the unoccupied states of adsorbed C_6F_6 on Cu(111) for coverages between half a monolayer to multilayers have been mapped out by NEXAFS spectroscopy. From the polarization anisotropy, orientation of this perfluorinated molecule has been determined at all the above mentioned coverages. Most importantly, effects of perfluorination reflected in

absorption resonances have been discussed with a model suggesting differences in the electronic structure among various adsorbate layers.

5.1 Bond polarization and image-potential screening in adsorbed C_6F_6 on Cu(111)

Abstract

The orientation of hexafluorobenzene (C_6F_6) on the Cu(111) surface has been determined for different coverages with the help of Near Edge X-ray Absorption Fine Structure (NEXAFS) Spectroscopy and X-ray Photoelectron Spectroscopy (XPS). The adsorption geometry and the bonding mode of C_6F_6 differ significantly in comparison to its hydrocarbon analog C_6H_6. C_6F_6 is found to adsorb on Cu(111) with the ring plane parallel to the surface for coverages below 10ML. Next to the distinct multilayer, bilayer and monolayer phases we also present evidence of sub-monolayer (i.e. 1/2 ML) coverage with different electronic structure. These findings are explained in a phenomenological model based on fluorine's property as a σ-acceptor and a π-donor and the resulting bond polarization within the molecule, which is stabilized by image-potential screening within the substrate [1].

Introduction

Organic thin films are receiving increased attention due to their importance in developing molecular electronics. As the electronic and optical properties of these films depend crucially on orientation and long range ordering of the organic molecule chosen, the adsorption behavior of organic molecules and their multilayer growth on single crystal surfaces are of relevance to the field. In particular, planar aromatic molecules are good candidates as they have a delocalized electronic structure and the film properties like the HOMO-LUMO band gap can easily be tuned by varying the ring substituent. From gas phase studies fluorination of hydrocarbon rings has been known to stabilize the molecular orbital levels [80]. Inverse photoemission studies [81] and photoabsorption and photodetachment investigations [82] report that perfluorination of benzene lowers the σ^* level even below the π^* orbital inverting their order. In particular, charge from the carbon backbone to the fluorine is donated in the σ system, accompanied by backdonation within the π system towards carbon[83]. Furthermore, protonation of the carbon ring increases the π donating ability of fluorine[83].

We chose to investigate the adsorption and multilayer growth mode of C_6F_6 molecules on Cu(111) as negative ion resonances of C_6F_6 are well known [82] and Cu(111) is one of the best characterized surfaces [84]. Moreover the unoccupied molecular resonance of C_6F_6 falls into the band gap of the Cu(111), making charge transfer dynamics

[1] This paper has been accepted for publication as Paper III : S. Vijayalakshmi, A. Föhlisch, P. S. Kirchmann, F. Hennies, A. Pietzsch, M. Nagasono, W. Wurth [79] Surf. Sci. (2006).

accessible by time resolved two photon photoemission (tr-2PPE) studies [85]. The orientation of the molecules depends on their interaction with the underlying substrate as well as between their neighbors. Adsorption characteristics of the nonfluorinated analog benzene, has been studied on a variety of substrates [77, 86–89]. On Cu(111), benzene adsorbs with its aromatic ring almost parallel to the surface [74] while in the second layer, the molecules are perpendicular to the underlayer [75] leading to a 'T' geometry. But at higher coverages, the molecules are oriented randomly [76] due to weak intermolecular (van der Waals type) interaction. For C_6F_6, high crystallinity in the solid has been reported [90]. The fluorine atom of one C_6F_6 molecule points to the center of the carbon backbone of the neighboring molecule in order to minimize the electrostatic repulsion between the molecules.

Near Edge X-ray Absorption Fine Structure Spectroscopy (NEXAFS) with its polarization dependence has proven to be a powerful tool to determine the electronic structure, molecular orientation and local bond length within molecular adsorbates [22]. In this work, we have determined using NEXAFS spectroscopy, the adsorption geometry of hexafluorobenzene on Cu(111) for the submonolayer, full monolayer, double layer and multilayer coverages which we compare to the adsorption mode of benzene on the Cu(111) surface.

Experiment

The experiments were performed at beam line UE56/1(SGM) at the synchrotron facility BESSY II in Berlin. Our experimental setup consists of a transportable UHV surface science spectroscopy system at a base pressure below 2×10^{-10}mbar with a preparation and an analysis chamber. The preparation chamber is equipped with standard surface science preparation tools, i.e. sputter gun, quadrupole mass spectrometer, Low Energy Electron Diffraction. The main chamber houses a Scienta 2002 hemispherical photoelectron analyzer and a partial electron yield detector. A commercially available Cu(111) single crystal (purity $\geq$ 99.9%) was cleaned several times by Ar^+ sputtering and annealing cycles (at 875K) until negligible amounts of contamination was found on the surface. The cleanliness of the crystal was checked by C1s, O1s and Cu valence XPS. Hexafluorobenzene obtained from Sigma-Aldrich (purity $\geq$ 99.5%) was further purified by freeze-pump-thaw cycles. The adsorption behavior of C_6F_6 on Cu(111) has been previously studied by Thermal Desorption Spectroscopy (TDS)[16, 17]. C_6F_6 was found to adsorb and desorb molecularly on the Cu(111) surface and formation of monolayer, bilayer and multilayer phases were identified. In this study, the TDS spectrum of C_6F_6/Cu(111) is reproduced (see footnote 1 for details) and the various layers have also been characterized by C1s XPS. C K-edge NEXAFS spectra were acquired for each of the distinct coverages observed, by monitoring the C-KLL Auger yield with the electron kinetic energy 242 eV $< E_K <$ 262eV. The correct preparation of the intended coverage

was ensured by recording C1s XPS each time, immediately after preparing a particular one, making use of the information about binding energy shift (between 0.5ML/1ML and 2ML/10ML) and peak intensity relationship (between 0.5ML and 1ML or 2ML and 10ML). The excitation bandwidth was set to ∼53meV. Using an variable polarization undulator, the polarization of the linearly polarized radiation can be switched by 90°. Thus the electric field vector could be aligned normal to the surface plane and within the surface plane. The degree of linear polarization was greater than 99%. The angle of incidence was 7°. The direction of photoelectron detection is in the plane normal to the incident photon beam at 45 ° with respect to the surface normal. The radiation damage of the adsorbate was minimized by scanning the sample during measurement.

Results and discussion

In Fig. 1 we show C1s photoelectron spectra of C_6F_6 layers at different coverages. Starting from a multilayer, prepared around 80K, the different known coverages of C_6F_6 on the Cu(111) surface were obtained by heating the sample at a rate of 1K/s according to thermal desorption spectroscopy data (TDS)[2] given in the right panel of Fig. 5.5 [16, 17].

We can directly distinguish the different layers of C_6F_6 obtained in TDS in their C1s photoelectron spectra. The bilayer is formed by heating to 158K with an C1s binding energy of E_{C1s}=288.16±0.1eV identical to the C1s binding energy of the multilayer. Heating to 165K yields a single peak shifted to lower binding energy of E_{C1s}=287.51±0.1eV which we interpret as the formation of a full monolayer. Further heating to 185K reduces the C1s signal by a factor of two without a change of the C1s binding energy. Thus, this high temperature coverage we assign as the formation of a half monolayer.

Based on this coverage assignment we turn to the polarization resolved C1s NEXAFS spectra depicted in Fig. 5.6, with the electric field vector $\vec{E}$ of the incident radiation parallel as well as perpendicular to the surface. The NEXAFS spectra were normalized to the photon flux and the spectrum of the clean Cu(111) substrate was subtracted. The orbital ordering for C_6F_6 molecule is
(core) $2a_{1g}$, $4e_{1u}$, $4e_{2g}$, $5a_{1g}$, $1b_{2u}$, $4b_{1u}$, $5e_{1u}$, $1a_{2u}$, $5e_{2g}$, $1e_{1g}$, $1b_{1g}$, $6e_{1u}$, $1a_{2g}$, $6e_{2g}$, $2b_{2u}$, $2a_{2u}$, $2e_{1g}$ (HOMO), $1\pi^*e_{2u}$(LUMO), σ^*b_{1u}, $2\pi^*b_{2g}$,σ^*e_{2g} and additional continuum resonances.

For all C_6F_6 coverages, we observe a strong NEXAFS polarization anisotropy, directly indicating orientational order within the adsorbate system. For all coverages,

[2]TDS spectrum in QMS mode was acquired in a different experimental set up and the Thermal Desorption spectrum in ion gauge pressure mode (measurement of pressure sensed by the ion gauge during the C_6F_6 desorption from the surface) was taken in the current experimental chamber in order to match the temperature scale in two modes

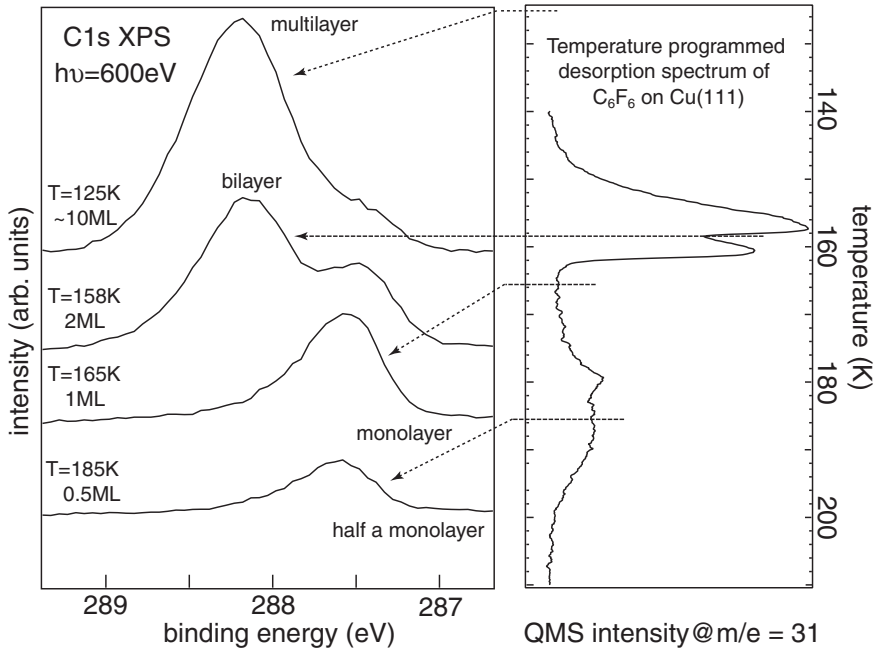

Figure 5.5: Carbon 1s photoelectron spectra of different C_6F_6 coverages on Cu(111) prepared by heating the multilayers to the temperatures indicated in the Thermal Desorption Spectrum (TDS) of C_6F_6 on Cu(111) at a rate of 1K/s. XPS spectra are shifted vertically (offset) for better clarity.

two distinct π^* resonances (for half a monolayer at 288.1eV and 292.2eV) are observed for $\overrightarrow{E}$ normal to the surface and were suppressed for in plane polarization. Analogous to the NEXAFS spectrum of monolayer benzene on Cu(111), these features can be assigned to the $1\pi^*$ and $2\pi^*$ resonances, respectively. This polarization dependence indicates for all investigated coverages in plane orientation of the C_6F_6 molecules. The small π^* intensity for the parallel polarized light may arise from a small molecular tilt and the fact that the sample is mounted at 7° grazing incidence.

This observation is supported by the polarization dependence of σ states, which are strong for in plane polarization and are suppressed for $\overrightarrow{E}$ normal to the surface. In particular, as seen in Fig.2b we assign the spectral feature around 289eV to the σ^*_{C-F} bond. Also the continuum or shape resonances (σ^*) at 296.2eV, 299.4eV and 305.2eV, indicate an in plane orientation of the C_6F_6. The features around 290.3-293eV could be due to Rydberg like transitions that broaden with increasing coverage. The observed states are in good agreement with those obtained from Inner Shell Electron Energy Loss Spectroscopy (ISEELS) measurements on gas phase C_6F_6 and the Rydberg states around 290.3-293eV were not reported [80]. As the coverage is increased from half a monolayer to ∼10ML, the shoulder on the lower binding energy side and higher binding energy side of the σ^*_{C-F} (around 289eV) and the states ∼ (291-292eV) respectively

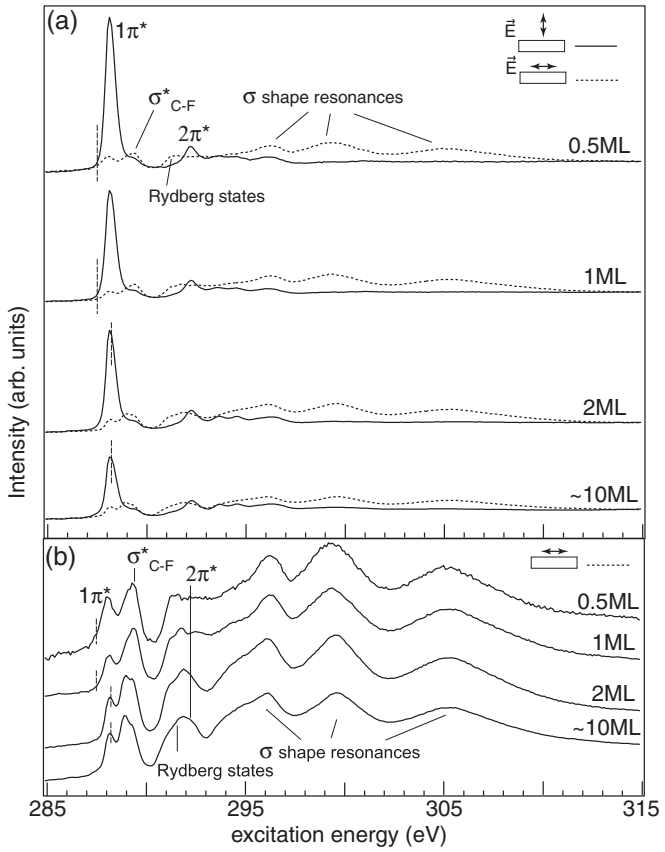

Figure 5.6: (a) Polarization dependent Carbon K-edge Near edge X-ray absorption spectra of C_6F_6 on Cu(111) at 0.5ML, 1ML, 2ML and multilayer (10ML) coverages. The Fermi level position is indicated by a vertical dashed line in each spectrum. (b) NEXAFS spectra for in plane polarization. All the spectra are shifted vertically (offset) for better clarity.

increase in intensity. Likewise the σ shape resonance around 296.2eV exhibits a shoulder at its lower energy side which then also shows increasing intensity with increasing coverage. As this resonance (at 296.2eV) is located above I_P, the shoulder development may be due to multielectron excitations. Although the other σ resonances do not exhibit any observable shift, the one around 299.4eV at half a monolayer moves to higher energy gradually with the increasing coverage and is found at 299.8eV for the thick multilayer.

Next to the polarization dependence, we observe a significant decrease of the $1\pi^*$ and $2\pi^*$ resonance intensities with increasing coverage for out of plane polarization. This decrease is strong in going from half a monolayer to full monolayer, weak from full monolayer to bilayer and from bilayer to 10ML coverage. A change of the molecular orientation at higher coverage can be ruled out, since no corresponding increase in π^* intensities is observed for in plane polarization. We have performed the experiments in such a way as to avoid saturation due to the high $1\pi^*$ cross section. In particular,

saturation can be disregarded as the variation in $1\pi^*$ intensity is accompanied by the analogous behavior of the weak $2\pi^*$ resonance.

In comparison to the adsorption geometry of benzene the one of C_6F_6 is significantly different. In particular, benzene in monolayer coverage adsorbs with almost flat configuration on the Cu(111) surface [74] and forms in the bilayer a 'T'-like configuration with the ring plane of the second layer perpendicular to the surface plane. Furthermore, multilayers of benzene are disordered. In contrast, C_6F_6 molecules are oriented in planar configuration in the range from submonolayer to multilayers.

In order to explain our observations we propose a phenomenological model based on the electron affinity of fluorine in combination with image-potential formation within the substrate. This is accompanied by the metallic dynamic screening of the core-excited final state of NEXAFS.

The large electron affinity of fluorine causes bond polarization within the C_6F_6 molecule. i.e., fluorine acts as a σ-acceptor and π-donor with respect to the carbon ring [83]. Furthermore, protonation of the carbon ring is known to increase the π donating ability of fluorine[83]. In total, partial negative charge accumulates on the fluorine atoms and partial positive charge on the carbon ring. On the metal surface, the π-backdonation from fluorine to the carbon ring is reduced upon adsorption, as the planar adsorption geometry leads to significant overlap of the π-states with substrate states. The result is the increase of unoccupied π-states at the carbon atoms, leading to the enhancement of the unoccupied carbon $1\pi^*$ and $2\pi^*$ x-ray absorption resonances for half a monolayer and the monolayer in comparison to the bilayer, multilayer and the gas phase.

Effectively, adsorption leads to an increase of the partial positive charge at the carbon ring and negative charges on the fluorine atoms in C_6F_6, which induce mirror charges of opposite sign in the metallic substrate. Thus, the bond polarization within the adsorbed C_6F_6 molecules is stabilized energetically (Fig. 5.7) similar to the formation of an ionic lattice of coadsorbed CO and K on Ni(100) [91]. We could also view this reduction of the fluorine π donating ability due to the influence of the substrate just as the opposite effect known from protonation of the carbon ring, which increases the π donating ability of fluorine[83].

Comparing 0.5ML and 1ML coverage, the smaller distance between the adsorbed molecules at 1ML partly counteracts the stabilizing effect of the substrate mirror charges, as the negative partial charges of the fluorine atoms between neighboring molecules repel each other. This causes in comparison to half monolayer coverage, the weaker π^* resonances for the full monolayer, arranging into the (3x3)C_6F_6/Cu(111) superstructure [13].

The second layer adsorbs on the charge pattern of the monolayer template, leading to preferential orientation while accommodating coulomb forces between the molecules. As a result, the bilayer and the multilayers inherit the orientation of the monolayer

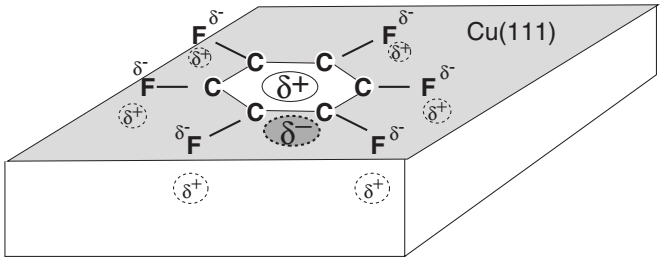

Figure 5.7: Schematic sketch of the interaction between adsorbed C_6F_6 and the Cu(111) substrate. Fluorine acts as a σ-acceptor and π-donor with respect to the carbon ring. On the metal surface, the π-back donation to the carbon is reduced, leading to bond polarization within the molecule, which is stabilized energetically through the image-potential formation within the substrate.

in contrast to the nonfluorinated C_6H_6 molecules that form disordered multilayers. Furthermore, π-backdonation from the fluorine towards the carbon ring is increasing towards higher coverage, seen in the decreasing unoccupied π-states at the carbon atoms. This leads with increasing coverage to the observed decrease of the NEXAFS C1s $1\pi^*$ and $2\pi^*$ resonance intensities.

We also observe that the $1\pi^*$ and $2\pi^*$ resonance position with respect to the Fermi level (given by the respective C1s binding energy, vertical dashed line in Fig. 5.6) lowers with increasing coverage. For 0.5ML and 1ML, the resonance position at 288.1eV is found 0.6eV above E_{Fermi}, whereas this absorption resonance position coincides with the Fermi level at 2ML and 10ML coverage. Stabilization of the π^* resonances with increasing thickness is in agreement with 2PPE experiments [85] where also a shift of the resonance position towards the Fermi level with increasing coverage has been observed. Due to the core- excited final state in NEXAFS, the $1\pi^*$ X-ray absorption resonance position is lowered towards the Fermi level, and especially for higher coverages even to a partial filling since the adsorbate resonance is pulled partly below the Fermi level. Whereas in 2PPE that involves no core-hole, the $1\pi^*$ orbital is lowered to a lesser extent and stays above the Fermi level.

Conclusions

C_6F_6 is found to adsorb on Cu(111) with the ring plane parallel to the surface for coverages below 10ML. From the combination of XPS and NEXAFS we can distinguish multilayer, bilayer and monolayer phases and observe additionally at sub-monolayer coverage (i.e. 1/2 ML) an adsorbate species with a different electronic structure in comparison to the full monolayer. In particular, the C_6F_6 $1\pi^*$ and $2\pi^*$ resonances exhibit in NEXAFS with increasing adsorbate coverage a decrease in intensity and a shift towards the Fermi level. This adsorption behavior of C_6F_6 is in sharp contrast to

the geometry of the non-fluorinated analog C_6H_6 where the molecules adsorb in a flat geometry for monolayer coverage and adopt a 'T'-like molecular arrangement in the bilayer and random orientation in the multilayer.

We explain our findings regarding the molecular orientation and the electronic structure of adsorbed C_6F_6 and the multilayer formation in a model of bond polarization within the molecule and image-potential screening in the substrate. In fluorinated hydrocarbons, fluorine acts as a σ-acceptor and a π-donor where the bond polarization within the molecule is driven by the high electron affinity of fluorine. Upon adsorption of C_6F_6 onto the Cu(111) surface, π-back donation from the fluorine to the carbon ring is reduced due to the interaction with the metal. Energetically, the increased charge separation within the molecular unit is stabilized by the response in the metallic substrate, where image-potential screening leads to the formation of mirror charges. Additionally, adsorbate-adsorbate interaction plays an important role going from sub-monolayer to full monolayer coverage. With reduced adsorbate-adsorbate distance the repulsive forces between the negative charges on the fluorine atoms increasingly counteract the effect of bond polarization within the adsorbed molecules. The charge pattern within the full monolayer then acts as a template for second layer growth and also molecules adsorbing subsequently inherit the in plane molecular orientation.

Acknowledgments

We are grateful for the support given by S. Cramm and the BESSY II crew. Financial support was given by the Deutsche Forschungsgemeinschaft under Schwerpunktprogramm 1093 "Dynamik von Elektronentransferprozessen an Grenzflächen".

Chapter 6

Auger resonant Raman spectroscopy for an aromatic molecule with equivalent atoms

Quantification of Raman channels and CT Auger channels is the primary requirement in determining the CT times in core-hole clock spectroscopy. The challenge in molecular systems coupled to a substrate is to identify and separate out different autoionization channels. Atomic autoionization decay spectrum is simple to analyze. On the other hand, in molecular systems the spectral features get more complex as the size of the molecule increases due to interference effects and due to an increasing number of channels. Hence separation and quantification of various channels also become more and more difficult and in some cases it is impossible to separate them. Alternative routes have been adapted in several cases. One such well-known example is the molecular C_{60} coupled to Au(110) substrate [18, 92]. Due to the mixing of different channels on adsorbing on a substrate, participant channels which are relatively easier to separate have been made use instead in order to determine CT times. Variation of their intensity served as a indirect measure of variation of CT times relative to the isolated molecule. The basic idea of the following paper is to review in several molecular systems the core–hole–clock spectroscopy investigations and to find a method to determine CT times from the core-excited C_6F_6/Cu(111) for various adsorbate coverages. Several different procedures have been tried out to ultimately determine the best method which suits this system particularly.

Fig. 6.1 shows various core-decay processes namely, participator Auger, spectator Auger and CT decay after resonant excitation by x-ray absorption to a discrete adsorbate resonance coupled to the substrate and the normal Auger decay process after excitation far above the absorption threshold. Valence photoemission similar to partici-

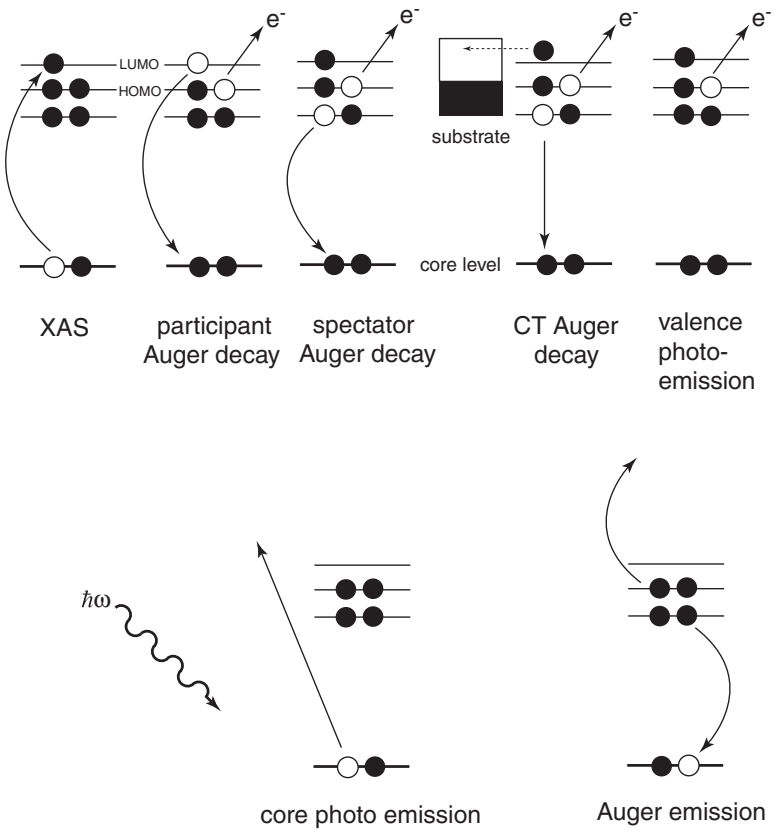

Figure 6.1: Core excitation-deexcitation scheme for an atom

pator decay is also shown. Schematic description of the spectral features corresponding to Fig. 6.1 is also depicted in Fig. 6.2.

Autoionization decay for larger molecular systems coupled to a substrate continuum consists of spectator, participator and CT Auger channels which mix-up giving complex spectral envelope, shown in Fig. 6.2.

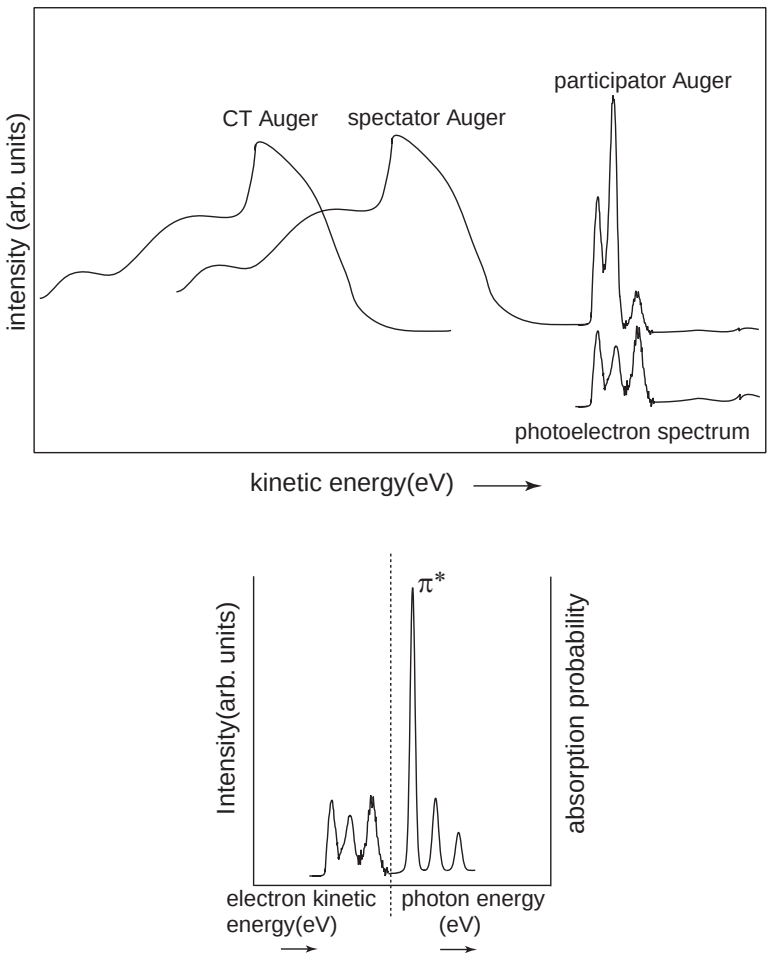

Figure 6.2: Spectral output for various core excitation-decay processes

6.1 Investigation of charge transfer dynamics in C_6F_6/Cu(111) with core–hole–clock spectroscopy

Abstract

We have calculated the charge transfer times from the core-excited adsorbate C_6F_6 on to the substrate with core–hole–clock spectroscopy for the adsorbate coverages of 1/2ML, 1ML, 2ML and 10ML. Adsorbed C_6F_6 presents several challenges in core–hole–clock spectroscopy investigations. As a polyatomic system, the C-KVV autoionization decay spectrum is complex due to vibronic coupling, mixing of various decay features due to charge transfer from the core-excited molecule to the neighboring molecules, charge transfer to the substrate and by polarization effects. Especially, the various autoionization channels like spectator, participator and charge transfer (CT) Auger are energetically too close for meaningful separation which is essential for CT times calculations. Therefore, we made use of the autoionization spectrum of isolated gas phase molecule which should contain only non-CT channels to extract the CT-Auger counterparts for the coupled systems. After trying out various other procedures with certain approximations we find this method giving access to absolute timescales and is best of all the others. All the methods show similar trend of charge transfer times for various adsorbate coverages and the absolute charge transfer times for the adsorbate coverages of 1/2ML, 1ML, 2ML and 10ML are found to be 3.5±0.2fs, 3.5±0.1fs, 6±0.3fs and 32±1fs respectively [1].

Introduction

The transfer of electrons across interfaces constitutes an elementary step in many technologically important applications like the electron injection and photovoltaic energy conversion in a Graetzel cell [2] but is also of general interest concerning the ultrafast relaxation of quasi-particle excitations. Ultrafast dynamics of core-excited states can be studied experimentally with the core–hole–clock method on the femtosecond [18, 25, 29, 30, 33, 34, 46, 62, 63, 65, 67–69] and attosecond timescale [24], which is at the limit of what is accessible with tr-2PPE due to the temporal length of the laser pulses. The basis to the core–hole–clock method is that in polyatomic systems on the timescale of the finite core-hole lifetime, different autoionization final states can be reached. Autoionization of a free atom will only have a single core-excited intermediate state. In contrast, in a polyatomic system the excited state created by X-ray absorption can lead due to electronic and/or vibrational coupling to relaxation in the core- excited state. Based on the branching ratio of the different autoionization final states due to

[1] This section is intended for publication as Paper IV : S. Vijayalakshmi, A. Föhlisch, F. Hennies, A. Pietzsch, M. Nagasono, W. Wurth [93].

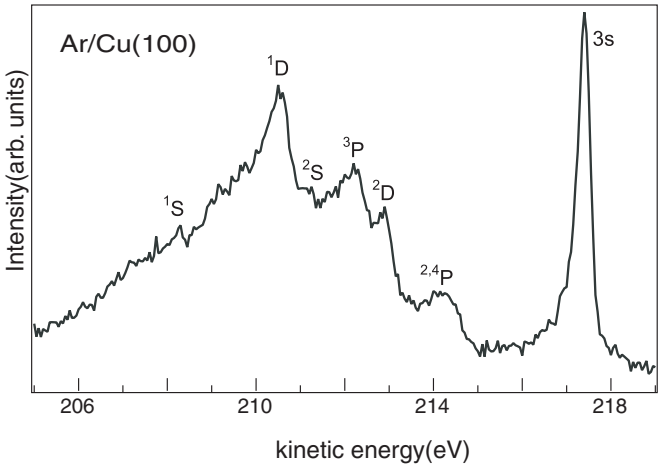

Figure 6.3: Autoionization spectrum of the $Ar2p_{3/2}^{-1} \rightarrow 4s^1$ on resonance for monolayer of physisorbed Ar/Cu(100)

the dynamic processes in the core-excited state, a survival probability of the initially excited state is given as a rate equation. Thus, for an atomic adsorbate with weak next neighbor interaction, two autoionization final states can be observed: a) The adsorbate core-excited state remains atomically localized. b) The adsorbate core-excited state couples via resonant charge transfer to delocalized (itinerant) substrate states, leading to a charge transfer final state. Hence, the branching ratio of these two autoionization channels (I_{loc}/I_{CT}) directly relates the core-hole lifetime τ to the survival probability of the atomically localized adsorbate core-excited state. The charge transfer time τ_{CT} obeys the relation:

$$\frac{I_{loc}}{I_{CT}} = \frac{\tau_{CT}}{\tau}.$$

Since Raman channels show linear dispersion with the exciting radiation and CT-Auger channels don't, as in Fig. 2.4, autoionization decay of a resonantly excited atom adsorbed on a metal is e.g. monolayer of Ar/Cu can be clearly separated into CT(normal Auger decay) and non-charge transfer components (Raman i.e spectator and participator) Fig. 6.3. In fact, there is no contribution of participator intensity to I_{Raman} for the atomic cases as it is restricted by dipole selection rules. As the spectator Auger (Raman) components are shifted from the CT Auger components by 2 eV, quantification of the two channels and extraction of charge transfer time from the above formula are trivial. Similar is the case of chemisorbed S/Ru [94].

To apply core–hole–clock spectroscopy to an molecular adsorbate, we need to consider two questions: a) What is the nature of the core-excited state, as the symmetry properties of the molecular unit allows molecularly delocalized symmetry adapted core-hole excited states, b) What are the possible electronic (CT) and the additional vibrational relaxation processes in the core- excited state.

In the present work, we investigate the dynamic timescales of the charge transfer from the molecular adsorbate C_6F_6 on to Cu(111) using core–hole–clock spectroscopy at the carbon atom. In our investigation we modify the molecular interaction by variation of the layer thickness between half a monolayer and multilayer coverages. As difficulties were encountered in obtaining charge transfer times for this symmetric molecular system alternative strategies with simple approximations were followed to extract the numbers. Autoionization decay of the isolated molecule in the gas phase provided extensive information on the nature of the system and served as reference in obtaining absolute time scales.

This paper is organized as follows.

1. We start by discussing the core–hole–clock spectroscopic measurements on the system including the gas phase.

2. Next, we assign the autoionization spectral features for the gas phase molecule. Here we discuss the so called spectator model in identifying the shape of the spectator Auger feature and examine the validity of the model for the C_6F_6 molecule by comparing for the other molecules in the literature.

3. Concerning the adsorbate system, overlapping of the CT Auger channel with that of resonant Auger is discussed starting from a simple diatomic molecule to a giant C_{60} and analytical difficulties encountered in separating various channels namely, CT,spectator and participator Auger.

4. Procedures followed to separate the charge transfer contributions from non-charge transfer channels in few other molecules are pointed out and the need to follow a different procedure for C_6F_6 is indicated.

5. Alternative methods are introduced which particularly suit the present system in extracting charge transfer times including the use of tr-2PPE measurement and eventually the charge transfer times obtained from various methods are compared to conclude on the best method that would suit our system.

In core–hole–clock spectroscopy, an carbon 1s electron of C_6F_6 molecule is resonantly excited to its nominally unoccupied $1\pi^*$ orbital and the autoionization decay of the excited state is monitored by measuring C-KVV Auger spectra. The de-excitation spectra are then quantitatively analyzed for contributions from charge-transfer and non-charge transfer channels so as to determine the charge transfer time or the survival probability of the initially excited state.

Experiment

The core–hole–clock experiments for the condensed/adsorbed molecule were performed at beamline UE56/1(SGM) at BESSY II, Berlin with our transportable UHV surface science spectroscopy system at a base pressure below 2×10^{-10} mbar housing a Scienta 2002 hemispherical photoelectron analyzer and a partial electron yield detector. The

Cu(111) single crystal (purity $\geq$ 99.9%) was cleaned by cycles of Ar^+ sputtering and annealing to 875K. Cleanliness was checked by X-ray photoelectron spectroscopy. The crystals were cooled to 100K and C_6F_6/Cu(111) multilayers were prepared. With thermal desorption spectroscopy the mono, bi and multilayer were prepared which can easily be distinguished by the chemical shift of their C1s core-level binding energies. The bandwidth of the exciting synchrotron radiation was set to $\sim$ 50meV. At 7° grazing incidence, the electric field vector $\overrightarrow{E}$ of the incident radiation was switched between perpendicular and parallel to the surface plane by moving the undulator. The direction of photoelectron detection was in the plane normal to the incident photon beam at 45 ° with respect to the surface normal. The Scienta SES 2002 was operated at $\sim$ 50eV pass energy at a bandwidth of $\sim$ 50meV. The samples were scanned during measurement to minimize the radiation induced dissociation of C_6F_6. Auger resonant Raman spectroscopy for the free gas molecule was performed in a different experimental set up at the beamline BL411 in Lund. The gas pressure was maintained at 3.5-7.5$\times 10^{-6}$ mbar during the measurement. Otherwise the similar settings were followed for data acquisition as that of the adsorbed molecular system.

Results

From the polarization dependent NEXAFS measurements, the C_6F_6 molecule has been found to lie on the Cu(111) surface with its aromatic ring parallel to the surface plane for the coverages of 0.5ML, 1ML, 2ML and for 10ML, Fig. 6.4. The $1\pi^*$ orbital, the lowest unoccupied resonance and $2\pi^*$ resonance positions are found to be at 288.1eV and 292.2eV for all the coverages. The $1\pi^*$ resonance of the gas phase C_6F_6 molecule was found to lie at 287.7eV (not shown in Figure). The unoccupied resonances are labelled as in Fig. 6.4 in comparison with gas phase ISEELS spectrum [80].

Having found the energy positions of unoccupied resonances, we set out to acquire the C-KLL autoionization decay of the C_6F_6 molecule from the resonantly excited C1s$\rightarrow 1\pi^*$ state. Since autoionization decay of an isolated gas molecule would contain only Raman channels (spectator and participator Auger), an attempt to separate the spectator Auger shape from that of the participator Auger is made for the isolated C_6F_6 gas molecule. As a first step in the on-resonance decay spectrum participator features which are similar to one-hole state photoemission features are assigned by comparing with the photoemission spectrum obtained 5.2eV below resonance, Fig. 6.5. The photoemission spectrum is in very good agreement with the previously reported gas phase valence spectrum obtained using He(II) source [95]. The assignments are made with the help of earlier studies [96].

All of the photoemission lines can satisfactorily be assigned. Different relative intensities of the participator channels in comparison to valence photoemission is due to the different matrix elements for the two processes. Participator intensities are

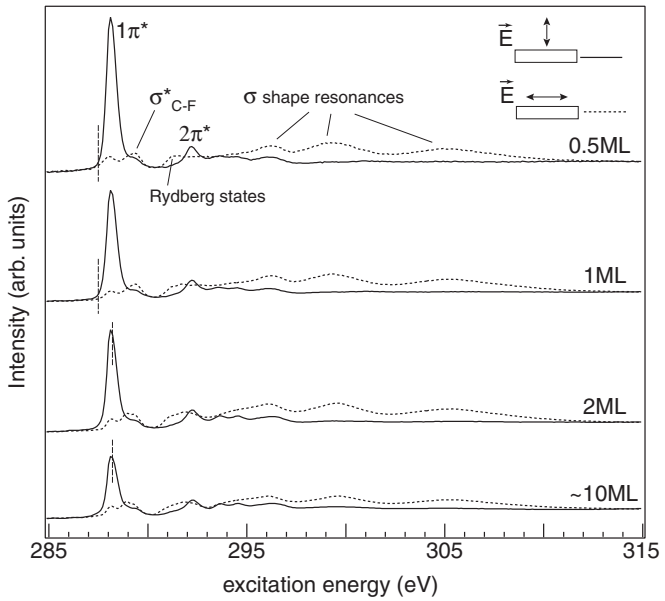

Figure 6.4: C K-NEXAFS spectrum of C_6F_6/Cu(111) for the adsorbate coverage from submonolayer to multilayer with the incident light parallel and perpendicular to the surface plane.

governed by coloumb matrix elements whereas the normal photoemission intensities are ruled by the dipole matrix elements. The participator lines with similar final state symmetry as the core-excited state show enhancement and while those with different final state symmetry than core-excited state are enhanced too little. After identifying participator lines we follow the so called spectator model to separate the spectator region from the participator features. The core ideas of this model are discussed below.

Spectator model:

In a simplistic approach, the autoionization decay spectrum of a isolated atomic or molecular species is broken into two individual components, namely, participator Auger and spectator Auger (due to localization of the excited electron). The participator component can be assigned by comparing it with the valence photoelectron spectrum whereas the spectator Auger can be considered as a off-resonant Auger component shifted due to couloumb interaction with the extra electron in the valence antibonding orbital. One can think of the spectator Auger as the satellites (2h-1e) to the photoemission too. However, the spectator channel intensities are governed by couloumb operators rather than dipole matrices and therefore it is more appropriate to consider them as off-resonance Auger counterpart. Thus the spectator component is considered similar to conventional Auger decay for well-screened states but with the core-excited electron watching the decay passively. But the kinetic energy of the spectator decay features

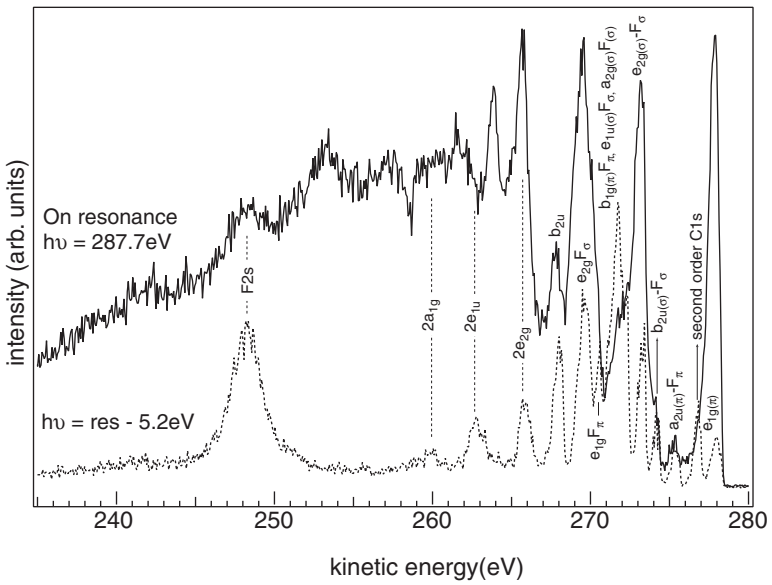

Figure 6.5: C-KLL autoionization spectrum of C1s$^{-1}1\pi^*$ state (excitation energy hν=287.7eV) and photoionization spectra at 5.2eV below resonance from gas phase C_6F_6.

should be shifted uniformly away from the conventional Auger decay features due to the couloumb interaction of the spectator electron. Such a model, called spectator model was presented by Moddeman et al. [97] to understand autoinization spectra of isolated species. Fig. 6.6 shows the spectator model schematically.

Moddeman et al. were able to give experimental proof of this hypothesis by studying several small molecules. The (e,2e) electron coincidence technique in autoionization decay of gaseous CO molecule after C1s-$2\pi^*$ excitation with electron beam revealed simultaneously the lineshapes of conventional Auger and spectator Auger [98, 99]. Analogously for the autoionization decay initiated by photon excitation spectator model can be discussed. Auger resonant Raman studies on gaseous CO are largely prevalent. In particular, the decay dynamics after C1s$\rightarrow 2\pi^*$ has been investigated in detail both experimentally and theoretically [99, 100]. The decay spectrum consisted of participator and spectator Auger components. Spectator model here was realized to account the features of the spectator decay features quite well.

Using the spectator model, spectator and participator components of the autoionization spectrum obtained for gaseous C_6F_6 for the excitation at $1\pi^*$ resonance were identified and separated. Assignment of the spectral features as spectator Auger and participator Auger are shown in Fig. 6.7.

The spectator shape so obtained for C_6F_6 is different than that of its standard Auger shape displayed in the upper panel. The sharp peak around 264.5eV in the resonant decay spectrum is absent in the standard Auger spectrum and there is no corresponding feature in the direct photoemission spectrum either. Thus we attribute

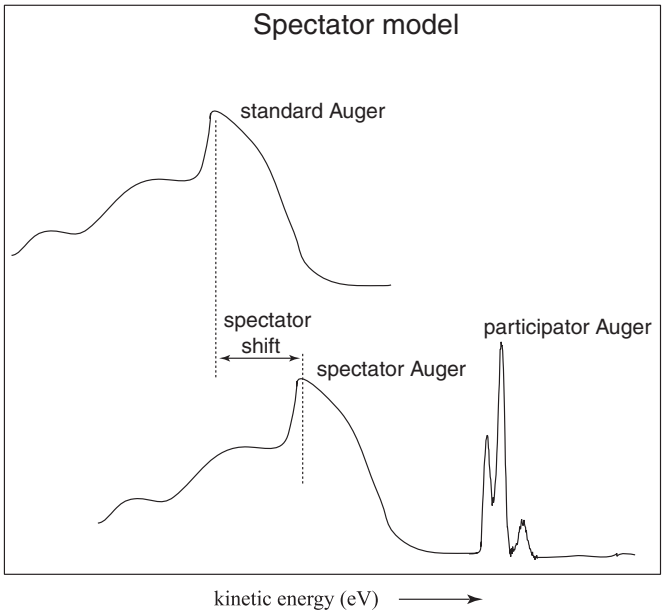

Figure 6.6: Schematic representation of the spectator model

this feature to be belonging to the spectator component may be arising due to strong resonant enhancement of low energy satellite to the photoemitted electron (K.E. around 263eV). We will below go through several other molecules for which similar aspects were studied.

The case of Nitrogen:

The spectator model was applied to the N_2 which is isoelectronic with CO. The deexcitation spectrum of gas phase N_2 resulting after N1s$\rightarrow 1\pi^*$ resonant excitation initiated by electron bombardment. The agreement in terms of intensities between the off-resonant Auger spectrum and the spectator spectrum is not very good. The spectator spectrum turned out to be less complicated than the off-resonant Auger spectrum albeit the other way is expected. So, the model is not satisfactory for the homonuclear diatomic molecule [98, 101]. The spectator electron is not only responsible for the shift of the spectator channel with respect to the off-resonance Auger spectrum, but also couples with the spin and angular momentum of the two final state holes and changes the overall spectator spectral shape [101].

Designation of participator lines with reference to photoionization spectrum also would work only upto certain extent since vibrational progressions due to coupling with electronic transitions may modify the spectral shape. In the high resolution Auger resonant Raman spectrum of gas phase CO [100], of adsorbed N_2 on a Xe spacer layer

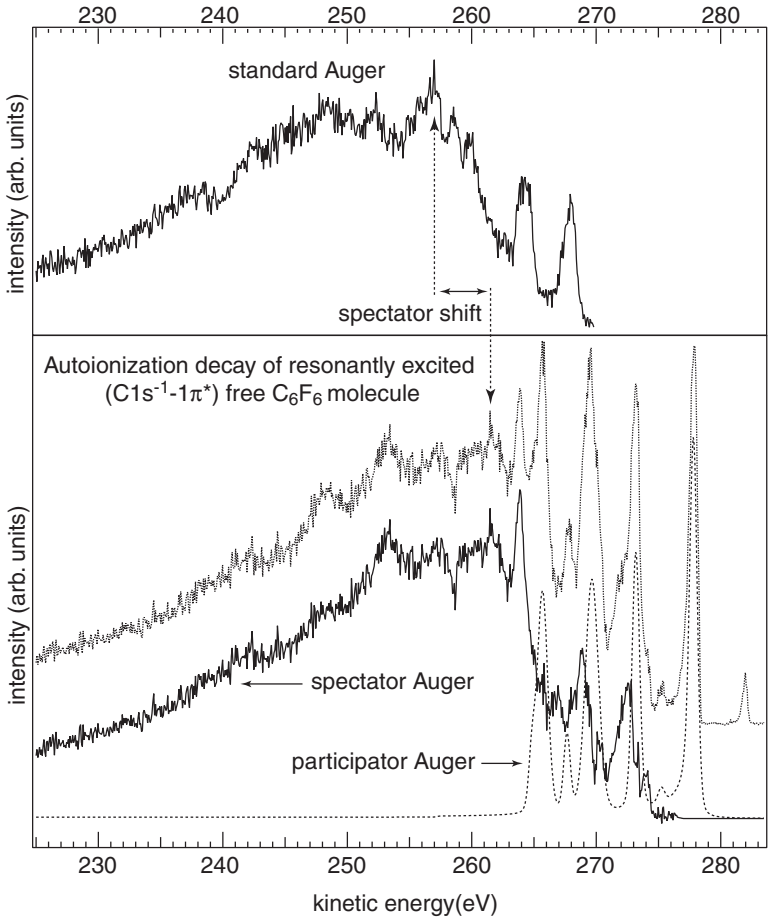

Figure 6.7: For free C_6F_6 molecule (a) Conventional C-KLL Auger spectrum after excitation into the continuum resonance (b) Decomposition of autoionization spectrum obtained after C1s→ $1\pi^*$ excitation into spectator and participator components. The spectator shift was found to be 4.5eV.

on Pt(111) [102] and of several other molecules, vibronic coupling effects accompanied by dramatic changes in the participator Auger spectrum were revealed [103–107].

Molecular O_2:

The resonant Auger decay of molecular Oxygen for the O1s→$1\pi^*$ excitation in the gas phase on the contrary to CO and N_2 is much more complex [108–110]. The identity of the spectator and participator channels are lost as the core-excited electron enters already half-filled $1\pi^*$ level and the electron becomes indistinguishable from the rest of the electrons in the $1\pi^*$. The strong correlation of resonantly excited electrons with its neighbors add further complications in the decay spectrum by introducing spin-split

effects. Thus, the simple correspondence between standard Auger spectrum and the spectator Auger spectrum again breaks down.

Disentanglement of various decay channels in adsorbates

To quantify the charge transfer times at different coverages, one would have to decompose the autoionization spectrum measured at resonance maximum into the spectator and the CT Auger contributions. We will go through the literature to learn how CT and non-CT channels are identified for simple systems as well as in complicated systems.

For isolated molecules dynamics of the core-excited state is governed by the lifetime of the core-hole and the nuclear motion in the excited state. If the energetic separation of the vibrational levels are comparable to the excited state lifetime width for instance in N_2, O_2, CO, etc. containing low-Z atomic elements, the vibrational motion may couple with the electronic decay (vibronic coupling). Diatomic molecules have only stretching vibrational freedom. On the other hand, polyatomic molecules if linear undergo bending or if planar distort towards pyramidal geometry when excited. As a result, decay of the core-hole leads to complicated spectrum.

With high resolution synchrotron sources vibronic coupling is revealed in the resonant Auger spectroscopy [111, 112] of isolated molecules and condensed molecules [113]. However, for adsorbed molecules, the vibrational levels are broadened due to coupling to the substrate. For the strongly coupled CO on Pt(111), the vibrational fine structure is not any more clearly visible even in the absorption spectrum [66]. Consequently, understanding of vibronic coupling effects in the decay spectra becomes extremely difficult. Further complications in the decay dynamics occur when the molecules are coupled to the substrate states due to extra molecular relaxation effects namely from a neighboring adsorbate or the underlying substrate.

For instance, on adsorption, the spectator and CT Auger channels can be concurrently seen as in the case of physisorbed N_2/Graphite[46]. The N1s$\rightarrow 1\pi^*$ excitation resonance lies below the Fermi level and as a consequence, the decay spectrum after resonant excitation consists only spectator and participator channels. For the excitation far-above resonance, in addition to the expected normal Auger channel, spectator and participator Auger features were also found due to charge transfer from the substrate to the adsorbate resonance. The normal Auger channel was identified by comparing with the standard Auger decay spectra when the adsorbate was decoupled from the substrate with Xe spacer layer. The spectator envelope definitely looks very different from the standard Auger shape again stressing the inadequacy of the spectator model. Similar observations were made for adsorbed N_2 on other substrates [66, 114].

Eventhough the interpretation of spectator lines as uniformly shifted off-resonant Auger spectrum is a crude approximation, extension of this model to larger adsorbed

molecules in multilayers was quite successful [81]. Indeed the model worked only for a few molecules.

Spectator model is inadequate for C_2H_4 in describing the spectator Auger channel obtained after C1s-b2g(π^*) excitation. Configuration interaction was known to play significant role in determining the line shape of the spectator decay [115]. The measurements though were made on multilayers formed on a metal substrate, there is no mention on possible mixing of CT Auger fraction (CT to the neighboring molecules) with the spectator part [116]. In case of benzene multilayers on Cu(111) the decay spectrum after C1s$\rightarrow 1\pi^*$ excitation was interpreted to consist only spectator and participator channels, a pure autoionization spectrum. Charge transfer to neighboring molecules was ruled out on the timescale of C1s core-hole [76].

In the case of condensed films of furan and pyrrole, spectator model was applied to understand electron correlation effects. For the autoionization decay after C1s$\rightarrow\pi^*$ excitation, the resulting participator peaks after subtracting the uniformly shifted far-off Auger spectrum could be explained with valence photoemission spectra only in the outer valence region. On the other hand, participator peaks in the inner valence region where the single-particle picture breaks down, could not be explained satisfactorily. Presence of unexplained sharp features in the spectator region was suspected due to configuration interactions in the final state. Alternatively, the explanation is that the spectator model could be invalid or change of spectator lineshape due to inhomogeneous charging.

Dissociative type:

This is an extreme case of vibronic coupling. The nuclear motion in the excited molecules may even result in dissociation of the core-excited state into fragments. Diatomic molecules (HF, HCl, HBr, HI, Br_2, Cl_2)[117–122], triatomics (H_2S O_3, H_2O) [123–125], polyatomics (CF_4)[126, 127] and hydrides (PH_3)[128] undergo ultrafast dissociation as a result of core-excitation into the highly antibonding σ^* unoccupied states. The electronic decay spectra have been studied and the rate of dissociation is comparable to the core-hole decay rate. As dynamic continuum of energies is available in the dissociating fragments, no linear dispersion of the kinetic energy of the emitted Auger electron with photon energy will be observable. Hence, CT Auger and spectator Auger in such cases would essentially mix and show similar behavior upon variation of excitation energy.

Autoionization spectral characteristics

The C-KVV autoionization decay spectrum resulting after excitation on $1\pi^*$ resonances are displayed in Fig. 6.8 along with the photoelectron spectrum obtained at far below resonance and the standard Auger spectrum obtained at far above resonance. All the

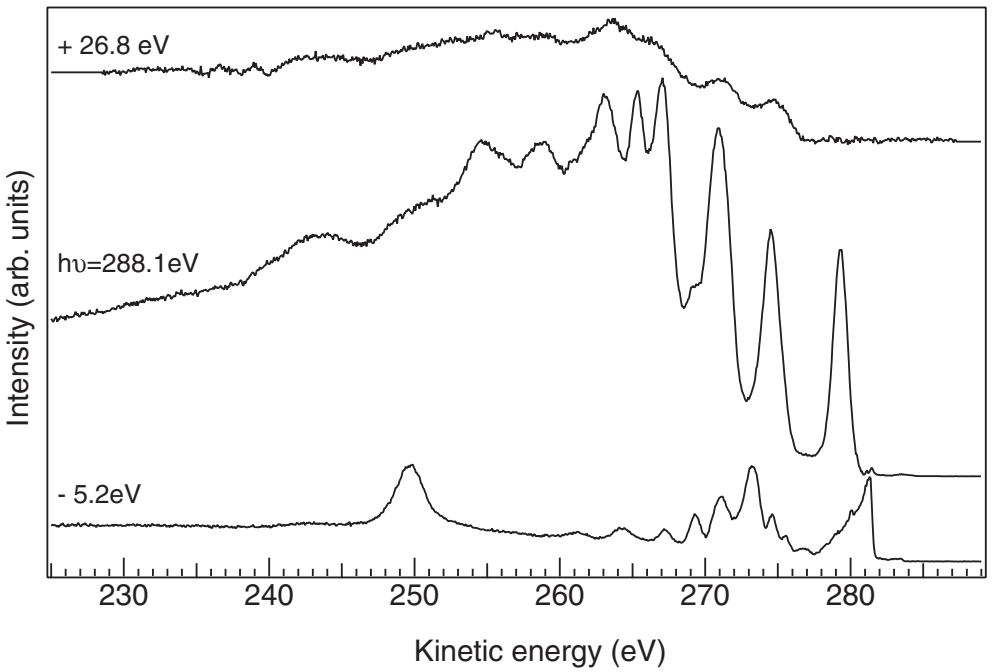

Figure 6.8: For 10ML C_6F_6/Cu(111) pure photoionization spectrum for the excitation far below π^* resonances (shifted by +5.2eV, autoionization spectrum for the C1s excitation on $1\pi^*$ resonance, pure Auger for excitation in the continuum.

three spectra correspond to 10ML coverage of C_6F_6. The contribution from the substrate is quite small and adsorbate originating features are prominent at this coverage.

Participator intensities for all the coverages showed Fano type profile [129, 130]. The Fano type resonance of participator lines is due to the mixing of single-hole configurations from direct and resonant transitions and is frequency dependent [27, 112, 131**?**]. The features in the photoemission spectrum and in the standard Auger spectrum can be compared with the gas phase spectra except the solid state broadening. The standard Auger spectrum shows well defined features comparable to that from the gas phase Auger spectrum, see also [132].

The photoionization and normal Auger spectra are identical for all the investigated coverages though normal Auger spectra are structureless for the 0.5ML and 1ML compared to 2ML and 10ML coverage due to interaction with the substrate states. Those spectra for 10ML serve as representatives of all coverages. However, the resonantly excited spectrum ($1\pi^*$) exhibits obvious changes when the adsorbate coverage is varied. Fig. 6.10 shows C-KLL decay spectra of the resonantly excited $C1s^{-1}\pi^{*1}$ state, for free C_6F_6 molecule and C_6F_6 of 0.5ML, 1ML, 2ML and 10ML adsorbed on Cu(111). The spectra are shifted with respect to each other due to difference in core-hole screening processes under different environments.

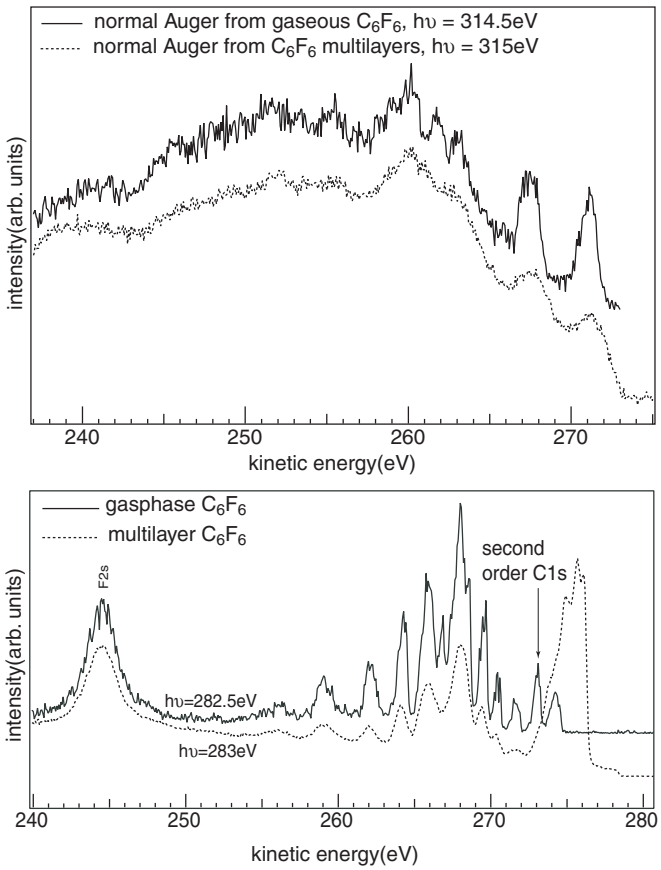

Figure 6.9: For 10ML C_6F_6/Cu(111) and gaseous C_6F_6 molecule (a)standard Auger spectra obtained for the excitation in the continuum (b)normal photoemission spectra for the incident radiation 5.2eV below the $1\pi^*$ resonance.

From Fig. 6.10, on increasing the C_6F_6 coverage from 0.5ML-10ML the $C1s^{-1}1\pi^*$ decay spectrum evolves gradually towards gas phase decay spectrum. Whereas the decay spectrum of the isolated molecule should contain only non-charge(spectator Auger and participator Auger) transfer channels, that for adsorbed C_6F_6 leads to the autoionization spectrum as a mixture of charge transfer (normal Auger) and non-charge transfer (spectator Auger and participator Auger) components due to coupling of the molecular resonance with neighbors.

What is explicit from the decay spectra is that participator features are broadened for adsorbed molecules than for gaseous molecule. The second conclusion is that enhancement of various participator features remain identical upon variation of the adsorbate coverage. The participator features show variation of the peak shapes for the excitation across resonance due to interference effects at the core-excited intermediate state.

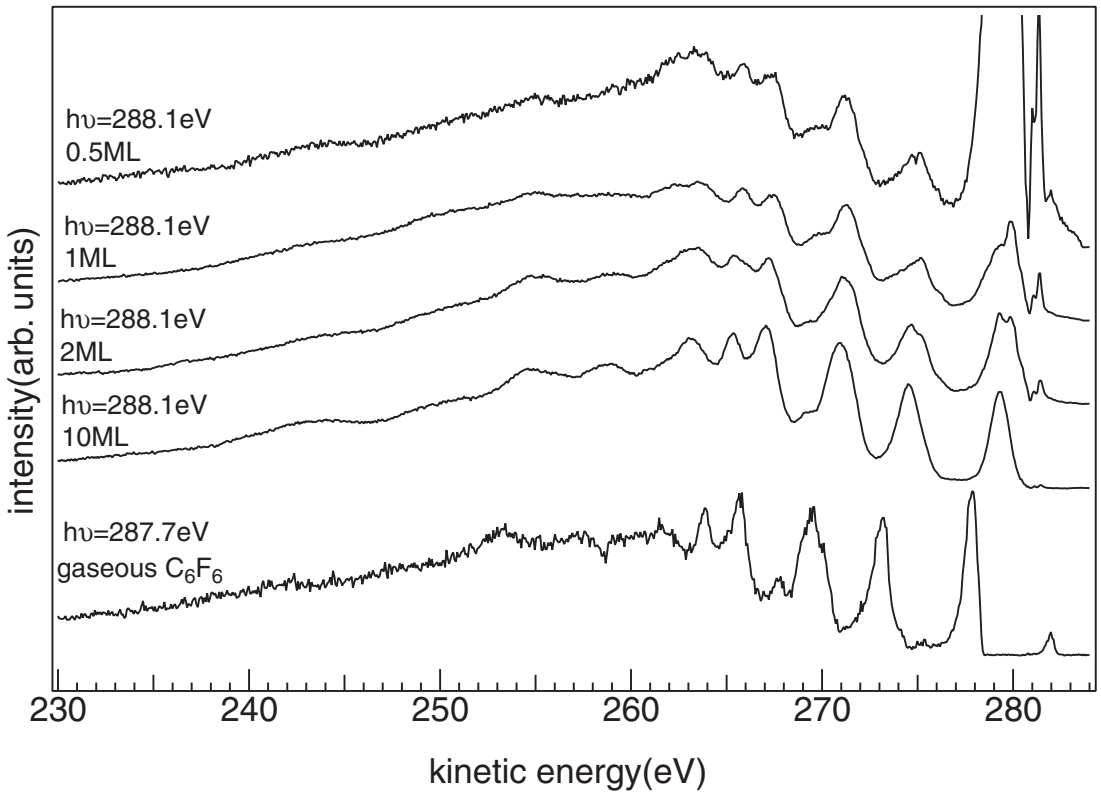

Figure 6.10: C-KLL autoionization spectra obtained after resonantly excited (C1s→$1\pi^*$) state of free C_6F_6 molecule and of 10ML, 2ML, 1ML and 0.5ML of C_6F_6 adsorbed on Cu(111)

Consequences of Jahn-Teller coupling in non-linear molecules:

On first inspection the linear dependence of the spectator Auger and participator Auger on the excitation energy is not obvious as it mixes together with the constant K.E. normal Auger channel. For the participator channels, non-linear dependence on the excitation energy was observed for just below and above resonance. Deviation in linear dependence of the participator peaks could be due to vibronic coupling in the excited state caused by Jahn-Teller type distortion (see below). It is followed from the Jahn-Teller theorem that as the $1\pi^*$ orbital is doubly degenerate in the ground state, excitation of the C1s electron into $1\pi^*$ lifts the degeneracy by lowering the molecular symmetry. As a consequence, the two orbitals are displaced vertically by a small amount as shown in Fig. 6.11. For larger molecules the vibrational levels are closely spaced and slight vertical displacement of the vibrational levels cause vibronic coupling.

The non-linear dispersion of the participator and spectator lines cannot be tracked exactly, if the exciting radiation is broader than the separation of between the vibra-

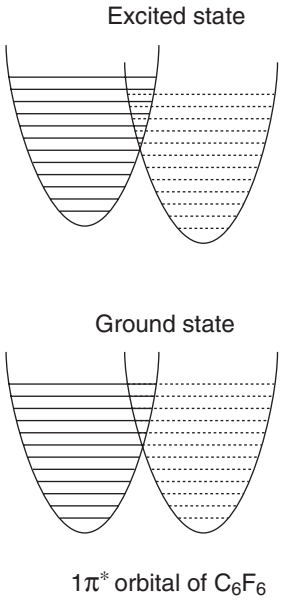

Figure 6.11: Schematic representation of Jahn-Teller effect and vibronic coupling in C_6F_6

tional states of the final state resonance. However, the overall spectral shape gets modified due to energy conservation.

In non-linear polyatomic molecules prevalence of Jahn-Teller effect leads to vibronic coupling in the core-excited intermediate state. Gaseous samples of BF_3, BCl_3, were studied by Auger resonant Raman spectroscopy near B1s→2pπ^* resonance. For BF_3, the spectator Auger spectral structure and the intensity distribution differs from the standard Auger spectrum [133]. In another investigation by Simon et al. the spectator Auger stays at constant kinetic energy whereas the participator Auger peaks show linear dispersion as the excitation energy is varied across resonance. On combining quantum mechanical calculations it was found that the stable/unstable nature of the potential energy curves of the final-states along the co-ordinate of out-of-plane vibration mode [134] is responsible for the dispersive/nondispersive behavior of participator/spectator Auger lines. The participator lines also showed vibrational fine structure and asymmetric line shape towards higher binding energies due to the specific excitation of giant out-of-plane bending mode in the intermediate core-excited state [135].

For BCl_3, the participator Auger decay shows evidence of dynamical Auger emission. Theoretical model based on vibronic coupling due to Jahn-Teller and Pseudo Jahn-Teller indicate multistate vibronic coupling and complex nuclear dynamics in the core-excited intermediate state [127].

Spectator vs CT Auger

The broad low kinetic energy spectral region around 230-265eV which is due to both charge transfer Auger and spectator Auger decay show gradual changes on increasing the adsorbate coverage whereas the sharp participator peaks look pretty much similar. On moving from isolated molecule to the condensate we can expect charge transfer to the neighboring molecules whereas at much lower adsorbate coverages charge transfer to the neighboring molecule as well as to the substrate is expected. This region evolves steadily from submonolayer to multilayer coverage and the features get sharper at higher coverages. The multiplet splitting due to coupling of the spectator electrons with the valence electrons might result in dramatic changes in this region. In addition, effects due to spectator and normal Auger mixing might also be expected.

The C-KVV autoionization spectrum of C_6F_6 is quite broad and decomposition of different channels for such a big molecule (in the framework of Auger electron spectra) is complicated further by the aromatic character which reduces the spectator shift and possibly by the involvement of vibrational motions in the molecule.

Possible Charge transfer mechanism

We will first derive the nature of the initially excited state to look for possible charge transfer channels. In molecules which contain equivalent atoms like C_2H_2, C_6H_6 delocalized nature of the core wave functions were realized in the ground state. Eventhough core orbitals are considered to be localized (non-bonding) they still participate in bonding-antibonding interactions in homogeneous symmetric environment. With high resolution photoelectron spectroscopy, the feable bonding of core orbitals and localization through dynamic symmetry breaking on ionization were proved, supporting theoretical computations [136]. Recently, this has been proved even for N_2 molecule with double slit experiment [137].

Similarly, the 6 C1s orbitals in the C_6F_6 molecule where all the carbon atoms are equivalent should interact weakly though forming bonding and antibonding orbitals which are delocalized in the ground state. Thus C1s core excitation is considered as coherent excitation of all the 6 carbon atoms and the excited electron again being placed in the strongly delocalized π orbital. Based on this concept expected excited state dynamics behavior of C_6F_6 is illustrated in the scheme below.

For an adsorbed C_6F_6 molecule, when the C1s electron is excited to the $1\pi^*$ orbital, electronic relaxation may occur by symmetry breaking and localization of the core-hole and the electron on one of the carbon atom (relaxation I). This is called dynamic symmetry breaking and such relaxation process results in vibronic coupling and shows up as a spectator Auger channel which does not show linear dispersion with incident photon energy as the vibrational motion consumed the extra energy. Since the electronic motion is roughly 1200 times faster than the nuclear motion and π type

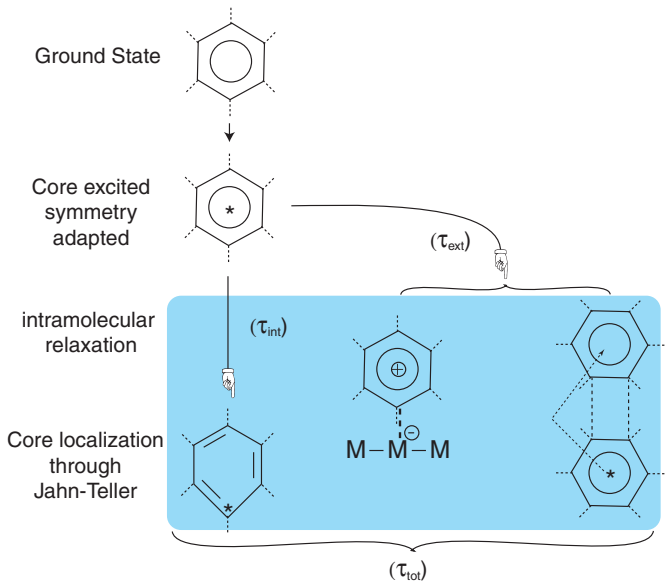

Figure 6.12: charge transfer mechanism in core-excited C_6F_6

electrons can screen the hole effectively, on localization of the core-hole, the electron is also coupled to it which may cause participator type decay which will not show linear dispersion with incident photon energy. The non-linear dispersion of the participator and spectator lines cannot be tracked exactly, if the exciting radiation is broader than the separation of between the vibrational states of the final state resonance. However, the overall spectral shape gets modified due to energy conservation.

Alternatively, the delocalized core-excited state may relax by transferring the electron to the neighboring molecule or to the substrate. These processes will have normal Auger characteristics (constant kinetic energy) as a charge transfer Auger channel. The excited electron-hole pair may hop to the neighboring molecule by polarization that would again show linear dependence on the excitation energy. However, it is a slow process comparing other decay. On the other hand, the initial core-excited delocalized state will appear as a spectator Auger and participator relaxation channels that would show excitation energy dependence.

Thus, the decay spectrum of the excited state has complicated structure as both CT and non-CT relaxation processes overlap and become indistinguishable. The spectator shift is smaller in aromatic systems compared to linear molecules. Besides, the polarization due to neighboring molecules reduces the spectator shift further.

Access to charge transfer times

In the literature various methods have been utilized to extract charge transfer times when the spectator and Auger components mix and were difficult to be separated. We will here go through three different cases of study.

Case 1 : CO/Ru(0001)

CO interacts strongly with transition metal surfaces. The coupling results in charge flow from the molecule to the substrate. It is interesting to know how fast the electron transfers from the chemisorbed molecule to the substrate and therefore, O1s-$2\pi^*$ excitation and decay dynamics for adsorbed CO/Ru(0001) has been studied by the resonant Auger Raman spectroscopy [29]. The decay of the O1s$\rightarrow 2\pi^*$ excited state shows very small percentage of participator decay and a large amount of normal Auger type intensity. This wide normal Auger feature resembles and stays at the same kinetic energy as the off-resonant Auger spectrum. However, this region must also have contribution from the dispersive spectator channel but can not be directly identified for estimation. In the resonant Auger decay of CO isolated from the Ru(0001) by Xe overlayers no charge transfer to the metal should occur and only spectator and participator Auger decay will be present. Hence the ratio of participator to spectator can be taken from the physisorbed CO (CO/Xe/Ru(0001)). The spectator contribution for O1s$\rightarrow 2\pi^*$ in CO/Ru(0001) is then calculated from the participator intensity and the known participator to spectator ratio. Contribution of the spectator channel in the case of chemisorbed CO/Ru amounted only 10%. Such a small fraction of spectator intensity obviously can not be seen if is hidden under the overwhelming normal Auger channel.

NO also strongly adsorbs on Ni(111)[138] and the autoionization spectrum after C1s$\rightarrow\pi^*$ excitation is predominantly of CT-Auger decay identical to the off-resonance Auger spectra. Similar procedure as applied for CO/Ru can be utilized here also to quantify various decay channels.

Case2 : BINA/TiO_2

Another different approach was taken in the charge transfer study of Bi-isonicotinic acid (BINA) adsorbed on TiO_2 [139]. BINA is a technologically important molecule acting as a ligand molecule in the so called coordination complex N_3, one of the most efficient dyes to-date. The rate of excited electron transfer from BINA to the unoccupied band of TiO_2 after N1s$\rightarrow$LUMO, N1s$\rightarrow$LUMO+1 and N1s$\rightarrow$LUMO+2 excitation in BINA is the central issue. The shapes of autoionization spectra after the N1s$\rightarrow$LUMO, N1s$\rightarrow$LUMO+1 and N1s$\rightarrow$LUMO+2 excitations are different from the off-resonance Auger spectrum, neglecting 1h-participator peaks. The broad low kinetic energy was

reconstructed by a model made with off-resonance Auger spectral shape for CT contribution and the off-resonant Auger spectrum shifted by spectator shift for spectator contribution. Off-resonant Auger spectrum shifted by the spectator shift (no CT) was added with off-resonant Auger spectrum (CT) both of varied weights in order to match the broad region of the original decay spectra for each of the three excitations. Residual intensities obtained after subtracting the model spectrum from the original decay spectrum were satisfactorily assigned to participator type decay on comparison with normal photoemission spectrum. This procedure is applicable when the spectator and CT Auger contributions are comparable.

Case3 : C_{60}

In larger molecular systems the limitation comes even in separating the participator decay channels from that of spectator decay. For example, the autoionization spectrum of C_{60} consists of both Auger like broad features attributable to spectator decay and sharp features due to participator decay. However, on the high binding energy region of the normal PES spectrum the states become less separable and lead to broadening. Indeed it becomes virtually impossible to distinguish the original contribution of the spectator from that of the participator. Thus, on coupling to the metal all the three channels, CT-Auger, spectator and participator decay mix together and it is less meaningful to try to identify and separate each of them. Similar difficulties are at the extreme, for graphite. In such situations, use of alternative methods is a wise solution to extract charge transfer times. One such way was developed to determine the charge transfer times in solid C_{60} [92]. In a simplified procedure, participator peaks which were verifiable were exclusively used. The autoionization decay of coupled system consists of a pure participator peak which gets enhanced when the molecules are separated by Xe matrix. As the participator intensity corresponds to the localization of the excited electron at the core-hole site, the decrease in the participator intensity in the coupled systems is due to electron transfer from excited state molecule to the neighbors on the timescale of the core-hole. Using the formula below the charge transfer times were quantified.

$$\frac{\tau_C}{\tau_C + \tau_{CT}} = \frac{I_{iso}}{I_{iso} - I_{coup}} \tag{6.1}$$

Charge transfer rates across the interface of metal-porphyrin complex (Fe-TPP)on FeS_2 surface has been calculated using the above formula [140].

Determination of charge transfer times

Having gone through the literature for various procedures adopted to extract charge transfer times with core–hole–clock spectroscopy, we would move on to device a method which suits our system.

We developed a new strategy here in order to extract charge transfer times after trying out a number of other procedures few of which are mentioned. In previous investigations on multilayer adsorbates namely, C_2H_4 and C_6H_6 charge transfer to neighboring molecules was considered not to contribute to the resonant decay spectrum and only spectator and participator decay features were claimed to exist. But, in C_6F_6 multilayers we speculate electron transfer to surrounding molecules/substrate to occur very slowly though. Hence, the multilayer decay spectrum obtained after resonant excitation contains not only spectator and participator Auger decay but also CT-Auger type decay. When the charge transfer is very slow compared to localization at the excited molecule, CT-Auger will be obscured by the overwhelming spectator intensity.

Method 1: Absolute charge transfer times from core–hole–clock spectroscopy

The autoionization spectrum of the free gaseous molecule should contain only non-charge (spectator Auger and participator Auger) transfer channels. Hence, CT contributions in the adsorbate autoionization spectra can be obtained by subtracting autoionization spectrum of the isolated molecule. The spectra for various adsorbate coverages are subtracted by the substrate contribution. The normal photoionization contribution was subtracted from each of the 5 decay spectra (0.5ML,1ML,2ML,10ML and gaseous C_6F_6) after which they are normalized for similar background. On subtracting autoionization of the gaseous molecule of necessary weightage (non-CT Auger in Fig.3) from the decay spectrum for each of the coverages, charge transfer Auger conterparts were obtained. The resonantly enhanced spectator feature labelled (SA) in Fig. 7.3 was used as a benchmark to subtract sufficient amount of the non-CT component. The participant feature at $\sim$279eV which is due to the HOMO had to be neglected in the calculation since it is hybridized with substrate valence states. The ratio of non-CT to CT channels obtained in this way changes significantly when increasing the coverage. From this ratio charge transfer times as a function of coverage have been calculated (and hence for the monolayer coverages very different from the gas phase feature). To check the influence of the neglected amount of HOMO intensity we added a contribution derived from the gas phase autoionization spectrum. However, charge transfer times do not differ within the error bars if the intensity of HOMO feature is omitted.

Charge transfer times thus obtained for 0.5ML, 1ML, 2ML and 10ML of adsorbate coverages with CHC method are 3.5$\pm$0.2fs, 3.5$\pm$0.1fs, 6$\pm$0.3fs and 32$\pm$1fs respectively.

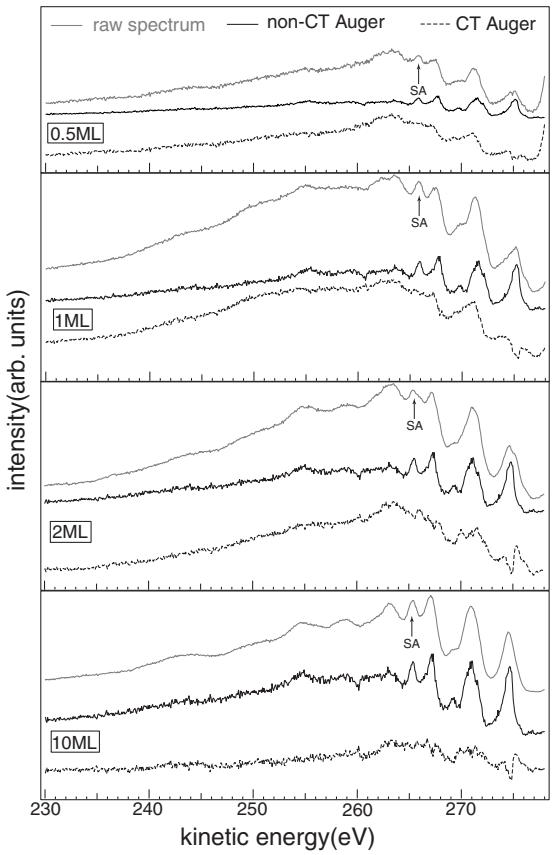

Figure 6.13: Decomposition of C-KLL autoionization decay spectra from the $C1s^{-1}1\pi^*$ state of C_6F_6 molecule adsorbed on Cu(111). CT Auger is obtained by subtracting sufficient amount of non-CT Auger components (autoionization spectrum from gaseous molecule) from the raw spectrum, for the adsorbate coverages 0.5ML, 1ML, 2ML and 10ML.

6.1.1 Method 2 : Relative charge transfer times from gas phase spectrum

Since participator channels are indicative of the strength of localization of the excited electron, by quantifying participator features charge transfer times can be calculated indirectly as in the case of C_{60} [92]. Since the relative intensities of the participator features remains identical for all the coverages, only one of them is needed to quantify while determining charge transfer times, at best the participator feature set P2 which does not get contribution from the substrate d-bands. If the autoionization spectrum from gas phase molecule serves as a reference with no charge transfer, the charge transfer times for the coupled phases can be calculated with the formula 6.2.

The participator peak set P2 for 0.5ML and 1ML show identical area and its intensity increases as the coverage increases, Figure. 6.14. The trend in charge transfer times

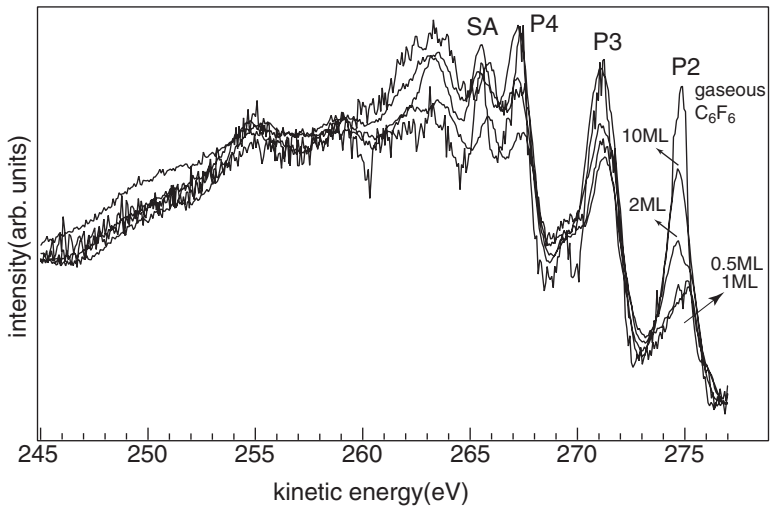

Figure 6.14: C-KLL autoionization spectra from free C_6F_6 molecule, 0.5ML, 1ML, 2ML and multilayers of C_6F_6 on Cu(111) from resonantly excited C1s→$1\pi^*$ state.

as the coverage is increased also is obvious from Figure. 6.14. However, P2 consists of several states and (spectator+CT) Auger region also contributes to the intensity of P2 feature. Therefore, the calculated CT times are not so accurate as method 1.

Method 3 : Combining tr-2PPE with CHC

In another method localization time of the electron in the $1\pi^*$ orbital of the core-excited molecule can be taken from the tr-2PPE measurements. Direct measurement of charge transfer time is possible with tr-2PPE technique. Charge transfer times have been obtained with this method for identical coverages of C_6F_6 on Cu(111) as CHC. As the bilayer is sharply distinguishable in TPD, the excited state lifetime found in the time resolved measurements for 2ML can be approximated to that in core–hole–clock method and charge transfer rates for the other coverages can be calculated on the basis of the modification in the participator intensity from the formula derived below 6.2. This method is again not a reliable one as the excited states in the two spectroscopic techniques are of different nature and the excited states are coupled differently to the substrate band structure [141] in addition to the overestimation of P2 intensities.

$$\frac{\tau_{CT}}{\tau_C} = \frac{ep(1+c)}{T - ep(1+c)} \tag{6.2}$$

Where T = total area of the decay spectrum; e = ratio of the participator P2 to the total participator intensity (obtained from gas phase); c = spectator to the total participator ratio, unknown, to be calculated using the charge transfer time of bilayer molecules in tr-2PPE measurement.

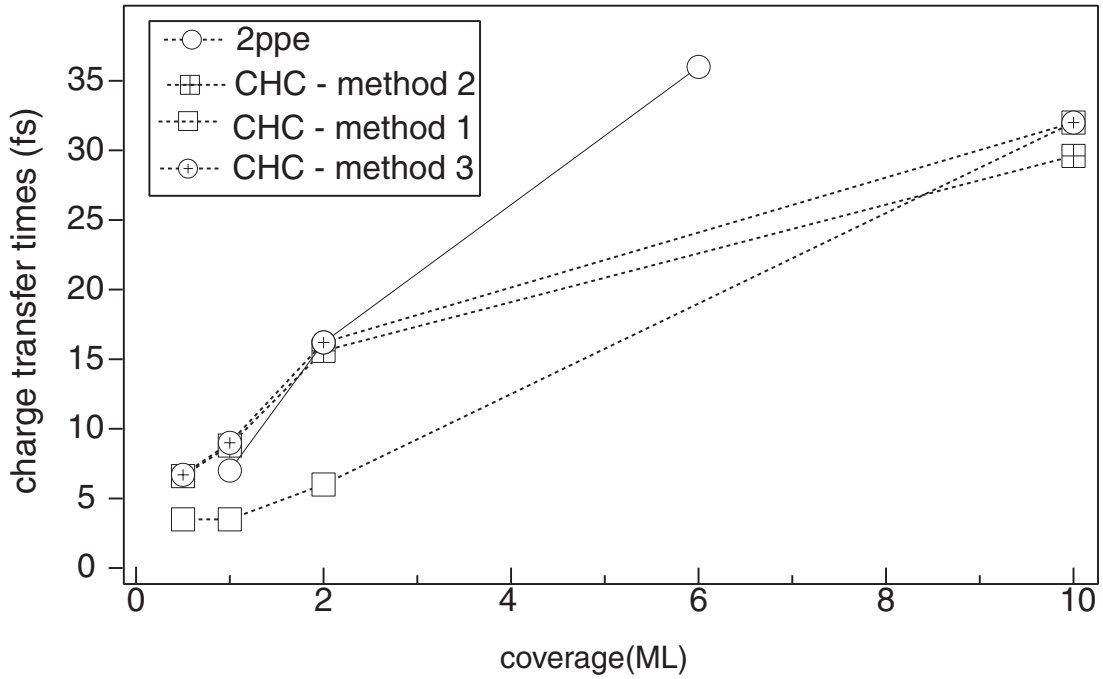

Figure 6.15: charge transfer times from the core-excited C_6F_6 molecule in 0.5ML, 1ML, 2ML and multilayers of C_6F_6 on Cu(111) utilizing different procedures and charge transfer times from the anionic C_6F_6 molecule on Cu(111) from tr-2PPE measurement.

Charge transfer times calculated with the above three methods are plotted in Fig. 6.15 in comparison to the times obtained from tr-2PPE. The trend in charge transfer times as the coverage is increased also is obvious, supporting our calculation procedure. However, the most reliable calculation of all the three methods is that from method:1.

Conclusions

In this paper, we have demonstrated with C_6F_6 molecule, a different method to calculate charge transfer times from the core-excited state adsorbate to the substrate from the core-hole decay spectrum. In essence we used autoionization spectrum of the free C_6F_6 molecule which contains only Raman channels to separate CT Auger counterparts in the coupled system. We have applied several other methods with certain approximations to obtain charge transfer times. All the methods showed similar trend in the charge transfer times across various coverages. However, use of gas phase autoionization spectrum in extracting CT Auger area is the best we find of all the methods. In fact, we can get absolute values from this method. The calculated charge transfer times

for 1/2ML, 1ML, 2ML and 10ML adsorbate coverages are 3.5±0.2fs, 3.5±0.1fs, 6±0.3fs and 32±1fs respectively.

In situations where the charge transfer/no charge transfer channels in resonant core-hole decay spectrum are very close and are not discernible, alternative method as this demonstrated here is very fruitful. The examples cited from the literature clearly will indicate the difficulties encountered in such molecules and the potential use of this method. However, this method is valid only when the ground state and the excited state geometry of the molecule is not significantly changed upon adsorption on a substrate.

Acknowledgements

This work has been funded by the Deutsche Forschungsgemeinschaft through SPP 1093.

Chapter 7

Investigations of charge transfer dynamics at interfaces with two different approaches

Charge transfer process at surfaces and interfaces can be studied via traditional pump-probe techniques, i.e., time resolved two-photon photoemission (tr-2PPE) or Core–Hole–Clock (CHC) method. These two techniques have been exploited in various adsorbate systems to study charge transfer dynamics in the femtosecond region, mainly to calculate the lifetime of excited states. Though each of the techniques has its own advantages and limitations, it is interesting to check how the techniques look at the system under study and what information do they provide about the system.

The pump-probe laser techniques operate in the direct time domain making the excited state lifetimes accessible directly. However, the resolution is limited by the temporal width of the laser pulse. CHC operates indirectly in the time domain i.e., the lifetime information is obtained from the branching ratio of non-CT channels to CT channels in the deexcitation spectrum. As CHC uses the core–hole–clock as the internal reference in calculating CT times very short lifetimes down to sub-femto seconds can be accessed. In contrast to pump-probe optical excitation which is focussed on the whole valence region, the element specificity of CHC is advantageous in an heterogeneous environment for instance, to distinguish between the $C1s^{-1}$ $2\pi^1$ and $O1s^{-1}$ $2\pi^1$ excited states. The important difference between the two techniques is that the initial excitation involve in pump-probe method is via substrate-adsorbate charge transfer but the initial excitation occurs in CHC at the adsorbate. Therefore in CHC spectroscopy charge transfer from the neutral core-excited state on to the underlying substrate is studied, in tr-2PPE, charge transfer from the anionic adsorbate resonance to the substrate states is derived.

For an atomic adsorbate, the excited state dynamics from the two techniques are easier to understand. However, for a molecular adsorbate, the dynamics of the excited state is much more complex due to differences in the excited intermediate states of anionic and neutral core-excited in nature. Charge transfer dynamics in molecular C_{60} has been investigated by both spectroscopic techniques. Molecular solid of C_{60} is very interesting to study as $C_{60}K_3$ forms superconducting phase. Distance-dependence of excited-state lifetimes and the rates of quenching by the metal substrate (Cu(111)) was studied by tr-2PPE for the coverages ranging from 2ML to 40ML. The initial excitation was concluded to occur within the molecular film rather than metal-to-molecule interfacial charge transfer as the 2PPE spectrum showed little changes on increasing the film thickness from 2 to 40ML. The rate of charge transfer between the excitons in C_{60} and the Cu substrate is found to depend exponentially on distance [12]. Core–hole–clock spectroscopic investigations on C_{60} also indicate decreased charge transfer rate on increasing the coverage from monolayer to multilayers [18, 92].

An interesting question is if similar information is derived on the excited state lifetime from both direct and indirect time domain. Thus, it is the goal of the following article to compare the two spectroscopic techniques on the system C_6F_6/Cu(111) for the adsorbate coverages of submonolayer to multilayers. C_6F_6/Cu(111) system is suitable to study by both pump-probe spectroscopy and Auger resonant Raman spectroscopy. The C_6F_6 molecular resonance falls into the band gap of Cu(111); the molecular resonance is stabilized by the band gap and hence favors the application of pump-probe technique that probes charge transfer dynamics in the regime of around 10fs. The system suits the study by core–hole–clock spectroscopy investigations as well.

7.1 Comparative study of charge transfer dynamics in C_6F_6/Cu(111) : Comparison of core–hole–clock method and time resolved two-photon photoemission

Abstract

We have investigated the charge transfer dynamics in the molecular adsorbate system C_6F_6/Cu(111) with time resolved two-photon photoemission and soft X-ray spectroscopy (Core–hole–clock (CHC) method) for adsorbate coverages ranging from 0.5 monolayer to multilayers and have compared the excited molecular states obtained with the two methods. Both methods give an increase of the excited state lifetime as the adsorbate coverage is increased. However, the absolute times are different. The difference in the charge transfer times obtained from the two techniques is accounted by the different nature of the initially excited state and as a consequence of the different coupling to the substrate band structure [1].

Introduction

The transfer of electrons across interfaces constitutes an elementary step in many technologically important applications like the electron injection and photovoltaic energy conversion in a Graetzel cell [2] but is also of general interest concerning the ultrafast relaxation of quasi-particle excitations. Time resolved two-photon photoemission (tr-2PPE) has been a traditional tool for the study of excited state dynamics at surfaces and interfaces occurring on a timescale of about 10fs [7, 10]. Alternatively, core-excited states can be used to study ultrafast dynamics of adsorbates with the core–hole–clock method on the femtosecond [18, 25, 29, 30, 33, 34, 46, 62, 63, 65, 67–69] and attosecond timescale [24] which is at the limit of what is accessible with tr-2PPE due to the temporal length of the laser pulses.

For comparison of the results obtained with the two techniques one has to take into account the fundamental differences in the excited states probed by the two methods. While tr-2PPE creates a negative ion resonance via indirect population through hot electrons created in the substrate, CHC creates a neutral resonance with a localized core-hole on the adsorbate. In case of a single, atomic adsorbate, the excited intermediate resonance is in both anionic and neutral excited form. Consequently, also relaxation of the excited state is typically governed by the same physics. However, with a different energetic position with respect to the substrate states the relaxation dynamics varies. In a polyatomic molecular system on the other hand, the excited state created by X-ray

[1] This section is intended for publication as Paper V : S. Vijayalakshmi, A. Föhlisch, F. Hennies, A. Pietzsch, M. Nagasono, W. Wurth, P. S. Kirchmann, U. Bovensiepen, M. Wolf [142].

absorption/hot electron attachment can relax due to electronic and/or vibrational coupling to the surrounding substrate atoms or molecules or within the molecule. These relaxation processes may be very different for the anionic or neutral excited states.

In core–hole–clock spectroscopy, based on the branching ratio of different autoionization final states due to dynamic processes in the core-excited state, a survival probability of the initially excited state is given as a rate equation. Thus, for an atomic adsorbate with weak next neighbor interaction, two autoionization final states can be observed: a) The adsorbate core-excited state remains atomically localized. b) The adsorbate core-excited state couples via resonant charge transfer to delocalized (itinerant) substrate states, leading to a charge transfer final state. Hence, the branching ratio of these two autoionization channels (I_{loc}/I_{CT}) directly relates the core-hole lifetime τ to the survival of the atomically localized adsorbate core-excited state. The charge transfer time τ_{CT} obeys the relation:

$$\frac{I_{loc}}{I_{CT}} = \frac{\tau_{CT}}{\tau}$$

In tr-2PPE the lifetime of the anion created by hot electron attachment to an atomic adsorbate can be obtained from cross correlation measurements made by varying the time delay between the pump and probe laser pulses while monitoring the photoexcited electron from the atomic resonance.

To apply core–hole–clock spectroscopy to an molecular adsorbate, we need to consider two questions: a) What is the nature of the core-excited state, as the symmetry properties of the molecular unit allows molecularly delocalized symmetry adapted core-hole excited states, b) What are the possible electronic (CT) and vibrational relaxation processes in the core-excited state. In tr-2PPE also, similar questions should be thought through regarding the initially created molecular anion.

In the present work, we investigate the timescales of the dynamic charge transfer from the molecular adsorbate C_6F_6 to Cu(111) and C_6F_6 neighbors respectively using core–hole–clock spectroscopy at the carbon atom and in direct comparison to tr-2PPE measurements. In our investigation we modify the molecular interaction with the substrate by variation of the layer thickness between half a monolayer and multilayer coverages. As for a complex system separation of the CT channels from their non-CT counterparts with the core–hole–clock method is difficult, a number of alternative strategies were adopted [143] to obtain the branching ratios. Finally the charge transfer times obtained from core–hole–clock spectroscopy are compared with those from tr-2PPE measurements. The charge transfer times independently obtained in the two methods show similar trends although the absolute times differ.

Comparison of the spectroscopic techniques

The principle of the tr-2PPE technique is compared with the core–hole–clock method in figure 7.1 for the molecular adsorbate system C_6F_6/Cu(111). The basic idea behind

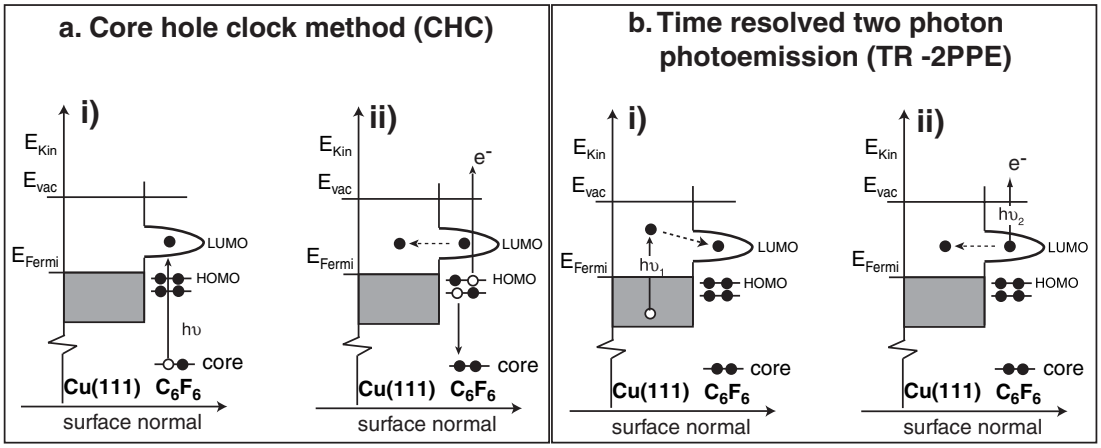

Figure 7.1: a) Core–hole–clock method (CHC) b)Time-resolved 2PPE spectroscopy (tr-2PPE).

the two spectroscopic methods is to measure the intermediate lifetime, in this case that of $C_6F_6^{(-)}$ (with tr-2PPE) or $C_6F_6^{(*)}$ (with CHC). The intermediate state in CHC is a core-excited neutral molecule and is created by exciting one of the core electrons of C_6F_6 molecule to its nominally unoccupied molecular orbital ($1\pi^*$) i.e., C1s$\rightarrow 1\pi^*$. The core-hole lifetime then serves as an internal clock to monitor the probability of the excited electron to be present (spectator decay) or absent (CT-Auger decay) at the core-excited site during the hole lifetime. Deexcitation of the core-hole gets contribution from the spectator decay, participator decay and CT - Auger decay, the participator decay being when the excited electron participates in the core-decay process. On the other hand, the intermediate state in tr-2PPE is anionic in nature and is obtained when hot electrons populating the states above E_F in the substrate (pump process) subsequently tunnel to the unoccupied molecular resonance. The probe pulse which after a time delay probes the intermediate electronic state and photoemits the electron from the molecular resonance measures the population of the intermediate state which decreases with time due to elastic tunnelling of the electron at molecular resonance back to the substrate states or inelastic scattering of the excited electron with other electrons.

Since tr-2PPE probes the adsorbate resonance in the time domain, lifetime of the adsorbate anionic resonance is directly measured. In contrast, branching ratio of the Raman to the CT Auger channel is used in CHC to calculate the charge transfer or the excited state lifetime in reference to the core-hole lifetime. The time resolution is limited by the temporal width of the pump-probe pulse in tr-2PPE whereas the core-hole lifetime controls the time resolution in CHC.

Experiment

Core–hole–clock experiments were performed at beamline UE56/1(SGM) at BESSY II, Berlin with our transportable UHV surface science spectroscopy system at a base pressure below 2×10^{-10} mbar housing a Scienta 2002 hemispherical photoelectron analyzer and a partial electron yield detector. Time resolved 2PPE measurements were carried out in a different experimental set-up in Berlin. The laboratory set-up combines an ultrahigh vacuum chamber (base pressure $<10^{-10}$mbar) for sample preparation and photoelectron spectroscopy with a tunable femtosecond laser system. The Cu(111) single crystal (purity $\geq$ 99.9%) was cleaned by cycles of Ar^+ sputtering and annealing to 875K for 1Min and 670K for 5min for CHC and tr-2PPE respectively. While in CHC the cleanliness was checked by X-ray photoelectron spectroscopy, the surface quality before tr-2PPE measurements was inspected with Low Energy Electron Diffraction (LEED) and within the resolution of Auger Electron Spectroscopy no contamination from O or C was observed. Also, the work function, energetic positions, linewidths and lifetimes of the Cu(111) surface (SS) and IP state were monitored by 2PPE to confirm the surface quality. According to earlier investigations, this is a very sensitive surface characterization method because, e.g., terrace steps lead to increased scattering rates [**?**]. For CHC measurements the crystals were cooled to 100K and C_6F_6/Cu(111) multilayers were prepared. With thermal desorption spectroscopy the mono, bi and multilayer were prepared which can easily be distinguished by the chemical shift of their C1s core-level binding energies. For tr-2PPE measurements C_6F_6 was adsorbed on Cu(111) at substrate temperatures of 140-160K depending on the desired coverage. The substrate temperatures were chosen appropriately to prevent the adsorption of subsequent layers, as has been reported earlier [13]. Thermal Desorption Spectroscopy (TDS) was routinely used to determine the adsorbate coverage (θ) from the integrated desorption yield, recorded at the mass of the most prominent C_6F_6-fragment (CF^+, 31amu). C_6F_6 coverages were investigated between 0.5 and 6ML, where 1ML coverage is defined by saturation of the monolayer desorption feature between 165K and 205K in TDS [144]. All 2PPE measurements were performed at a substrate temperature of 100K.

In core–hole–clock spectroscopy, the bandwidth of the exciting synchrotron radiation was set to $\sim$ 50meV. At 7° grazing incidence, the electric field vector $\vec{E}$ of the incident radiation was switched between perpendicular and parallel to the surface plane by moving the undulator. The direction of photoelectron detection was in the plane normal to the incident photon beam at 45 ° with respect to the surface normal. The Scienta SES 2002 was operated at $\sim$ 50eV pass energy at a bandwidth of $\sim$ 50meV. The samples were scanned during measurement to minimize the radiation induced dissociation of C_6F_6. Autoionization spectra from the gaseous C_6F_6 molecule were obtained in a different experimental chamber at the beamline BL411 in Lund. The gas pres-

sure during the measurement was maintained at 3.5-7.5 $\times 10^{-10}$ mbar. The parameters for data acquisition was identical to that of adsorbate including the electron energy resolution.

For the 2PPE measurements, a regenerative amplifier (Coherent RegA 9050) operating at 200kHZ repetition rate is employed, which generates pulses with a duration of (FWHM)[2] [145] of 55fs at a centre wavelength of 800nm (1.55eV). The RegA output beam pumps two optical parametrical amplifiers (OPAs), operating in the near-infrared (1100-1300nm/1.13-0.95eV) and visible (470-730nm/2.64-1.70eV) spectral regimes. Subsequent doubling and quadrupling of the OPA output allows to generate photon energies in the visible (2.25-1.91eV) and near ultraviolet (UV) (4.51-3.82eV) range. The extensive tunability allows us to carefully tune the laser photon energies to specific resonances of the molecule-metal interface and to follow their dynamics. The dispersion introduced by the optical path to both the visible (p-polarization) and UV pulses is pre-compensated with the use of prism pair compressors, thus resulting in nearly Fourier-transform-limited pulses with durations as short as 28fs (FWHM)[145] at the position of the sample. The UV pulses are temporally delayed with respect to the visible pulses and are then focussed on to the sample surface with polarizations parallel to the plane of incidence (p-polarization). The beam spots exhibit a Gaussian profile with a diameter of 100-150μm, resulting in typical fluences of 100μJcm^{-2} for the visible and 20μJcm^{-2} for the UV light. The size and overlap of the two laser beams are inspected with a CCD camera placed outside the UHV chamber in line with the sample position.

Results

Unoccupied states

In Fig. 7.2, the X-ray absorption spectra (a) of the mono, bi and multilayers (10ML), relative to the Fermi edge are shown for in and out of plane orientation of the electric field vector in comparison to 2PPE spectra (b) for mono, bi and multilayers (6ML) relative to the Fermi level. The unoccupied states are labelled as in fig. 7.2.

In XAS the $1\pi^*$ and $C-F\sigma^*$ resonances appear around 0.6eV and 4.7eV above the E_F. From the polarization dependence of the $1\pi^*$ and $C-F\sigma^*$ states, flat adsorption geometry of the C_6F_6 molecules are revealed. In two photon photoemission spectra obtained at zero delay between the pump and probe pulses the feature at E-E_F=2.5eV is due to hot electrons. The two high kinetic energy peaks of E-E_F=3.8eV and 4.15eV seen at 1ML adsorbate coverage are due to surface and image states. The $1\pi^*$ molecular resonance occurs at 3.13eV above E_F for 1ML coverage and shifts towards lower energies

[2]The laser pulse duration is inferred from the width of the cross correlation traces of the photoelectron yield assuming a sech^2(t) pulse envelope. See also [145]

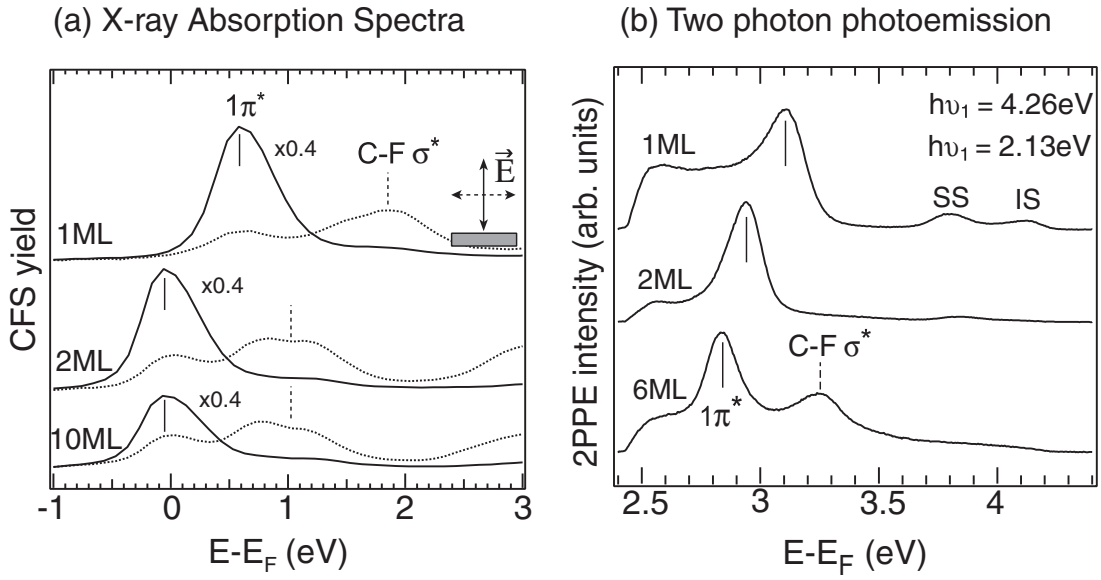

Figure 7.2: CHC vs 2PPE (a)Polarization dependent NEXAFS spectra. (b)2PPE spectra, as a function of coverage.

with increasing coverage showing similar trend as in X-ray absorption spectrum for unoccupied states. However, the shift is smaller than in XAS. The $C-F\sigma^*$ resonance can be observed only for 6ML coverage in 2PPE. Thus we observe for the $1\pi^*$ and $C-F\sigma^*$ states in XAS, the similar trend in 2PPE (b), which allows us to choose nominally the same states to perform the core–hole–clock and time resolved 2PPE investigations.

Autoionization (CHC) vs cross correlation (tr-2PPE)

In Fig.3, C-KLL resonant Auger decay of the core-excited state $C1s^{-1}1\pi^*$ of adsorbed C_6F_6, for the adsorbate coverages of 0.5ML, 1ML, 2ML and 10ML are displayed along with their respective CT and non-CT components underneath and in fig.4, the cross correlation curves obtained for the $1\pi^*$ C_6F_6 molecular resonance for the adsorbate coverages, 1ML, 2ML, 3ML and 6ML with tr-2PPE measurements are depicted.

In the autoionization spectra shown in Fig.3, sharp features above ∼267eV kinetic energy are mainly due to participator Auger decay. The broad feature below 267eV are due to both spectator and normal Auger decay resulting from CT. The later two decay features have almost similar peak shapes and here in C_6F_6 are indistinguishable. The participator decay region also overlap to certain extent with the other two decay features. To quantify the charge transfer times at different coverages, one would have to decompose the autoionization spectrum into non-CT (spectator+participator) and CT Auger contributions. The C-KVV Auger spectrum is quite broad and decomposition

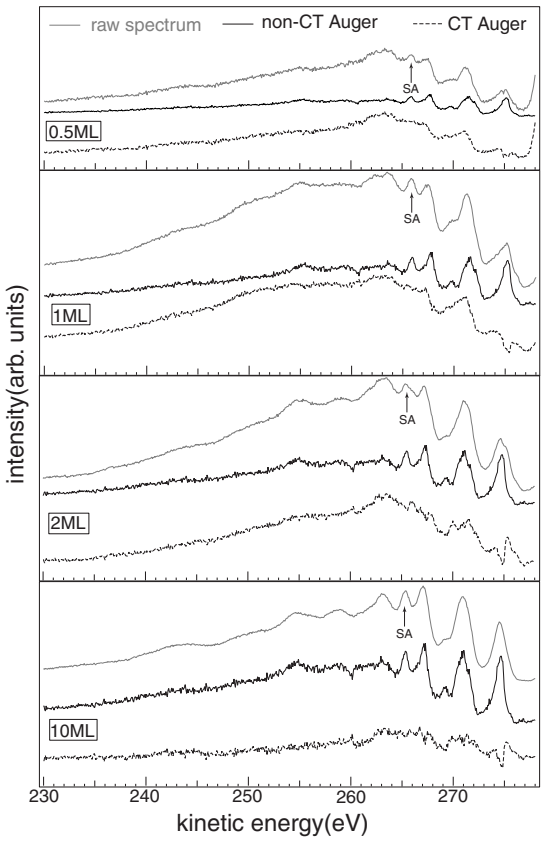

Figure 7.3: Decomposition of C-KLL autoionization decay spectra from the $C1s^{-1}1\pi^*$ state of C_6F_6 molecule adsorbed on Cu(111). CT Auger is obtained by subtracting sufficient amount of non-CT Auger components (autoionization spectrum from gaseous molecule) from the raw spectrum, for the adsorbate coverages 0.5ML, 1ML, 2ML and 10ML.

for such a big molecule (in the framework of Auger electron spectra) is complicated further by the aromatic character which reduces the spectator shift and possibly by the involvement of vibrational motions of the molecule. We solved this issue by making use of the autoionization spectrum of the gaseous molecule that should contain only non-charge (spectator Auger and participator Auger) transfer channels. Substrate contribution is subtracted from the spectra for various adsorbate coverages. The normal photoionization contribution was subtracted from each of the 5 decay spectra (0.5ML,1ML,2ML,10ML and gaseous C_6F_6) after which they are normalized for similar background. On subtracting autoionization of the gaseous molecule of necessary weightage (non-CT Auger in Fig.3) from the decay spectrum for each of the coverages, charge transfer Auger counterparts were obtained. The resonantly enhanced spectator feature labelled in figure 3 was used as a benchmark to subtract sufficient amount of the non-CT component. The participant feature $\sim$279eV which is due to

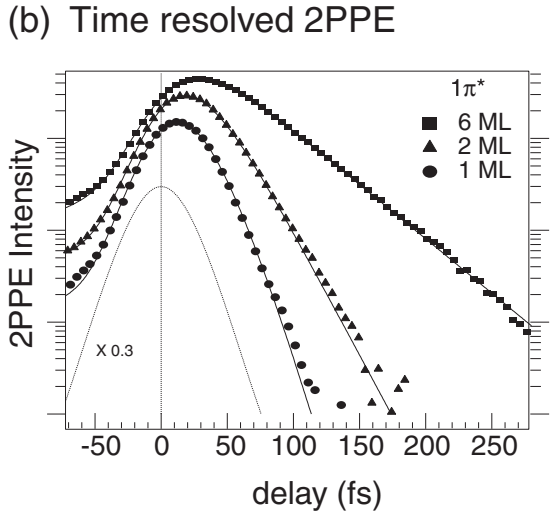

Figure 7.4: Semi-logarithmic presentation of cross correlations of $1\pi^*$ anionic C_6F_6 molecular resonance obtained for 1ML, 2ML and 6ML of C_6F_6/Cu. The positive delay of the peak maxima increases while the decay rate decreases with coverage. Both changes reflect the increase in the lifetime of the excited state electron population. The rise and decay times are extracted from fits (-) of a delayed rise mechanism. The non-vanishing intensity for negative delays is attributed to hot electrons pumped by the visible and probed by the UV laser pulses. In the fits this is taken into account by a second single exponential decay for Δt <0.

the HOMO had to be neglected in the calculation since it is hybridized with substrate valence states. The ratio of non-CT to CT channels obtained in this way changes significantly when increasing the coverage. From this ratio charge transfer times as a function of coverage have been calculated. To check the influence of the neglected amount of HOMO intensity we added a contribution derived from the gas phase autoionization spectrum. However, charge transfer times do not differ within the error bars if the intensity of HOMO feature is omitted.

Charge transfer times thus obtained for 0.5ML, 1ML, 2ML and 10ML of adsorbate coverages with CHC method are 3.5±0.2fs, 3.5±0.1fs, 6±0.3fs and 32±1fs respectively.

Next, we turn to the results from tr-2PPE measurements. Tr-2PPE measurements enable us to measure the lifetime of the electron in the unoccupied molecular resonance. Fig. 7.4 shows the cross-correlation curves for the $1\pi^*$ resonance in logarithmic scale obtained by recording 2PPE intensity as a function of pump-probe delay at various adsorbate coverages. Information on time zero and laser pulse duration was retrieved from the clean Cu(111) surface after thermal desorption of the adlayer. The analysis of the cross correlation signals within a rate equation model yields the corresponding decay times [13]. The charge transfer times obtained for 1ML, 2ML and 6ML from tr-2PPE are 7±3fs, 16.2±3fs and 36±3fs respectively.

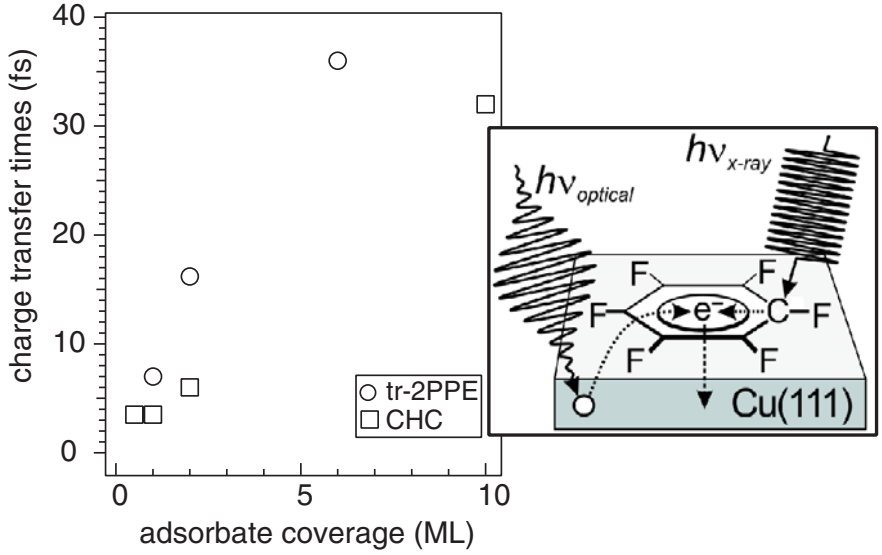

Figure 7.5: Charge transfer times obtained for various coverages of C_6F_6 adsorbed on Cu(111) independently with tr-2PPE and with CHC

Discussion

Comparison of charge transfer times

The charge transfer times so obtained are plotted in Fig. 7.5. In both measurements the charge transfer time decreases with increase in adsorbate coverage. Thus a similar trend is observed though absolute values differ.

To compare and get further insight into the observed trend of charge transfer times obtained in the two spectroscopic techniques, we should consider the following factors.
1. Nature of the excited state
2. Energetic position of the excited states with respect to the substrate band structure and role of the substrate electronic structure.

1. Nature of the excited states

Nature of the excited state and pathways of charge transfer can be compared for the two methods.

In single molecules which contain equivalent atoms like C_2H_2, C_6H_6 or C_6H_6 symmetry adapted core wave functions are an adequate description for the ground state [144, 145]. When a C1s electron is excited to the LUMO in these molecules the excited state is still a state with the full molecular symmetry i.e. the core-hole and the excited electron can be found with equal probability on all equivalent atoms. However, the 1s hole-electron pair can subsequently localize on a single carbon atom through Jahn-Teller distortion of the molecule. Since this intramolecular relaxation process which

involves vibronic coupling is also present for isolated molecules in the gas phase it will not affect our analysis.

When the molecules are in an adsorbate layer or a molecular thin film with long range order the electronic states will of course form bands. Upon resonant excitation of the C1s to the $1\pi^*$ a localized Frenkel exciton will be formed as a result of the strong Coulomb interaction of the excited electron with the core-hole. The width of the exciton band will be fairly small since hopping of the exciton to a neighboring molecule occurs via Förster mechanism and is comparatively slow. Hence this delocalization process is not important on the timescale of the core-hole lifetime and will not affect the core-hole decay. The only process which affects the core-hole decay process is resonant charge transfer of the excited electron from a single molecule to the metal substrate and/or inelastic scattering of the excited electron to substrate states. Hence we conclude that core-hole clock spectroscopy is sensitive to the CT of the excited electron initially localised on a single molecule to the metal substrate.

In tr-2PPE, the molecule in the ground state becomes anionic when a hot electron from the underlying substrate tunnels to the $1\pi^*$ resonance band. The excited electron is delocalized (quasi-free electron) and its energy dispersion as a function of $k_{\|}$ shows a shallow parabolic behavior. The decay of this delocalized state via resonant tunnelling to the metal substrate or inelastic scattering is monitored by the tr-2PPE experiment.

2. Role of the substrate electronic structure

For 0.5ML and 1ML coverages of C_6F_6 charge transfer occurs at a faster rate from the molecule to the substrate as the molecules are in close proximity to the metal. Interaction of the molecules close to substrate can be verified by the asymmetric shape of the C1s XP spectral line for these coverages that indicates metallic screening upon creation of the C1s core-hole [146] and the asymmetric peak shape A, Fig.2.

The difference in charge transfer times between the two methods may then be due to the position of the molecular resonance/core-excited state with respect to the Fermi level. The band structure of Cu [84] has been extensively studied. The surface electronic structure of Cu(111) exhibits a wide band gap in the direction normal to the surface in the -5.83eV to -0.69eV energy range. In Fig. 7.6(b) is shown the energetic position of the core-excited $C_6F_6{}^{(*)}$ and the position as well as the energy dispersion of $C_6F_6{}^{(-)}$ with respect to E_F for various adsorbate coverages.

On comparing at $k_{\|}$=0, the molecular resonance in tr-2PPE stays higher than the core-excited resonance in CHC for all the coverages. i.e. the excited electron at $k_{\|}$=0 finds itself at the mid of band gap for $C_6F_6^{(-)}$ state but is close to/on the E_F for 0.5ML,1ML / 2ML,multilayer coverages of the adsorbate for core excitation. For finite values of $k_{\|}$, the $C_6F_6{}^{(*)}$ state overlaps with the unoccupied substrate band, whereas the excited electron of $C_6F_6{}^{(-)}$ state increasingly delocalized in the adlayer as the

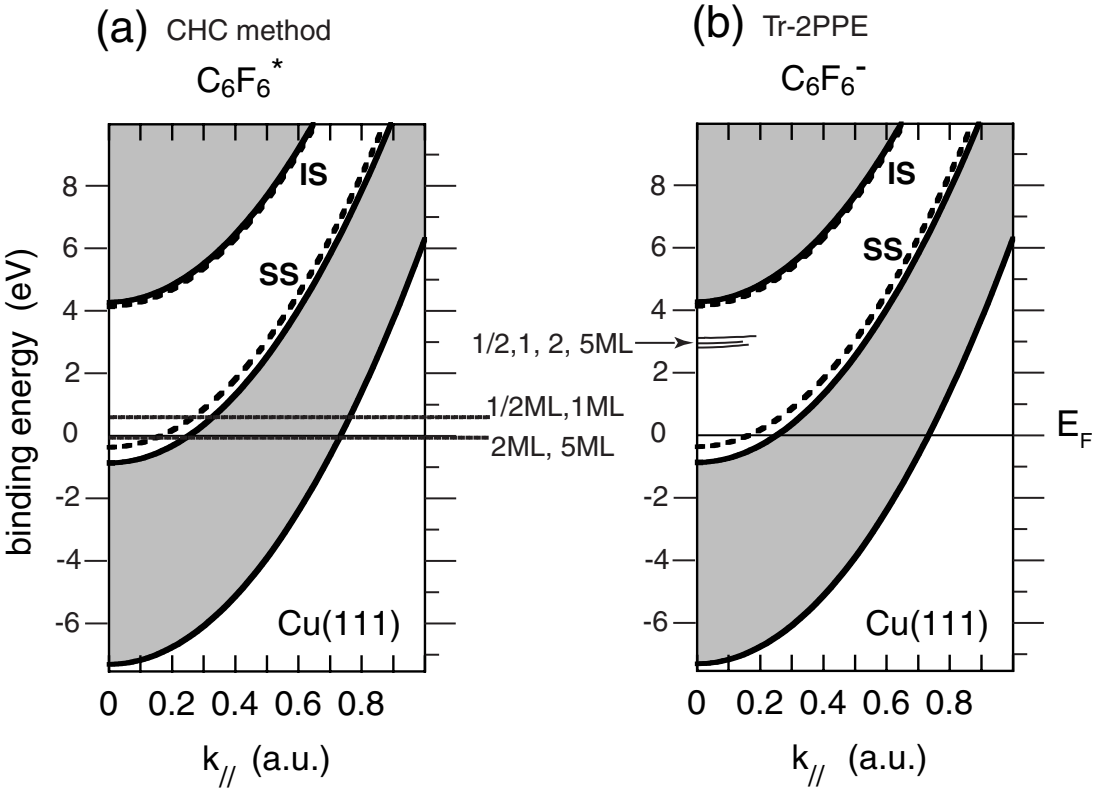

Figure 7.6: CHC vs 2PPE - charge transfer times: Energetic position of the intermediate states (a)$C_6F_6^{(*)}$ and (b)$C_6F_6^{(-)}$ for 0.5ML, 1ML, 2ML and multilayer coverages.

coverage is increased. Thus, for 0.5/1ML coverage the $C_6F_6^{(*)}$ state decays much faster than the $C_6F_6^{(-)}$ state. For increasing adsorbate coverages, the excited electron of $C_6F_6^{(-)}$ is increasingly localized inside the adsorbate layer due to spatial separation of the layers away from the underlying substrate. On the other hand, for higher coverages than 1ML the excited electron of $C_6F_6^{(*)}$ can either decay to the metal or can hop to the neighboring molecule by polarization; both the processes are slower for reasons of spatial or energetical separation respectively.

Conclusions

In this paper, we have compared for C_6F_6/Cu(111), charge transfer times (from the excited molecule) obtained with the core–hole–clock method and tr-2PPE spectroscopy. Both the methods show similar trend in the charge transfer times across various adsorbate coverages. The CT times from tr-2PPE are higher than those obtained from CHC method. The difference in the absolute timescales of CT between the methods is due

to different nature of initially excited state and the energetic position of the excited state with respect to the substrate electronic structure.

Higher electronic lifetimes from tr-2PPE measurements than from CHC are not surprising as the excited state resonance in tr-2PPE that lies higher in the bandgap needs larger $k_{\parallel}$ values of electron to tunnel to substrate than the electron in the lower lying resonance in CHC. However, the $C_6F_6{}^{(-)}$ state stays inside the band gap for all finite values of $k_{\parallel}$ at all adsorbate coverages, whereas the $C_6F_6{}^{(*)}$ state overlaps with the substrate unoccupied states.

Acknowledgements

This work has been funded by the Deutsche Forschungsgemeinschaft through SPP 1093.

Summary and outlook: Aspects of core–hole–clock spectroscopy

Summary

To summarize, in this thesis, characteristics of core–hole–clock spectroscopy as an experimental tool to study charge transfer dynamics in adsorbate systems have been investigated in detail. The study includes both atomic and molecular adsorbates coupled to metal substrates.

The basic assumption made in deriving the relation between charge transfer time and core-hole life time which is "the two decay events are independent" is checked for its validity by comparing the charge transfer times in the system S/Ru with two independent core-hole clocks. The charge transfer times are similar within the experimental uncertainty when the reference clock is changed from S(1s) to S(2s). The two different core-hole clocks have different decay rates and still do not influence the charge transfer decay rate. Thus the validity of the assumption is proved.

Next, the sensitivity of the core–hole–clock spectroscopy to fine changes in the substrate electronic structure has been checked for the monolayer of physisorbed Ar on Cu(111) and Cu(100) surfaces. Indeed, the differences are reflected in charge transfer times between obtained for the two systems, Ar/Cu(111) and Ar/Cu(100). Due to different coupling strength of the core-excited Ar to two different Cu surfaces, the charge transfer from Ar on Cu(100) is twice as fast as on Cu(111). Theoretical computations based on Wave Packet Propagation (WPP) method supports the observations though absolute charge transfer times differ from those obtained from the experiment.

Further, the CHC is compared with the traditional pump-probe laser technique (tr-2PPE) which measures charge transfer times directly in the time domain in contrast to CHC for the molecular system C_6F_6/Cu(111) for various adsorbate coverages.

Prior to this, the molecular adsorbate system was characterized with Temperature Programmed Thermal Desorption Spectroscopy and X-ray Photoelectron Spectroscopy and a clear distinction between different adsorbate coverages from submonolayer to multi-layers was established. It is inevitable in charge transfer dynamics studies to know exactly the adsorption geometry of the molecule on the substrate surface. Hence, the

Near Edge X-ray Absorption Fine Structure spectroscopy was utilized to determine the adsorbate geometry and it was found that hexafluorobenzene adsorbs with its aromatic ring plane parallel to the substrate surface for all the coverages ranging from 1/2ML to 10ML.

While extracting CT times, the tr-2PPE facilitates the determination of CT times especially with molecular systems as it operates in the time domain. On the other hand, the CHC method in a large molecule like C_6F_6 is faced with difficulties in separating and quantifying the CT channels from non-CT channels which is the primary requirement to calculate the CT times. Hence, a number of alternative approaches were undertaken and the accuracy of each of them were compared. The most accurate method of all was concluded which then was used to calculate CT times.

At last, the charge transfer (CT) times obtained with core–hole–clock spectroscopy with the tr-2PPE show similar trend as the adsorbate coverage was varied, the absolute times differ, however. The difference in CT times from the two techniques was accounted due to different nature of the initial excited state and the different coupling of the excited state with the substrate band structure. Whereas the excited state probed by tr-2PPE is anionic in nature, the excited state studied by CHC is a neutral core-excited state. The different nature of the excited states in turn determine the coupling with the underlying substrate and hence the charge transfer times.

Thus, an in-depth understanding of the core–hole–clock spectroscopy has been provided in this thesis by studying atomic and molecular adsorbates coupled to metal substrates.

Outlook

Clear understanding of charge transfer dynamics is essential, while applying the method for practical problems. Molecular adsorbate systems are most interesting candidates on the side of technological research. However, fundamental understanding of charge transfer dynamics pave the way to success of the technology. The very next appealing concept in electron transfer dynamics is the spin-dependent charge transfer or the spin-dependency of the excited state life time. CHC can be tested for its ability to detect differences in lifetimes between up and down spin of an excited electron. Further semiconductor surfaces are again the interesting ones in device physics. Hence, further CHC spectroscopic studies with semiconductor substrates is suggested for future research.

Bibliography

[1] E. Ilisca and K. Makoshi. *Electronic Processes at solid surfaces*. World Scientific, 2006.

[2] Brian O'Regan and Michael Graetzel. *Nature*, 353:737, 1991.

[3] O. Benka and M. Uda. *Phys. Rev. Lett.*, 56:1667, 1986.

[4] R. Kienberger, M. Hentschel, M. Uiberacker, Ch. Spielmann, M. Kitzler, A. Scrinzi, M. Wieland, Th. Westerwalbesloh, U. Kleineberg, U. Heinzmann, M. Drescher, and F. Krausz. *Science*, 297:1144, 2002.

[5] Ahmed H. Zewail. *Nobel Lecture*, 1999.

[6] Richard Haight. *Surf. Sci. Rep.*, 21:275, 1995.

[7] E. Knoesel, A. Hotzel, and M. Wolf. *Phys. Rev. B*, 57:12812, 1998.

[8] C. B. Harris, N.-H. Ge, R. L. Lingle, Jr., J. D. McNeill, and C. M. Wong. *Ann. Rev. Phys. Chem.*, 48:711, 1997.

[9] R. W. Schoenlein, J. G. Fujimoto, G. L. Eesley, and T. W. Capehart. *Phys. Rev. Lett.*, 61:2596, 1988.

[10] H. Petek, H. Nagano, M. J. Weida, and S. Ogawa. *J. Phys. Chem. B*, 105:6767, 2001.

[11] M. Bauer, S. Pawlik, and M. Aeschlimann. *Phys. Rev. B*, 55:10040, 1997.

[12] G. Dutton and X.-Y. Zhu. *J. Phys. Chem. B*, 105:10912, 2001.

[13] C. Gahl, K. Ishioka, Q. Zhong, A. Hotzel, and M. Wolf. *Faraday Discuss.*, 117: 191, 2000.

[14] T. Hertel, E. Knoesel, E. Hasselbrink, M. Wolf, and G. Ertl. *Surf. Sci.*, 317: L1147, 1994.

[15] A. Hotzel, K. Ishioka, E. Knoesel, M. Wolf, and G. Ertl. *Chem. Phys. Lett.*, 285: 271, 1998.

[16] T. Vondrak and X.-Y. Zhu. *J. Phys. Chem. B*, 103:3449, 1999.

[17] X.-Y. Zhu, T. Vondrak, H. Wang, C. Gahl, K. Ishioka, and M. Wolf. *Surf. Sci.*, 451:244, 2000.

[18] P. A. Brühwiler, O. Karis, and N. Mårtensson. *Rev. Mod. Phys.*, 74:703, 2002.

[19] G. S. Brown, M. H. Chen, B. Crasemann, and G. E. Ice. *Phys. Rev. Lett.*, 45: 1937, 1980.

[20] G. Bradley Armen, Helena Aksela, Teijo Åberg, and Seppo Aksela. *J. Phys. B*, 33:R49, 2000.

[21] M. N. Piancastelli. *J. Electron Spectrosc. Relat. Phenom.*, 107.

[22] J. Stöhr. *NEXAFS spectroscopy*, volume 25. Springer Series in Surface Science, 2003.

[23] A. Föhlisch, S. Vijayalakshmi, F. Hennies, W. Wurth, V. R. R. Medicherla, and W. Drube. Verification of the core–hole–clock method using two different time references : Attosecond charge transfer in c(4x2)s/ru(0001). *Chem. Phys. Lett. 434 (2007) 214.*

[24] A. Föhlisch, P. Feulner, F. Hennies, A. Fink, D. Menzel, D. Sanchez-Portal, P. Echenique, and W. Wurth. *Nature*, 436:373, 2005.

[25] J. Schnadt, P. A. Brühwiler, L. Patthey, J. N. O'Shea, S. Södergren, M. Odelius, R. Ahuja, O. Karis, M. Bässler, P. Persson, H. Siegbahn, S. Lunell, and N. Mårtensson. *Nature*, 418:620, 2002.

[26] O. Björneholm, A. Nilsson, A. Sandell, B. Hernnäs, and N. Mårtensson. *Phys. Rev. Lett.*, 68:1892, 1992.

[27] O. Karis, A. Nilsson, M. Weinelt, T. Wiell, C. Puglia, N. Wassdahl, N. Mårtensson, M. Samant, and J. Stöhr. *Phys. Rev. Lett.*, 76:1380, 1996.

[28] O. Björneholm, S. Sundin, S. Svensson, R. R. T. Marinho, A. N. de Brito, F. Gel'mukhanov, and H. Ågren. *Phys. Rev. Lett.*, 79:3150, 1997.

[29] C. Keller, M. Stichler, G. Comelli, F. Esch, S. Lizzit, W. Wurth, and D. Menzel. *Phys. Rev. Lett.*, 80:1774, 1998.

[30] C. Keller, M. Stichler, G. Comelli, F. Esch, S. Lizzit, D. Menzel, and W. Wurth. *Phys. Rev. B*, 57:11951, 1998.

[31] R. Feifel, F. Burmeister, P. Salek, M. N. Piancastelli, M. Bässler, S. L. Sorensen, C. Miron, H. Wang, I. Hjelte, O. Björneholm, A. N. de Brito, F. Gel'mukhanov, H. Ågren, and S. Svensson. *Phys. Rev. Lett.*, 85:3133, 2000.

[32] W. Wurth and D. Menzel. *Chem. Phys.*, 251:141, 2000.

[33] A. Föhlisch, D. Menzel, P. Feulner, M. Ecker, R. Weimar, K. L. Kostov, G. Tyuliev, S. Lizzit, R. Larciprete, F. Hennies, and W. Wurth. *Chem. Phys.*, 289:107, 2003.

[34] C. Keller, M. Stichler, A. Fink, P. Feulner, D. Menzel, A. Föhlisch, F. Hennies, and W. Wurth. *Appl. Phys. A*, 78:125, 2004.

[35] J. P. Gauyacq and A. G. Borisov. *Phys. Rev. B*, 69:235408, 2004.

[36] S. Vijayalakshmi, A. Föhlisch, F. Hennies, A. Pietzsch, M. Nagasono, W. Wurth, A. G. Borisov, and J. P. Gauyacq. *Chem. Phys. Lett.*, 427:91, 2006.

[37] F. Gel'mukhanov and H. Ågren. *Phys. Rep.*, 312:87, 1999.

[38] M. O. Krause and J. H. Oliver. *J. Phys. Chem. Ref. Data*, 8:329, 1979.

[39] C.-O. Almbladh and L. Hedin. *Handbook of Synchrotron Radiation*, North Holland, 1983.

[40] A. Föhlisch, O. Karis, M. Weinelt, J. Hasselström, A. Nilsson, and N. Mårtensson. *Phys. Rev. Lett.*, 88:027601, 2002.

[41] M. Weinelt, A. Nilsson, M. Magnuson, T. Wiell, N. Wassdahl, O. Karis, A. Föhlisch, N. Mårtensson, J. Stöhr, and M. Samant. *Phys. Rev. Lett.*, 78: 967, 1997.

[42] C. Schwennicke, D. Jürgens, G. Held, and H. Pfnür. *Surf. Sci.*, 316:81, 1994.

[43] D. Jürgens, C. Schwennicke, and H. Pfnür. *Surf. Sci.*, 381:174, 1997.

[44] L. Asplund, P. Kelfve, B. Blomster, H. Siegbahn, K. Siegbahn, R. L. Lozes, and U. I. Wahlgren. *Physica Scripta*, 16:273, 1977.

[45] S. Doniach and M. Sunjic. *J. Phys. C*, 3:285, 1970.

[46] O. Björneholm, A. Nilsson, A. Sandell, B. Hernnäs, and N. Mårtensson. *Phys. Rev. Lett.*, 68:1892, 1992.

[47] A. G. Borisov, J. P. Gauyacq, A. K. Kazansky, E. V. Chulkov, V. M. Silkin, and P. M. Echenique. *Phys. Rev. Lett.*, 86:488, 2001.

[48] M. Bauer, S. Pawlik, and M. Aeschlimann. *Phys. Rev. B*, 60:5016, 1999.

[49] J. P. Gauyacq, A. G. Borisov, and G. Raçeev. *Surf. Sci.*, 490:99, 2001.

[50] V. A. Ermoshin and A. K. Kazansky. *Phys. Lett. A*, 218:99, 1996.

[51] J. P. Gauyacq and A. G. Borisov. *Phys. Rev. B*, 69:235408, 2004.

[52] A. G. Borisov, A. K. Kazansky, and J. P. Gauyacq. *Phys. Rev. B*, 59:10935, 1999.

[53] S. Vijayalakshmi, A. Föhlisch, F. Hennies, A. Pietzsch, M. Nagasono, W. Wurth, A. G. Borisov, and J. P. Gauyacq. Surface projected electronic band structure and adsorbate charge transfer dynamics : Ar adsorbed on cu(111) and cu(100). *Chem. Phys. Lett.*, 427:91, 2006.

[54] P. M. Echenique, R. Berndt, E. V. Chulkov, Th. Fauster, A. Goldmann, and U. Höfer. *Surf. Sci. Rep.*, 52:219, 2004.

[55] R. Kosloff, G. Katz, and Y. Zeiri. *Faraday Discuss.*, 117:291, 2000.

[56] H. Guo, P. Saalfranck, and T. Seideman. *Prog. Surf. Sci.*, 62:239, 1999.

[57] S. Ogawa, H. Nagano, and H. Petek. *Phys. Rev. Lett.*, 82:1931, 1999.

[58] H. Petek, M. J. Weida, H. Nagano, and S. Ogawa. *Science*, 288:1402, 2000.

[59] A. G. Borisov, A. K. Kazansky, and J. P. Gauyacq. *Surf. Sci.*, 430:165, 1999.

[60] J. P. Gauyacq, A. G. Borisov, G. Raşeev, and A. K. Kazansky. *Faraday Discuss.*, 117:15, 2000.

[61] A. G. Borisov, J. P. Gauyacq, E. V. Chulkov, V. M. Silkin, and P. M. Echenique. *Phys. Rev. B*, 65:235434, 2002.

[62] M. Ohno. *Phys. Rev. B*, 50:2566, 1994.

[63] N. Mårtensson and A. Nilsson. *J. Electron Spectrosc. Relat. Phenom.*, 72:1, 1995.

[64] O. Karis, A. Nilsson, M. Weinelt, T. Wiell, C. Puglia, N. Wassdahl, N. Mårtensson, M. Samant, and J. Stöhr. *Phys. Rev. Lett.*, 76:1380, 1996.

[65] A. Sandell, O. Hjortstam, A. Nilsson, P. Brühwiler, O. Eriksson, P. Bennich, P. Rudolf, J. M. Wills, B. Johansson, and N. Mårtensson. *Phys. Rev. Lett.*, 78: 4994, 1997.

[66] W. Wurth, P. Feulner, and D. Menzel. *Physica Scripta*, T41:213, 1992.

[67] W. Wurth. *Appl. Phys. A*, 65:597, 1997.

[68] A. Sandell, P. A. Brüwiler, A. Nilsson, P. Bennich, P. Rudolf, and N. Mårtensson. *Surf. Sci.*, 429:309, 1999.

[69] W. Wurth and D. Menzel. *Chem. Phys.*, 251:141, 2000.

[70] D. C. Marinica, C. Ramseyer, A. G. Borisov, D. Teillet-Billy, and J. P. Gauyacq. *Surf. Sci.*, 540:457, 2003.

[71] K. Horn, C. Mariani, and L. Cramer. *Surf. Sci.*, 117:376, 1982.

[72] E. V. Chulkov, V. M. Silkin, and P. M. Echenique. *Surf. Sci.*, 437:330, 1999.

[73] J. P. Gauyacq and A. K. Kazansky. *Phys. Rev. B*, 72:045418, 2005.

[74] P. S. Bagus, K. Hermann, and C. Wöll. *J. Chem. Phys.*, 123:184109, 2005.

[75] M. Xi, M. X. Yang, S.K. Jo, B. E. Bent, and P. Stevens. *J. Chem. Phys.*, 101: 9122, 1994.

[76] D. Menzel, G. Rocker, H.-P. Steinrück, D. Coulman, P. A. Heimann, W. Huber, P. Zebisch, and D. R. Lloyd. *J. Chem. Phys.*, 96:1724, 1992.

[77] N. Witkowski, F. Hennies, A. Pietzsch, S. Mattsson, A. Föhlisch, W. Wurth, M. Nagasono, and M. N. Piancastelli. *Phys. Rev. B*, 68:115408, 2003.

[78] A. Pietzsch, F. Hennies, A. Föhlisch, W. Wurth, M. Nagasono, N. Witkowski, and M. N. Piancastelli. *Surf. Sci.*, 562:65, 2004.

[79] S. Vijayalakshmi, A. Föhlisch, P. S. Kirchmann, F. Hennies, A. Pietzsch, M. Nagasono, and W. Wurth. Bond polarization and image-potential screening in adsorbed c_6f_6 on cu(111). *Surf. Sci.*, 600:4972, 2006.

[80] A. P. Hitchcock, P. Fischer, A. Gedanken, and M. B. Robin. *J. Phys. Chem.*, 91: 531, 1987.

[81] R. Dudde, B. Reihl, and A. Otto. *J. Chem. Phys.*, 92:3930, 1990.

[82] L. G. Christophorou, P. G. Datskos, and H. Faidas. *J. Chem. Phys.*, 101:6728, 1994.

[83] T. X. Carroll, T. D. Thomas, H. Bergersen, K. J. Børve, and L. J. Sæthre. *J. Org. Chem.*, 71:1961, 2006.

[84] R. Courths and S. Hüfner. *Phys. Rep.*, 112:53, 1984.

[85] P. S. Kirchmann, P. A. Loukakos, U. Bovensiepen, and M. Wolf. *New Journal of Physics*, 7:113, 2005.

[86] F. P. Netzer. *Langmuir*, 7:2544, 1991.

[87] H. Hoffmann, F. Zaera, R. M. Ormerod, R. M. Lambert, L. P. Wang, and W. T. Tysoe. *Surf. Sci.*, 232:259, 1990.

[88] S. Aminpirooz, L. Becker, B. Hillert, and J. Haase. *Surf. Sci. Lett.*, 244:L152, 1991.

[89] A. C. Liu, J. Stöhr, C. M. Friend, and R. J. Madix. *Surf. Sci.*, 235:107, 1990.

[90] N. Boden, P. P. Davis, C. H. Stam, and G. A. Wesselink. *Molec. Phys.*, 25:81, 1973.

[91] J. Hasselström, A. Föhlisch, R. Denecke, A. Nilsson, and F. M. F. de Groot. *Phys. Rev. B*, 62:11192, 2000.

[92] P. A. Brühwiler, A. J. Maxwell, P. Rudolf, C. D. Gutleben, B. Wästberg, and N. Mårtensson. *Phys. Rev. Lett.*, 71:3721, 1993.

[93] S. Vijayalakshmi, A. Föhlisch, F. Hennies, A. Pietzsch, M. Nagasono, and W. Wurth. Investigation of charge transfer dynamics in c_6f_6/cu(111) with core–hole–clock spectroscopy. *in manuscript*, .

[94] A. Föhlisch, S. Vijayalakshmi, F. Hennies, W. Wurth, V. R. R. Medicherla, and W. Drube. *Chem. Phys. Lett.*, 434:214, 2007.

[95] C. R. Brundle, M. B. Robin, and N. A. Kuebler. *J. Amer. Chem. Soc.*, 94:1466, 1972.

[96] M. H. Palmer, W. Moyes, M. Spiers, and J. N. A. Ridyard. *J. Mol. Struct.*, 49: 105, 1978.

[97] W. E. Moddeman, T. A. Carlson, M. O. Krause, B. P. Pullen, W. E. Bull, and G. K. Schweitzer. *J. Chem. Phys.*, 55:2317, 1971.

[98] L. Ungier and T. D. Thomas. *J. Chem. Phys.*, 82:3146, 1985.

[99] H.-J. Freund and C.-M. Llegener. *Chem. Phys. Lett.*, 134:70, 1987.

[100] R. Feifel, L. Karlsson, M.-N. Piancastelli, R. F. Fink, M. Bässler O. Björneholm, K. Wiesner, C. Miron, H. Wang, A. Giertz, S. L. Sorensen A. Naves de Brito, and S. Svensson. *Phys. Rev. A*, 65:052701, 2002.

[101] W. Eberhardt, E. W. Plummer, I. W. Lyo, R. Murphy, R. Carr, and W. K. Ford. *J. De Physique*, C9:679, 1987.

[102] O. Björneholm, H. Tillborg, A. Nilsson, N. Mårtensson, H. Ågren, and C. M. Liegener. *Phys. Rev. Lett.*, 73:2551, 1994.

[103] T. X. Carroll and T. D. Thomas. *J. Chem. Phys.*, 86:5221, 1987.

[104] T. X. Carroll and T. D. Thomas. *J. Chem. Phys.*, 89:5983, 1988.

[105] T. X. Carroll, S. E. Anderson, L. Ungier, and T. D. Thomas. *Phys. Rev. Lett.*, 58:867, 1987.

[106] W. Eberhardt, J.-E. Rubensson, K. J. Randall, J. Feldhaus, A. L. D. Kilcoyne, A. M. Bradshaw, Z. Xu, P. D. Johnson, and Y. Ma. *Physica Scripta*, T41:143, 1992.

[107] R. Murphy, In-Whan Lyo, and W. Eberhardt. *J. Chem. Phys.*, 88:6078, 1988.

[108] D. Lapiano-Smith, K. Lee, C. I. Ma, K. Wu, and D. M. Hanson. *J. Electron Spectrosc. Relat. Phenom.*, 51:221, 1990.

[109] C. Puglia, A. Nilsson, B. Hernnäs, O. Karis, P. Bennich, and N. Mårtensson. *Surf. Sci.*, 342:119, 1995.

[110] K. Wandelt. *Surf. Sci. Rep.*, 2:1, 1982.

[111] V. Carravetta, F. Kh. Gel'mukhanov, H. Ågren, S. Sundin, S. J. Osborne, A. Naves de Brito, O. Björneholm, A. Ausmees, and S. Svensson. *Phys. Rev. A*, 56:4665, 1997.

[112] M. N. Piancastelli, M. Neeb, A. Kivimäki, B. Kempgens, H. M. Köppe, K. Maier, and A. M. Bradshaw. *Phys. Rev. Lett.*, 77:4302, 1996.

[113] F. Hennies, S. Polyutov, I. Minkov, A. Pietzsch, M. Nagasono, F. Gel'mukhanov, L. Triguero, M.-N. Piancastelli, W. Wurth, H. Ågren, and A. Föhlisch. *Phys. Rev. Lett.*, 95:163002, 2005.

[114] C. Puglia, P. Bennich, J. Hasselström, C. Ribbing, P. A. Brühwiler, A. Nilsson, Z. Y. Li, and N. Mårtensson. *Surf. Sci.*, 414:118, 1998.

[115] L. S. Cederbaum, W. Domcke, J. Schirmer, W. V. Niessen, G. H. F. Diercksen, and W. P. Kraemer. *J. Chem. Phys.*, 69:1591, 1978.

[116] W. Wurth and D. Menzel. *J. Electron Spectrosc. Relat. Phenom.*, 62:23, 1993.

[117] H. Aksela, S. Aksela, O.-P. Sairanen, A. Kivimäki, G. M. Bancroft, and K. H. Tan. *Physica Scripta*, T41:122, 1992.

[118] E. Kukk, H. Aksela, S. Aksela, F. Gel'mukhanov, H. Ågren, and S. Svensson. *Phys. Rev. Lett.*, 76:3100, 1996.

[119] H. Aksela, S. Aksela, M. Ala-Korpela, O.-P. Sairanen, M. Hotokka, G. M. Bancroft K. H. Tan, and J. Tulkki. *Phys. Rev. A*, 41:6000, 1990.

[120] S. Svensson, L. Karlsson, N. Mårtensson, P. Baltzer, and B. Wannberg. *J. Elect. Spectrosc. Rel. Phenom*, 50:C1–C7, 1990.

[121] P. Morin and I. Nenner. *Phys. Rev. Lett.*, 56:1913, 1986.

[122] I. Nenner, P. Morin, P. Lablanquie, M. Simon, N. Levasseur, and P. Millier. *J. Elect. Spectrosc. Rel. Phenom*, 52:623, 1990.

[123] K. Wiesner, A. Naves de Brito, S. L. Sorensen, N. Kosugi, and O. Björneholm. *J. Chem. Phys.*, 122:154303, 2005.

[124] M. N. Piancastelli, B. Kempgens, U. Hergenhahn, A. Kivimäki, K. Maier, A. Rüdel, and A. M. Bradshaw. *Phys. Rev. A*, 59:1336, 1999.

[125] S. Svensson, H. Aksela, A. Kivimäki, O.-P. Sairanen, A. Ausmees, S. J. Osborne, A. Naves de Brito, E. Nõmmiste, G. Bray, and S. Aksela. *J. Phys. B*, 28:L325, 1995.

[126] K. Ueda, M. Simon, C. Miron, N. Leclercq, R. Guillemin, P. Morin, and S. Tanaka. *Phys. Rev. Lett.*, 83:3800, 1999.

[127] K. Ueda, S. Tanaka, Y. Shimizu, Y. Muramatsu, H. Chiba, T. Hayaishi, M. Kitajima, and H. Tanaka. *Phys. Rev. Lett.*, 85:3129, 2000.

[128] Kiyoshi Ueda. *J. Electr. Spectrosc. Relat. Phenom.*, 88:1, 1998.

[129] U. Fano. *Phys. Rev.*, 124:1866, 1961.

[130] U. Fano and J. W. Cooper. *Rev. Mod. Phys.*, 40:441, 1968.

[131] R. Camilloni, M. Žitnik, C. Comicioli an K. C. Prince, M. Zacchigna, C. Crotti, C. Ottaviani, C. Quaresima, P. Perfetti, and G. Stefani. *Phys. Rev. Lett.*, 77: 2646, 1996.

[132] William J. Griffiths, Svante Svensson, Arnaldo Naves de Brito, Nestor Correia, Bjorn Wannberg, Marion L. Langford, Frank M. Harris, and Christoph M. Liegener Hans Ågren. *J. Chem. Soc. Faraday Trans.*, 89:1637, 1993.

[133] H. Kanamori, S. Iwata, A. Mikuni, and T. Sasaki. *J. Phys. B*, 17:3887, 1984.

[134] M. Simon, C. Miron, N. Leclercq, P. Morin, K. Ueda, Y. Sato, S. Tanaka, and Y. Kayanuma. *Phys. Rev. Lett.*, 79:3857, 1997.

[135] C. Miron, R. Feifel, O. Björneholm, S. Svensson, A. Naves de Brito, S. L. Sorensen, M. N. Piancastelli, M. Simon, and P. Morin. *Chem. Phys. Lett.*, 359: 48, 2002.

[136] V. Myrseth, K. J. Borve, K. Wiesner, M. Bässler, S. Svensson, and L. J. Saethre. *Phys. Chem. Chem. Phys.*, 4:5937, 2002.

[137] Daniel Rolles, Markus Braune, Slobodan Cvejanovic, Oliver Geßner, Rainer Hentges, Sanja Korica, Burkhard Langer, Toralf Lischke, Georg Prümper, Axel Reinköster, Jens Viefhaus, Björn Zimmermann, Vincent McKoy, and Uwe Becker. *Nature*, 437:711, 2005.

[138] H.-P. Steinrück, T. Pache, and W. Huber. *Physica Scripta*, 41:177, 1990.

[139] Joachim Schnadt, Anders Henningsson, Martin P. Andersson, Patrik G. Karlsson, Per Uvdal, Hans Siegbahn, Paul A. Brühwiler, and Anders Sandell. *J. Phys. Chem.*, 108:3114, 2004.

[140] M. P. de Jong, R. Friedlein, S. L. Sorensen, G. Öhrwall, W. Osikowicz, C. Tengsted, S. K. M. Jönsson, M. Fahlman, and W. R. Salaneck. *Phys. Rev. B*, 72: 035448, 2005.

[141] S. Vijayalakshmi, A. Föhlisch, F. Hennies, A. Pietzsch, M. Nagasono, W. Wurth P. S. Kirchmann, U. Bovensiepen, and M. Wolf. *in manuscript*, .

[142] S. Vijayalakshmi, A. Föhlisch, F. Hennies, A. Pietzsch, M. Nagasono, W. Wurth P. S. Kirchmann, U. Bovensiepen, and M. Wolf. Comparative study of charge transfer dynamics in c_6f_6/cu(111) : Comparison of core–hole–clock method and time resolved two-photon photoemission. *in manuscript*, .

[143] S. Vijayalakshmi, A. Föhlisch, F. Hennies, A. Pietzsch, M. Nagasono, and W. Wurth. *in manuscript*, .

[144] K. Ishioka, C. Gahl, and M. Wolf. *Surf. Sci.*, 454-456:73, 2000.

[145] C. Rulliere. *Femtosecond Laser Pulses*. Springer Series. 1998.

[146] S. Vijayalakshmi, A. Föhlisch, P. S. Kirchmann, F. Hennies, A. Pietzsch, M. Nagasono, and W. Wurth. *Surf. Sci.*, 600:4972, 2006.

Acknowledgements

I have been working as a Ph.D student under the supervision of Prof. Dr. Wilfried Wurth and Dr. Alexander Föhlisch from 2002 Oct. - 2006 Nov. As a foreigner to the place and to the work, during this four years of work I learnt a lot. I enjoyed very much working with my Ph.D work. I am grateful to my thesis supervisor for providing very good guidance and lots of patience to explain me physics aspects. I am thankful for my project supervisor Dr. Alexander Föhlisch for teaching me surface science concepts especially the condensed matter physics and the methods. Discussions during lunch time were very fruitful.

I thank Franz Hennies my labmate who also carried out project works with me. It was really great that Franz translated the German conversations during the experiments to me. Beamtime in Lund with Franz is an immemorable event. I am grateful for Annette's comments on my thesis. I am thankful for both of their unconditional help.

I thank Dr. Mitsuru and Edlira for cooperating at work.

I thank Sven and Holger for working in pace with me at the machine. I improved quite a bit of my German by chatting with them.

Collaborative work with Prof. Dr. J. P. Gauyacq and Dr. A. G. Borisov on the investigation of band gap effect on electron dynamics in Ar/Cu(100) and Ar/Cu(111) was very instructive and is gratefully acknowledged. I am very thankful to Prof. Dr. Martin Wolf, Dr. U. Bovensiepen, Patrick S. Kirchmann from Berlin collaborating in hexafluorobenzene/Cu(111) charge transfer dynamics project. I thank Patrick for his valuable comments and discussions regarding our joint project.

It was nice sharing the office with Dr. Michael Martins during the first 2 years of my Ph.D though we never spoke with each other much.

I like to also thank Leif, Mathhias, Jon and Wellhöfer for having fun at times.

My parents were taking extra care for me during my stay away from my family. It is a great pleasure for me to write my Ph.D thesis and see it in its full form.